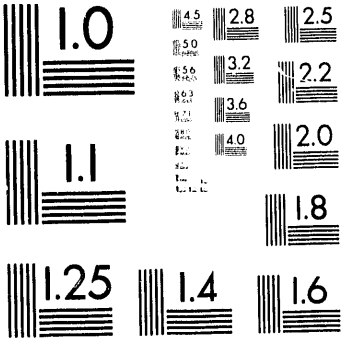
1.0
1.1
1.25
1.4
1.6
1.8
2.0
2.2
2.5
2.8
3.2
3.6
4.0
4.5
5.0
5.6
6.3
7.1

1 of 2

SAND92-2013
Unlimited Release
Printed August 1993

Distribution
Category UC-721

Uncertainty and Sensitivity Analyses for Gas and Brine Migration at the Waste Isolation Pilot Plant, May 1992

J.C. Helton[1], J.E. Bean[2], B.M. Butcher,
J.W. Garner[3], J.D. Schreiber[4],
P.N. Swift[5], and P. Vaughn[3]

ABSTRACT

Uncertainty and sensitivity analysis techniques based on Latin hypercube sampling, partial correlation analysis, stepwise regression analysis and examination of scatterplots are used in conjunction with the BRAGFLO model to examine two phase flow (i.e., gas and brine) at the Waste Isolation Pilot Plant (WIPP), which is being developed by the U.S. Department of Energy as a disposal facility for transuranic waste. The analyses consider either a single waste panel or the entire repository in conjunction with the following cases: (1) fully consolidated shaft, (2) system of shaft seals with panel seals, and (3) single shaft seal without panel seals. The purpose of this analysis is to develop insights on factors that are potentially important in showing compliance with applicable regulations of the U.S. Environmental Protection Agency (i.e., 40 CFR 191, Subpart B; 40 CFR 268). The primary topics investigated are (1) gas production due to corrosion of steel, (2) gas production due to microbial degradation of cellulosics, (3) gas migration into anhydrite marker beds in the Salado Formation, (4) gas migration through a system of shaft seals to overlying strata, and (5) gas migration through a single shaft seal to overlying strata. Important variables identified in the analyses include initial brine saturation of the waste, stoichiometric terms for corrosion of steel and microbial degradation of cellulosics, gas barrier pressure in the anhydrite marker beds, shaft seal permeability, and panel seal permeability.

[1]Arizona State University, Tempe, AZ
[2]New Mexico Engineering Research Institute, Albuquerque, NM
[3]Applied Physics, Inc., Albuquerque, NM
[4]Science Applications International Corporation, Albuquerque, NM
[5]Tech Reps, Inc., Albuquerque, NM

MASTER

ACKNOWLEDGMENTS

The support provided by D. R. Anderson, B. L. Baker, J. Berglund, W. Beyeler, S. C. Hora, H. J. Iuzzolino, R. P. Rechard, K. K. Rudeen, M. S. Tierney, K. Trauth, and other members of the 1991 performance assessment team for the Waste Isolation Pilot Plant is gratefully acknowledged. Special recognition is extended to M. G. Marietta and M. Fewell for their careful prepublication review of this document. The editorial support provided by the staff of Tech Reps, Inc., with special thanks to D. Marchand, F. Puffer, and M. Minahan, is also gratefully appreciated.

CONTENTS

Figures

Tables

1. INTRODUCTION

The Waste Isolation Pilot Plant (WIPP) in southeastern New Mexico is being developed by the U.S. Department of Energy (DOE) as a research and development facility to demonstrate the safe disposal of defense-generated transuranic waste (U.S. DOE, 1980; U.S. DOE, 1991). The WIPP must comply with various environmental regulations of the U.S. Environmental Protection Agency (EPA), including 40 CFR 268.6, *Petitions to allow land disposal of a waste prohibited under Subpart C of Part 268* (implementing the *Resource Conservation and Recovery Act* [RCRA, U.S. EPA, 1986]) and 40 CFR 191, Subpart B, the *Environmental Standards for the Management and Disposal of Spent Nuclear Fuel, High-Level and Transuranic Radioactive Wastes* (U.S. EPA, 1985). In support of the development of the WIPP and to provide perspective on compliance with various applicable regulations, Sandia National Laboratories (SNL) is conducting an ongoing performance assessment for the WIPP (Bertram-Howery and Hunter, 1989; Lappin et al., 1989). At present, a performance assessment is carried out each year to summarize what is known about the WIPP and to provide guidance for future work (Marietta et al., 1989; Bertram-Howery et al., 1990; WIPP PA, 1991a).

The 1991 WIPP performance assessment (WIPP PA, 1991a; 1991b; 1991c; Helton et al., 1992) is the first to model the generation of gas in the repository and the potential flow of this gas away from the repository. The primary focus of prior performance assessments for the WIPP has been on compliance with 40 CFR 191, Subpart B, which primarily involves radionuclide releases due to cuttings removal and transport by groundwater. The two phase (i.e., gas and brine) flow calculations performed for the 1991 WIPP performance assessment provide the first opportunity to investigate factors that may influence compliance with 40 CFR 268.6.

To provide perspective on factors influencing compliance with 40 CFR 268, three analysis cases were considered as part of the 1991 WIPP performance assessment:

Case 1: Fully Consolidated Shaft
Case 2: System of Shaft Seals with Panel Seals
Case 3: Single Shaft Seal without Panel Seals.

All three cases examine the undisturbed performance of the WIPP over 10,000 yr. Case 1 uses a model configuration identical to that used in the 1991 WIPP performance assessment for scenarios involving human intrusion during exploratory drilling for natural resources, with the significant difference that an intrusion does not occur. Because the Case 1 model configuration was designed to assess flow up a borehole, shafts are,

depending on preferred terminology, omitted or assumed to be fully consolidated. This assumption forces all significant fluid flow from the repository to occur horizontally through anhydrite layers above and below the waste panels. Cases 2 and 3 contain permeable shafts, with the result that both horizontal and vertical fluid migration is possible.

For each case, uncertainty and sensitivity analyses are performed to determine the factors affecting gas and brine movement away from the repository. Gas movement provides an indication of the extent to which volatile organic compounds (VOCs) might be transported away from the repository. Similarly, brine movement provides an indication of the extent to which heavy metals and other contaminants might be transported away from the repository by flowing brine. The uncertainty and sensitivity analyses use techniques based on Latin hypercube sampling, examination of scatterplots, partial correlation analysis and stepwise regression analysis (Helton et al., 1991; Helton, 1992).

A prior report describes the three analysis cases in detail and provides an overview of the manner in which the BRAGFLO computer program is used to model two-phase flow for these cases (WIPP PA, 1992). Additional information on BRAGLFO is available in Ch. 5 of WIPP PA, 1991b. In addition, WIPP PA, 1992 presents sensitivity analysis results based on the examination of scatterplots and the results associated with individual sample elements. The present report uses more formal procedures based on partial correlation analysis and stepwise regression analysis, although examination of scatterplots will also be used extensively.

As a reminder, there are two types of uncertainty in a performance assessment: stochastic uncertainty and subjective uncertainty (Ch. 3, WIPP PA, 1991a; Helton, 1983). Stochastic uncertainty refers to the fact that many different occurrences have a real possibility of taking place and is incorporated into a performance assessment through the probabilities for individual scenarios. Subjective uncertainty refers to the analysts' lack of knowledge with respect to values for parameters required in the computational implementation of a performance assessment and is incorporated into a performance assessment by developing distributions for imprecisely known parameters that characterize a degree of belief as to where the appropriate value to use in the analysis is located. The three analysis cases are equivalent to individual scenarios, and there is no consideration of their probability of occurrence. Thus, the results presented in this report do not involve stochastic uncertainty. Rather, the uncertainty and sensitivity analyses are studying the effects of subjective uncertainty.

2. CASE 1: FULLY CONSOLIDATED SHAFT

2.1 Summary Description*

Case 1 involves a single waste panel and employs the model configuration used for the undisturbed scenario in the 1991 WIPP performance assessment (Sects. 5.2.3 and 5.2.4, WIPP PA, 1991b). The computational implementation with BRAGFLO is based on an axisymmetric geometry (Fig. 2-1) and uses the gridding scheme shown in Fig. 2-2. The drift and shaft systems are omitted from the model, which is equivalent to the assumption of a sealing system that produces properties identical to undisturbed halite.

The single waste panel considered in Case 1 is represented as a cylinder with the same enclosed volume as the mean volume of the ten waste-disposal panels, including the volume occupied by the halite pillars separating the rooms (Fig. 2-3). Pillars are included in the panel volume to preserve the horizontal cross-sectional area through which brine inflow from the anhydrite interbeds could occur. This results in a cylinder having a radius of approximately 97 m. Porosity of the modeled panel is less than the porosity of the waste and backfill alone due to the presence of the low-porosity halite in the pillars. As discussed later, a correction is also made to approximate the room expansion that might occur from the presence of waste-generated gas. Initial brine saturation is also adjusted for the presence of the pillars, which are fully saturated with brine. These adjustments are discussed in the documentation for the 1991 preliminary comparison with 40 CFR 191, Subpart B (Sect. 3.4.8, WIPP PA, 1991c).

The region modeled with BRAGFLO includes Marker Bed 139 (MB139), which is an anhydrite interbed below the waste-disposal horizon, and Anhydrite Layers A and B above the panel (Fig. 2-2). These units are included in the model because they have higher permeability than the intact halite of the Salado Formation and therefore are preferred pathways for fluid flow. As modeled, Marker Bed 139 is 0.9 m thick and 2.9 m below the panel floor. Anhydrite Layers A and B are represented as a single layer 0.21 m thick, corresponding to the combined thickness of the two units, and are located 5.33 m above the floor of the panel at the elevation of Anhydrite Layer B. The thickness of the waste panel was uncertain and ranged from 2.67 m to 3.64 m. This variability resulted from uncertainty with respect to waste composition, which in turn controls waste porosity after compaction and thus panel height.

*Adapted from Section 2.2 of WIPP PA, 1992.

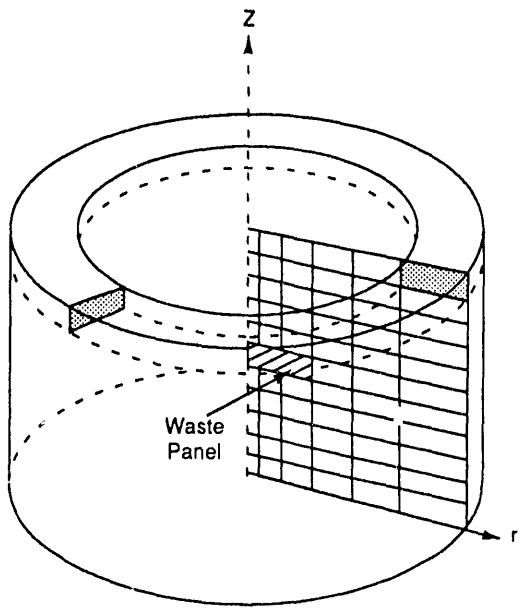

Figure 2-1. Schematic representation of an axisymmetric cylindrical model (Fig. 2-1, WIPP PA, 1992).

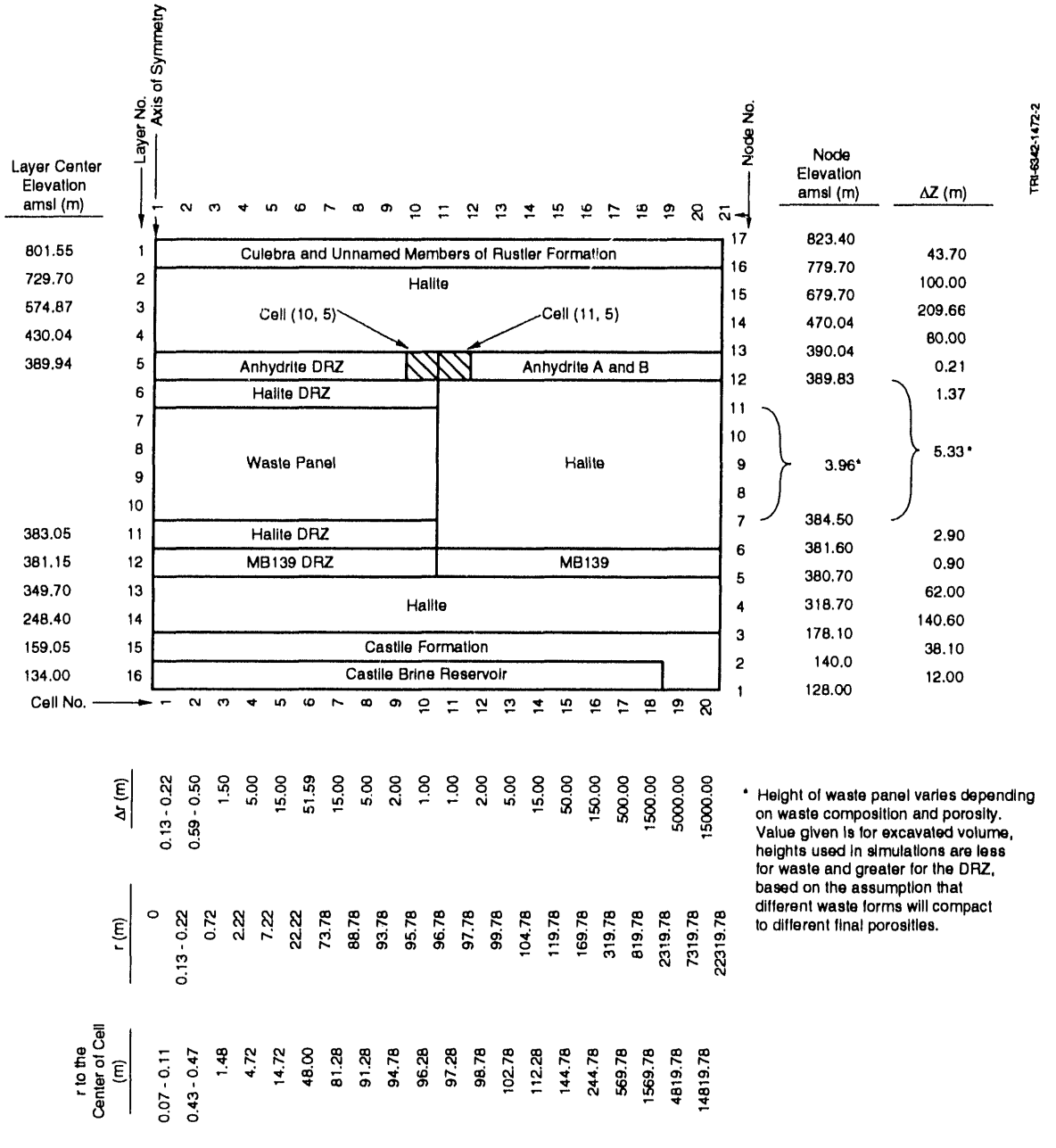

Figure 2-2. Gridding scheme employed with BRAGFLO for the cylindrical equivalent panel model used for Case 1 (Fig. 2-2, WIPP PA, 1992). Individual computational cells are identified with an ordered pair (i,j) of integers, where i designates the horizontal coordinate and j designates the vertical coordinate.

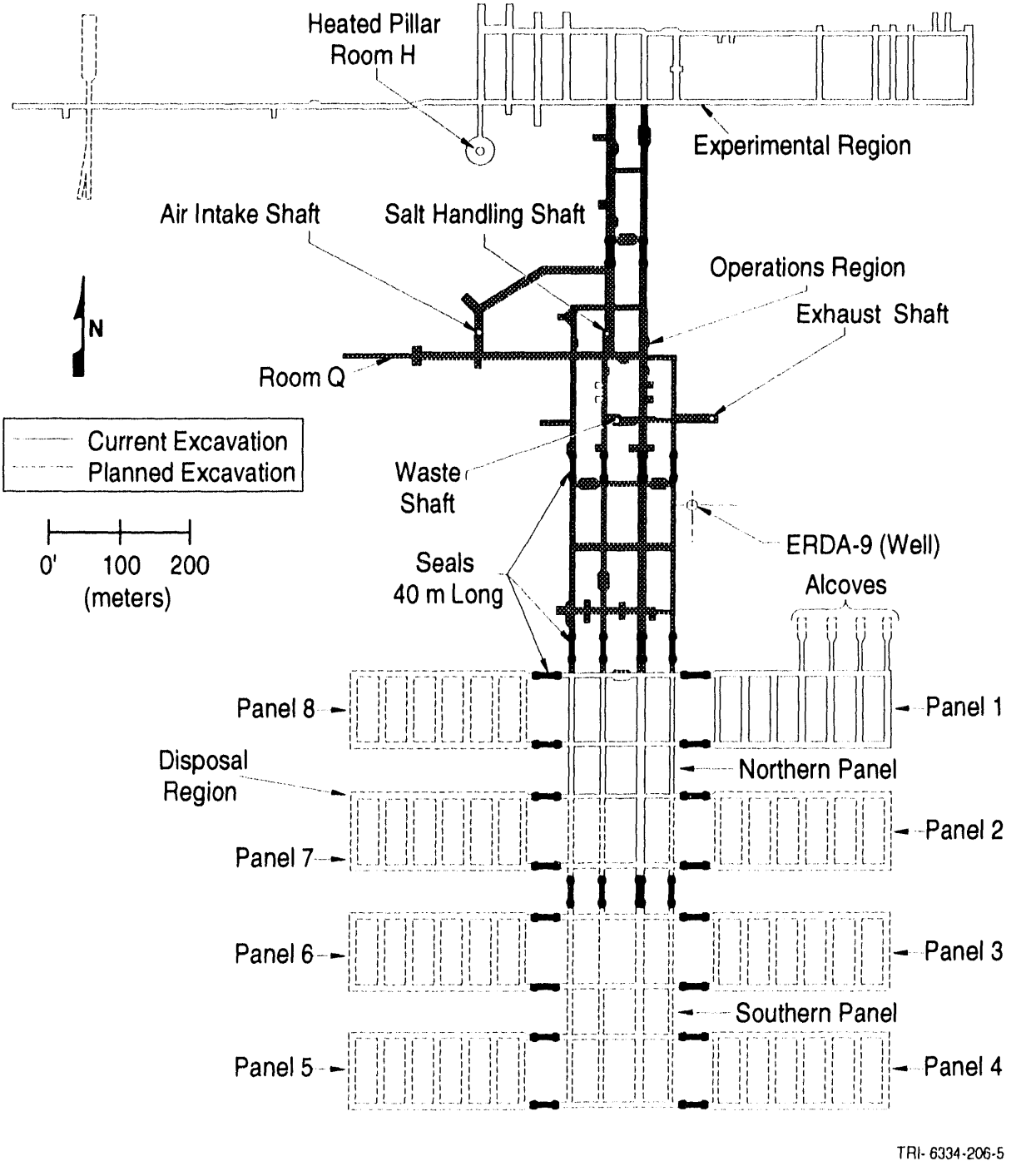

Figure 2-3. Excavated areas in the WIPP repository.

The disturbed rock zone (DRZ) surrounding the excavation is assumed to extend upward to the top of Anhydrite Layers A and B and downward to the base of Marker Bed 139. The lateral extent of the disturbed rock zone within the halite is not included in this model because the principal flow paths of interest are through the disturbed rock zone vertically to the anhydrite layers.

The modeled region extends laterally for a radius of approximately 22 km. This distance is a compromise value; a more-distant boundary might result in greater computational accuracy, but uncertainty in the geologic system being modeled increases away from the repository (Powers et al., 1978). The model extends upward to the Culebra Dolomite Member of the Rustler Formation and downward to the Castile Formation. These units are included because they represent potential sinks and sources, respectively, for brine flow in the system. For simplicity, the lower unnamed member of the Rustler Formation is combined with the Culebra Dolomite, and the two are modeled as a single unit with properties representative of the Culebra Dolomite. No flow in the direction normal to the horizontal boundary is assumed below the repository in the Castile Formation and above the repository in the Culebra Dolomite. Within the Culebra, the vertical far-field boundary is defined at a constant pressure, reflecting the Culebra's high transmissivity relative to adjacent layers and role as a sink for fluid flow.

2.2 Sampled Variables

The 14 imprecisely-known variables listed in Table 2-1 were used as input to BRAGFLO for the Case 1 uncertainty and sensitivity analyses. As discussed in the Introduction, the distributions indicated in Table 2-1 for the individual variables are characterizing subjective uncertainty. The Case 1 calculations used a Latin hypercube sample (McKay et al., 1979; Iman and Shortencarier, 1984) of size 60 from the 14 variables in Table 2-1. Further, the restrictive pairing technique developed by Iman and Conover (Iman and Conover, 1982; Iman and Davenport, 1982) was used to ensure that the correlations between uncorrelated variables were close to zero and that correlated variables had correlations close to their specified values. The resultant sample is listed in Table 3.1-2 of WIPP PA, 1992.**

**The 1991 performance assessment for the WIPP used a Latin hypercube sample of size 60 from 45 imprecisely known variables (Table B-2, WIPP PA, 1991b; Table 3-1, Helton et al., 1992). The BRAGFLO calculations for Case 1 are the BRAGFLO calculations performed for undisturbed panel behavior in the 1991 WIPP performance assessment. Further, the indicated variable values in Table 3.1-6 of WIPP PA, 1992 are the values obtained in this original sample of size 60 for the 14 variables in Table 2-1.

Table 2-1. Imprecisely Known Variables Used in BRAGFLO in the Estimation of the Behavior of an Undisturbed Waste Panel.

Variable	Definition
BRSAT	Initial liquid (brine) saturation of waste (dimensionless). Range: 0 to 2.76×10^{-1}. Median: 1.38×10^{-1}. Distribution: Uniform. Additional information: Section 3.4.9, WIPP PA, 1991c. Variable 1 in Latin hypercube sample is uniformly distributed on interval [0,1] and used to select value for BRSAT by preprocessor to BRAGFLO.
GRCORH	Scale factor used in definition of gas generation rate for corrosion of steel under humid conditions (dimensionless). Actual gas generation rate is GRCORH•GRCORI. Range: 0 to 5×10^{-1}. Median: 1×10^{-1}. Distribution: Piecewise uniform. Additional information: Memo from Brush, July 8, 1991, contained in Appendix A, WIPP PA, 1991c; Section 3.3.8, WIPP PA, 1991c. Variable 3 in Latin hypercube sample.
GRCORI	Gas generation rate for corrosion of steel under inundated conditions (mol/m^2 surface area steel•s). Range: 0 to 1.3×10^{-8} mol/m^2 s. Median: 6.3×10^{-9} mol/m^2 s. Distribution: Piecewise uniform. Additional information: Same as GRCORH. Variable 4 in Latin hypercube sample.
GRMICH	Scale factor used in definition of gas generation rate due to microbial degradation of cellulosics under humid conditions (dimensionless). Actual gas generation rate is GRMICH•GRMICI. Range: 0 to 2×10^{-1}. Median: 1×10^{-1}. Distribution: Piecewise uniform. Additional information: Same as GRCORH. Variable 5 in Latin hypercube sample.
GRMICI	Gas generation rate due to microbial degradation of cellulosics under inundated conditions (mol/kg cellulosics•s). Range: 0 to 1.6×10^{-8} mol/kg s. Median: 3.2×10^{-9} mol/kg s. Distribution: Piecewise uniform. Additional information: Same as GRCORH. Variable 6 in Latin hypercube sample.
MBPERM	Permeability (k) in anhydrite marker beds in Salado Formation under undisturbed conditions (m^2). Range: 8.5×10^{-21} to 1.8×10^{-18} m^2. Median: 7.8×10^{-20} m^2. Distribution: Piecewise uniform with a 0.8 rank correlation with SALPERM. Additional information: Memo from Beauheim, June 14, 1991, contained in Appendix A, WIPP PA, 1991c; Section 2.4.5, WIPP PA, 1991c. Variable 12 in Latin hypercube sample.
MBPOR	Porosity (ϕ) in anhydrite marker beds in Salado Formation under undisturbed conditions (dimensionless). Range: 1×10^{-3} to 3×10^{-2}. Median: 1×10^{-2}. Distribution: Piecewise uniform. Additional information: Section 2.4.7, WIPP PA, 1991c. Variable 13 in Latin hypercube sample.

Table 2-1. Imprecisely Known Variables Used in BRAGFLO in the Estimation of the Behavior of an Undisturbed Waste Panel (concluded).

Variable	Definition
MBPRES	Pressure (p) in anhydrite Marker Bed 139 under undisturbed conditions (Pa). Pressures at other elevations in the Salado Formation were varied hydrostatically relative to the sampled value for MBPRES. Range: 8.21×10^6 to 1.48×10^7 Pa. Median: 1.28×10^7 Pa. Distribution: Piecewise uniform. Additional information: Memos from Beauheim, June 14, 1991, and Howarth, June 12, 1991, contained in Appendix A, WIPP PA, 1991c; Section 2.4.6, WIPP PA, 1991c. Variable 11 in Latin hypercube sample.
MBTHPRES	Threshold displacement pressure (p_t) in anhydrite marker beds in Salado Formation (Pa). Range: 3×10^3 to 3×10^7 Pa. Median: 3×10^5 Pa. Distribution: Lognormal Additional information: Davies, 1991; memo from Davies, June 2, 1991, contained in Appendix A, WIPP PA, 1991c; Section 2.4.1, WIPP PA, 1991c. Variable 14 in Latin hypercube sample is normally distributed on [0,1] and used to select value for MBTHPRES by preprocessor to BRAGFLO; the actual value used for threshold displacement pressure, p_t, in BRAGFLO is log p_t = log (5.6×10^{-7}) - 0.346 log (MBPERM) + (4•MBTHPRES-2).
SALPERM	Permeability (k) in halite component of Salado Formation (m^2). Range: 2.0×10^{-22} to 1.4×10^{-19} m^2. Median: 5.7×10^{-21} m^2. Distribution: Piecewise uniform. Additional information: Memo from Beauheim, June 14, 1991, contained in Appendix A, WIPP PA, 1991c; Section 2.3.5, WIPP PA, 1991c. Variable 10 in Latin hypercube sample.
STOICCOR	Stoichiometric factor for corrosion of steel (dimensionless). Defines proportion of two different chemical reactions that take place during the corrosion process. Range: 0 to 1. Median: 5×10^{-1}. Distribution: Uniform. Additional information: Brush and Anderson in Lappin et al., 1989, p. A-6; Section 3.3.8, WIPP PA, 1991c. Variable 2 in Latin hypercube sample.
STOICMIC	Stoichiometric coefficient for microbial degradation of cellulosics (mol gas/mol CH_2O). Range: 0 to 1.67 mol/mol. Median: 8.35×10^{-1} mol/mol. Distribution: Uniform. Additional information: Brush and Anderson in Lappin et al., 1989, p. A-10; Section 3.3.9, WIPP PA, 1991c. Variable 9 in Latin hypercube sample.
VMETAL	Fraction of total waste volume that is occupied by IDB (Integrated Data Base) metals and glass waste category (dimensionless). Range: 2.76×10^{-1} to 4.76×10^{-1}. Median: 3.76×10^{-1}. Distribution: Normal. Additional information: Section 3.4.1, WIPP PA, 1991c. Variable 7 in Latin hypercube sample.
VWOOD	Fraction of total waste volume that is occupied by IDB combustible waste category (dimensionless). Range: 2.84×10^{-1} to 4.84×10^{-1}. Median: 3.84×10^{-1}. Distribution: Normal. Additional information: Section 3.4.1, WIPP PA, 1991c. Variable 8 in Latin hypercube sample.

The version of BRAGFLO used in the 1991 WIPP performance assessment did not include a model for the competing effects of creep closure of a waste panel and the resistance to and possible reversal of this process due to waste generated gas. As a compromise, the pore volume in a waste panel was initially set to the volume necessary to contain all the waste-generated gas that could be produced from the initial inventory of steel and cellulosics at lithostatic pressure (i.e., 14.9 MPa). As a result, initial pore volume was a function of STOICCOR (stoichiometric factor for corrosion of steel), STOICMIC (stoichiometric coefficient for microbial degradation of cellulosics), VMETAL (fraction of total waste volume occupied by IDB metals and glass waste category) and VWOOD (fraction of total waste volume occupied by IDB combustible waste category). This procedure resulted in a pore volume that was approximately equal to the pore volume of an uncompacted waste panel (i.e., at the time of repository closure) but was approximately five times the estimated pore volume of a waste panel for compaction at lithostatic pressure with no gas-related resistance. Additional discussion is provided in Section 3.4.8 of WIPP PA, 1991c.

One BRAGFLO calculation was performed for each of the 60 sample elements generated from the variables listed in Table 2-1. Thus, a total of 60 BRAGFLO calculations are available for analysis. The remainder of this chapter is devoted to an exploration of the resultant mapping from BRAGFLO input to BRAGFLO predictions.

In addition to the 14 sampled variables listed in Table 2-1, the calculations for Case 1 also required values for a number of additional variables that were fixed at their best-estimate values. These variables and their values are listed in Tables 3.1-1a and 3.1-1b of WIPP PA, 1992. Further, additional discussion of the BRAGFLO input for Case 1 is available in Section 3.1 of WIPP PA, 1992.

2.3 Uncertainty and Sensitivity Analysis Results

Given that gas migration into the marker beds (i.e., anhydrite layers) in the Salado Formation is the outcome of greatest interest for Case 1, a natural starting point is an exploration of gas generation. Gas generation has two sources: corrosion of steel and microbial degradation of cellulosics. Further, each of these gas-generating processes can take place under either inundated or humid conditions. Results relating to gas generation are presented in Sections 2.3.1, 2.3.2 and 2.3.3. Then, gas saturation and gas pressure in a waste panel are investigated in Section 2.3.4. Finally, lateral gas migration in the anhydrite marker beds is investigated in Section 2.3.5.

2.3.1 Gas Generation Due to Corrosion

A summary of the results for gas generation due to corrosion is given in Figure 2-4. The two upper frames in Figure 2-4 show cumulative gas generation as a function of time due to corrosion under humid conditions (upper left frame) and corrosion under inundated conditions (upper right frame). Each curve in the upper two frames results from a single Latin hypercube sample element (i.e., each frame has 60 curves, one for each sample element). Overall, the range of gas production under humid conditions is similar to the range of gas production under inundated conditions, although the largest gas production curves occur for inundated conditions.

Formal sensitivity analysis techniques based on partial rank correlation (Helton et al., 1991; Helton, 1992) can be used to investigate the variation in cumulative gas production shown in the upper two frames of Figure 2-4. Specifically, the lower two frames in Figure 2-4 show time-dependent plots of partial rank correlation coefficients between cumulative gas production and individual variables from Table 2-1. These coefficients were calculated on the basis of vertical slices through the cumulative gas production curves. Figure 2-4 and other similar figures in this presentation show the partial rank correlation curves for all sampled variables that had a partial rank correlation coefficient whose absolute value exceeded 0.5 for the particular dependent variable under consideration and were generated with the PCCSRC program (Iman et al., 1985). As a reminder, a positive rank correlation coefficient indicates that two variables tend to increase and decrease together, and a negative rank correlation coefficient indicates that, as one variable increases, the other tends to decrease.

As shown by the partial correlation results in the lower left frame of Figure 2-4, cumulative gas production due to corrosion under humid conditions tends to increase as GRCORH (scale factor used in definition of gas-generation rate for corrosion of steel under humid conditions) and GRCORI (gas-generation rate for corrosion of steel under inundated conditions) increase. The positive effects for GRCORH and GRCORI result because the actual gas-generation rate due to corrosion under humid conditions is defined by GRCORH•GRCORI. Thus, increasing each of these variables increases the rate at which gas is generated under humid conditions.

Cumulative Gas Production Due to Corrosion of Steel

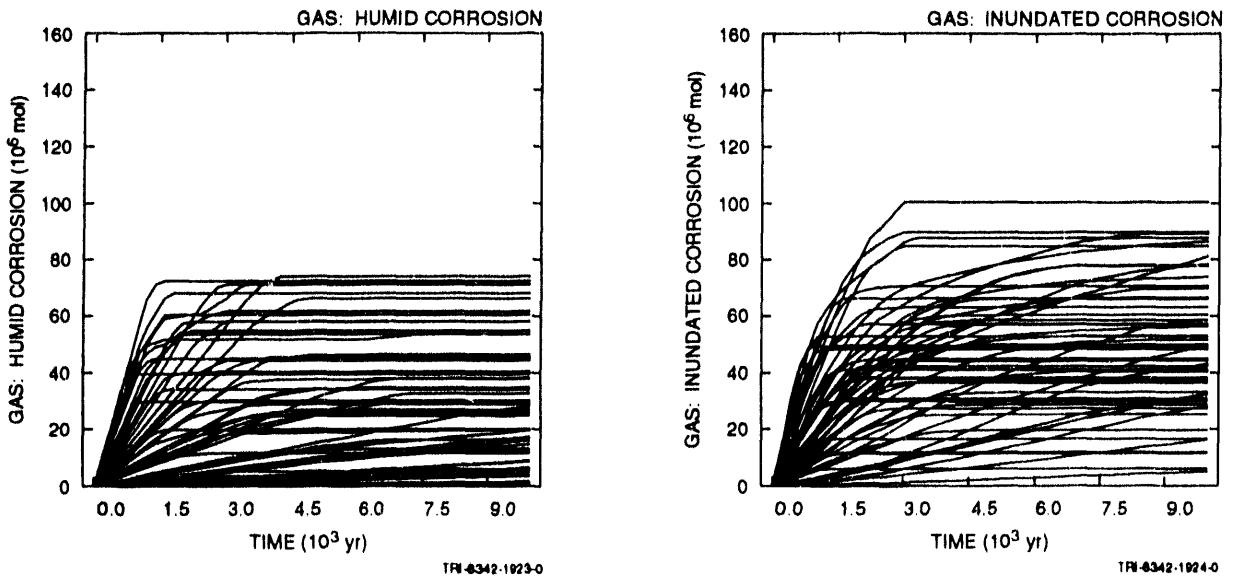

Partial Rank Correlation Coefficients for Cumulative Gas Production Due to Corrosion of Steel

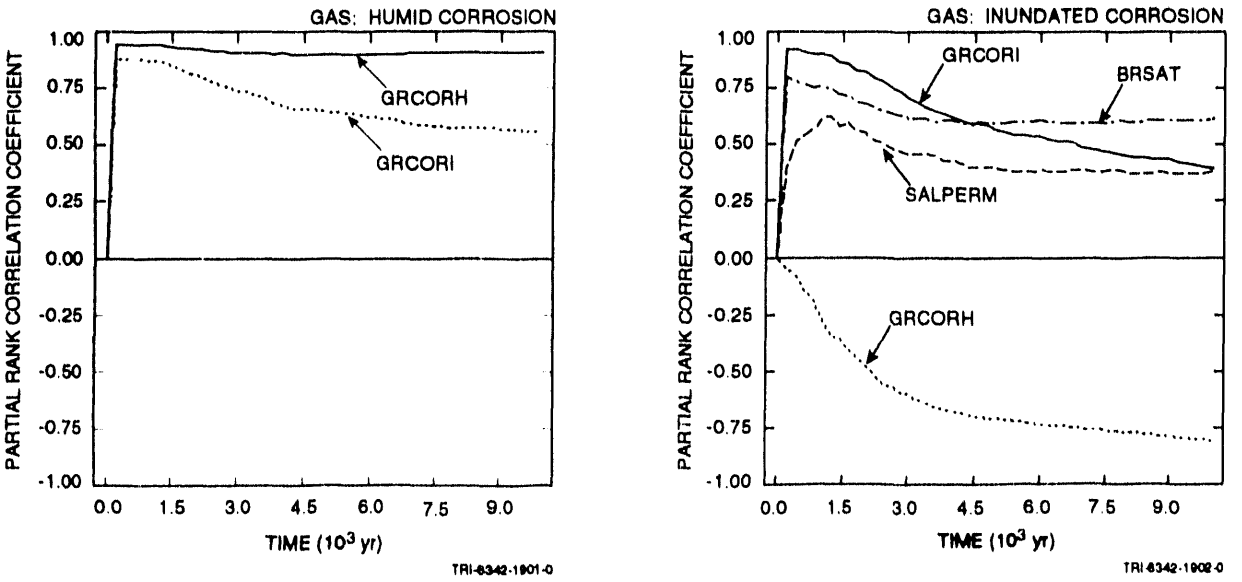

Figure 2-4. Uncertainty and sensitivity analysis results for gas generation due to corrosion of steel.

As shown by the partial correlation results in the lower right frame of Figure 2-4, cumulative gas production due to corrosion under inundated conditions tends to increase as GRCORI (gas-generation rate for corrosion of steel under inundated conditions), BRSAT (initial brine saturation of waste) and SALPERM (Salado halite permeability) increase and tends to decrease as GRCORH (scale factor used in definition of gas-generation rate for corrosion of steel under humid conditions) increases. The positive effects for GRCORI, BRSAT and SALPERM result because increasing GRCORI increases the rate at which gas is generated by corrosion under inundated conditions and increasing BRSAT and SALPERM increases the amount of steel that will be consumed by corrosion under inundated conditions. The importance of GRCORI decreases with time because, although GRCORI determines the rate at which gas is generated, it does not determine the total amount of gas that is generated. The negative effect for GRCORH results because the increased consumption of steel and brine by corrosion under humid conditions reduces the amount of gas that can be produced by the corrosion of steel under inundated conditions.

Stepwise regression analysis (Helton et al., 1991; Helton, 1992) can also be used to analyze the cumulative gas production results shown in Figure 2-4. As an example, the two regression analyses shown in Table 2-2 are for cumulative gas production over 10,000 yr due to corrosion under humid and inundated conditions, respectively. Thus, these two regression analyses are for the gas production values appearing above 10,000 yr in the two upper frames of Figure 2-4.

These analyses and other similar analyses in this report were performed with the STEPWISE program (Iman et al., 1980). A variable was required to be significant at the 0.02 α-level to enter a regression model and to remain significant at the 0.05 α-level to be retained in a regression model (Draper and Smith, 1981). A considerable amount of discretion was used in the selection of the stopping points for the individual regression analyses and took into account behavior of R^2-values, α-values, the PRESS criterion (Allen, 1971), scatterplots, and the entry of apparently spurious variables into the regression model. The analyses were tried with both raw (i.e., untransformed) data and rank-transformed (Iman and Conover, 1979) data. The regression analyses with rank-transformed variables typically yielded regression models with higher R^2 values and more reasonable variable selections than the regression analyses with raw data. Therefore, all the regression analyses presented in this report were performed with rank-transformed data.

The regression analysis in Table 2-2 for gas production under humid conditions indicates positive effects (i.e., positive regression coefficients) for GRCORH (scale factor used in definition of gas-generation

Table 2-2. Stepwise Regression Analyses with Rank-Transformed Data for Cumulative Gas Production over 10,000 yr Due to Corrosion under Humid and Inundated Conditions.

Total Gas Production over 10,000 yr (Humid Corrosion)				Total Gas Production over 10,000 yr (Inundated Corrosion)			
Step[a]	Variable[b]	SRC[c]	R^{2d}	Step[a]	Variable[b]	SRC[c]	R^{2d}
1	GRCORH	0.81	0.70	1	GRCORH	-0.66	0.40
2	GRCORI	0.27	0.76	2	BRSAT	0.37	0.52
3	SALPERM	-0.21	0.80	3	SALPERM	0.31	0.63
4	BRSAT	-0.18	0.83	4	GRCORI	0.21	0.67

[a] Steps in stepwise regression analysis
[b] Variables listed in order of selection in regression analysis
[c] Standardized regression coefficients in final regression model
[d] Cumulative R^2 value with entry of each variable into regression model

rate for corrosion of steel under humid conditions) and GRCORI (gas-generation rate for corrosion of steel under inundated conditions) and negative effects (i.e., negative regression coefficients) for SALPERM (Salado halite permeability) and BRSAT (initial brine saturation of waste). As indicated earlier, the positive effects for GRCORH and GRCORI result because the gas-generation rate for the corrosion of steel under humid conditions is GRCORH•GRCORI. The negative effects for SALPERM and BRSAT result from increasing the amount of steel corroded under inundated conditions and thus decreasing the amount of steel available for corrosion under humid conditions. The scale factor GRCORH is the most important variable and accounts for 70% (i.e., $R^2 = 0.70$) of the variability in gas generation due to corrosion under humid conditions. Further, GRCORI, SALPERM and BRSAT collectively account for an additional 13% of the variability (i.e., 83% - 70% = 13%).

The regression analysis in Table 2-2 for gas production under inundated conditions indicates positive effects for BRSAT (initial brine saturation of waste), SALPERM (Salado halite permeability) and GRCORI (gas-generation rate for corrosion of steel under inundated conditions) and a negative effect for GRCORH (scale factor used in definition of gas-generation rate for corrosion of steel under humid conditions). These effects result because increasing BRSAT and SALPERM increases the amount of steel exposed to corrosion under inundated conditions, increasing GRCORI increases the gas-generation rate under inundated conditions, and increasing GRCORH decreases the amount of steel available for corrosion under inundated conditions. The scale factor GRCORH is the most important variable and accounts for 40% of the variability in gas generation due to

corrosion under inundated conditions. Further, BRSAT, SALPERM and GRCORI collectively account for an additional 27% of the variability.

The variables GRCORI (gas-generation rate for corrosion of steel under inundated conditions) and GRCORH (scale factor used in definition of gas-generation rate for corrosion of steel under humid conditions) are used in the product GRCORH•GRCORI to define the gas-generation rate for the corrosion of steel under humid conditions. As a result, GRCORH•GRCORI is a natural candidate variable for inclusion in a stepwise regression analysis for gas production due to corrosion under humid conditions. As shown in Table 2-3, this inclusion results in GRCORH•GRCORI being the first variable selected in a stepwise regression analysis for total gas production over 10,000 yr due to corrosion under humid conditions, with 77% of the variability being accounted for. For comparison, the regression results summarized in Table 2-2 indicate that GRCORH by itself can account for 70% of the variability and that GRCORH and GRCORI together can account for 76% of the variability. As the stepwise regression analysis presented in Table 2-3 continues, GRCORI is picked in the third regression model (i.e., at step 3). However, unlike the results shown in Table 2-2 for gas generation under humid conditions, GRCORI now has a negative rather than a positive regression coefficient; also, the regression coefficient for

Table 2-3. Stepwise Regression Models with Rank-Transformed Data for Cumulative Gas Production over 10,000 yr Due to Corrosion under Humid Conditions. Four regression models were constructed; standardized regression coefficients and R^2 values are given for each of these models.

Variable[a]	Model 1: SRC[b]	Model 2: SRC	Model 3: SRC	Model 4: SRC
GRCORH•GRCORI	0.87	0.89	1.02	1.01
SALPERM	--	-0.25	-0.25	-0.25
GRCORI	--	--	-0.23	-0.23
BRSAT	--	--	--	-0.14
R^2 Value[c]	0.77	0.83	0.86	0.88

[a]Variables selected in regression models.
[b]Standardized regression coefficients for variables in model. Model i designates the ith model constructed in the stepwise regression analysis for i = 1,2,3,4 (i.e., the model constructed at step i).
[c]R^2 value for regression model.

GRCORH•GRCORI jumps from 0.89 to 1.02. This behavior results from the fact that GRCORH•GRCORI and GRCORI are correlated and hence are being played-off against each other in the regression analysis obtained at the third step of the stepwise regression analysis presented in Table 2-3. The final regression models presented in Tables 2-2 and 2-3 involve the same underlying variables (i.e., GRCORH, GRCORI, SALPERM, BRSAT) and can account for 83% and 88%, respectively, of the gas production under humid conditions. Thus, inclusion of GRCORH•GRCORI in the analysis results in a regression model that can account for somewhat more of the variability in gas production; at the same time, the interpretation of the analysis is made more difficult by the resultant instability in the regression coefficients for GRCORH•GRCORI and GRCORI (i.e., the regression coefficient for each variable depends on whether or not the other variable is in the regression model).

2.3.2 Gas Generation Due to Microbial Degradation

A summary of the analysis results for gas generation due to microbial degradation is given in Figure 2-5. The upper two frames in Figure 2-5 show cumulative gas generation due to microbial degradation under humid and inundated conditions, respectively. As comparison with the corresponding plots in Figure 2-4 shows, gas generation due to microbial degradation is approximately 50% or less of the gas generation due to corrosion. The range of cumulative gas generation shown in Figure 2-5 is slightly larger for inundated than for humid conditions.

The lower two frames in Figure 2-5 present sensitivity analysis results based on partial rank correlation coefficients as in Figure 2-4. For cumulative gas production under humid conditions, increasing each of STOICMIC (stoichiometric coefficient for microbial degradation of cellulosics), GRMICH (scale factor used in definition of gas-generation rate due to microbial degradation of cellulosics under humid conditions) and GRMICI (gas-generation rate due to microbial degradation of cellulosics under inundated conditions) increases gas production and increasing BRSAT (initial brine saturation) decreases gas production. Increasing STOICMIC increases the amount of gas produced per unit of cellulose consumed while increasing GRMICH and GRMICI increases the rate GRMIC•GRMIC of microbial degradation. Increasing BRSAT decreases the amount of gas produced under humid conditions by increasing the amount of cellulosics that will be consumed under inundated conditions. The importance of GRMICI decreases over time as the inventory is depleted. For cumulative gas production under inundated conditions, increasing each of STOICMIC, BRSAT, GRMICI and SALPERM (Salado halite permeability) increases gas production. The positive effects for BRSAT and SALPERM result from increasing the amount of cellulosics that will be consumed under inundated conditions.

Cumulative Gas Production Due to Microbial Degradation of Cellulosics

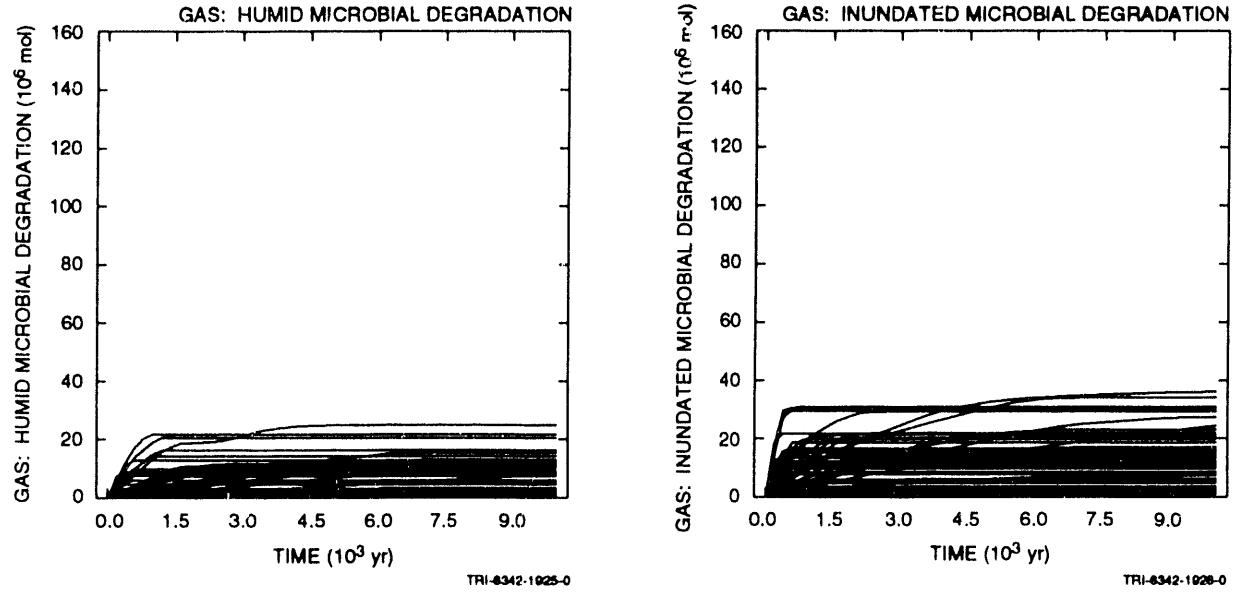

Partial Rank Correlation Coefficients for Cumulative Gas Production Due to Microbial Degradation of Cellulosics

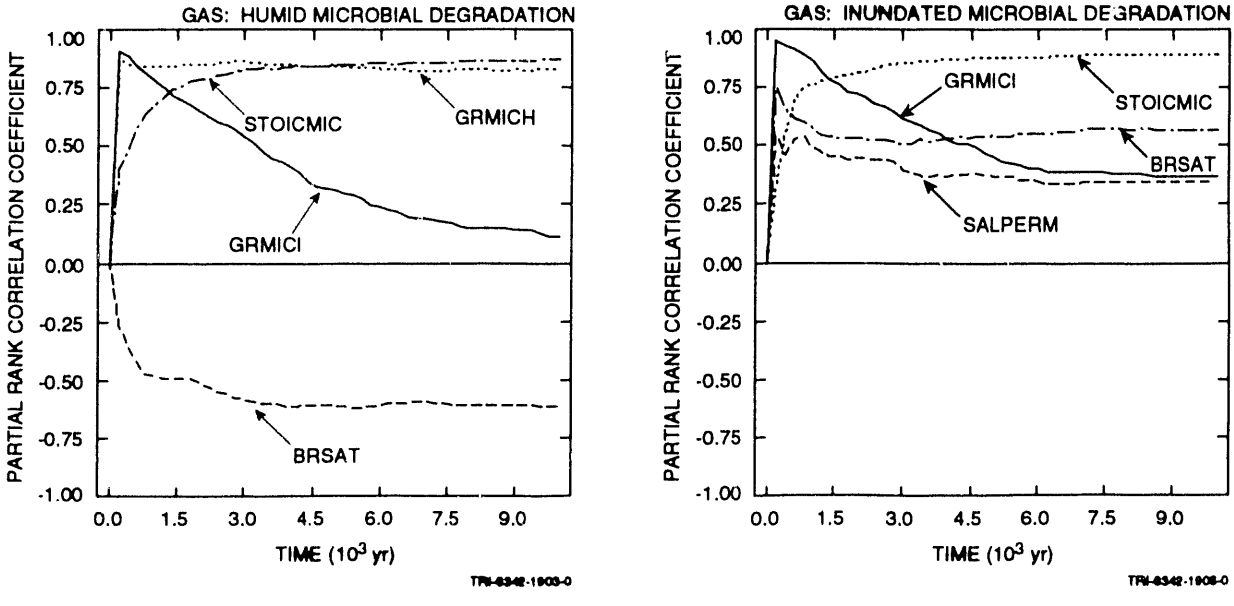

Figure 2-5. Uncertainty and sensitivity analysis results for gas generation due to microbial degradation of cellulosics under humid and inundated conditions.

The two regression analyses in Table 2-4 are for cumulative gas production over 10,000 yr due to microbial degrada ion under humid and inundated conditions, respectively. Thus, these tw regression analyses are for the gas-production values appearing above 10,000 yr in the two upper frames of Figure 2-5. For gas production under humid conditions, the variables STOICMIC (stoichiometric coefficient for microbial degradation of cellulosics), GRMICH (scale factor used in definition of gas-generation rate due to microbial degradation of cellulosics under humid conditions) and BRSAT (initial brine saturation) can account for 81% of the observed variability in gas production, with gas production tending to increase with increasing values for STOICMIC and GRMICH and tending to decrease with increasing values for BRSAT. For gas production under inundated conditions, the variables STOICMIC and BRSAT can account for 71% of the observed variability in gas production, with gas production tending to increase as each of these variables increases. When the three additional variables SALPERM (Salado halite permeability), GRMICI and VWOOD (fraction of total waste volume that is occupied by IDB combustible waste category) are added to the regression model, 81% of the variability in gas production can be accounted for, with gas production again tending to increase as each of these variables increases. The positive effects for SALPERM and VWOOD result because increasing SALPERM increases the amount of brine flowing into a waste panel and thus increases the amount of gas generation that will take place under inundated conditions and increasing VWOOD increases the amount of cellulosics available for microbial degradation.

2.3.3 Total Gas Production

The upper two frames in Figure 2-6 show total gas production due to corrosion and microbial degradation and were obtained by combining the corresponding results in Figures 2-4 and 2-5 for gas production under humid and inundated conditions. Typically, low gas production under humid conditions is associated with higher gas production under inundated conditions and vice versa. As a result, the gas-production curves in Figure 2-6 tend to lie farther above the abscissa than many of the individual curves in Figures 2-4 and 2-5. Overall, the gas production due to corrosion tends to be at least twice the gas production due to microbial degradation. Gas production due to microbial degradation has more curves close to zero than gas production due to corrosion because STOICMIC (stoichiometric coefficient for microbial degradation of cellulosics) was assigned a range of possible values that extends to zero, which results in no gas generation due to microbial degradation.

The lower two frames in Figure 2-6 present sensitivity analysis results based on partial rank correlation coefficients as in Figure 2-4. For cumulative gas production due to corrosion, increasing each of GRCORI

Table 2-4. Stepwise Regression Analyses with Rank-Transformed Data for Cumulative Gas Production over 10,000 yr Due to Microbial Degradation under Humid and Inundated Conditions.

Total Gas Production over 10,000 yr (Humid Degradation)				Total Gas Production over 10,000 yr (Inundated Degradation)			
Step[a]	Variable[b]	SRC[c]	R^{2d}	Step[a]	Variable[b]	SRC[c]	R^{2d}
1	STOICMIC	0.66	0.43	1	STOICMIC	0.79	0.65
2	GRMICH	0.55	0.73	2	BRSAT	0.27	0.71
3	BRSAT	-0.29	0.81	3	SALPERM	0.22	0.76
				4	GRMICI	0.16	0.79
				5	VWOOD	0.15	0.81

[a] Steps in stepwise regression analysis
[b] Variables listed in order of selection in regression analysis
[c] Standardized regression coefficients in final regression model
[d] Cumulative R^2 value with entry of each variable into regression model

(gas-generation rate for corrosion of steel under inundated conditions), GRCORH (scale factor used in definition of gas-generation rate for corrosion of steel under humid conditions) and BRSAT (initial brine saturation) tends to increase gas production and increasing STOICCOR (stoichiometric factor for corrosion of steel) tends to decrease gas production. Increasing GRCORI, GRCORH and BRSAT tends to increase the rate of gas production and hence cumulative gas production, with this effect becoming less important at later times due to exhaustion of either steel or brine in the waste panel. The negative effect for STOICCOR results because increasing STOICCOR increases the proportion of low-gas-producing reactions in the corrosion process. For cumulative gas production due to microbial degradation, GRMICI (gas-generation rate due to microbial degradation of cellulosics under inundated conditions) and BRSAT (initial brine saturation) have positive effects at early times and then decrease in importance. In contrast, STOICMIC (stoichiometric coefficient for microbial degradation of cellulosics) has an increasingly important positive effect with time and ultimately dominates the variability in cumulative gas production.

The two regression analyses in Table 2-5 are for cumulative gas production over 10,000 yr due to corrosion and microbial degradation, respectively. Thus, these two regression analyses are for the gas production values appearing above 10,000 yr in the two upper frames of Figure 2-6. The regression analysis for gas production due to corrosion selected the variables STOICCOR (stoichiometric factor for corrosion of

Cumulative Gas Production

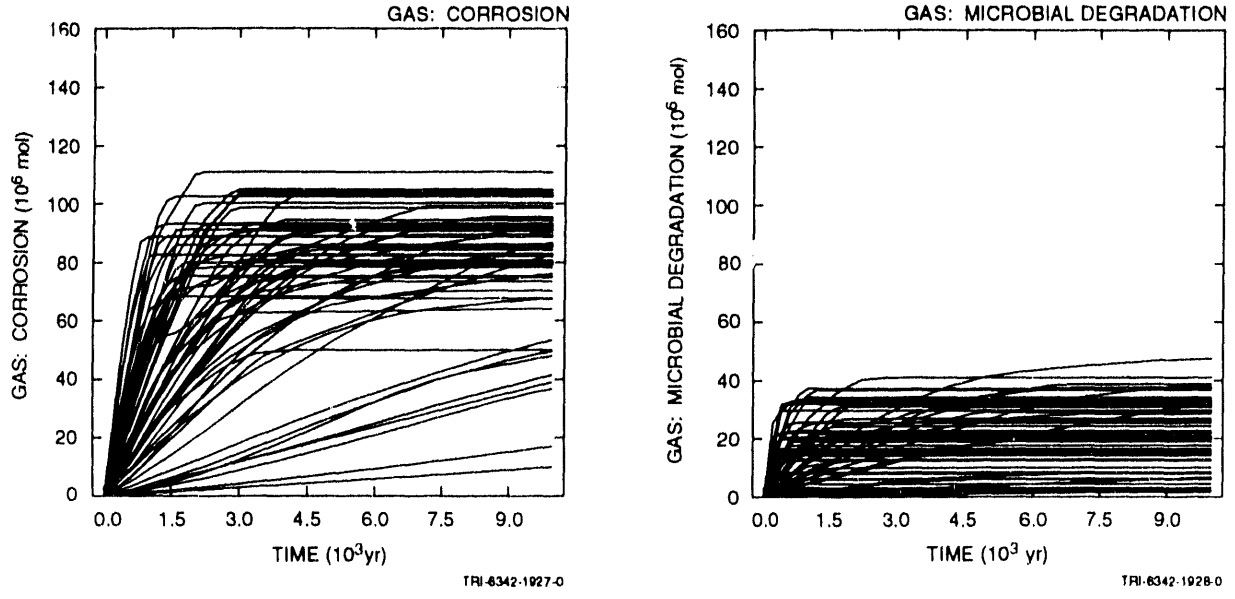

Partial Rank Correlation Coefficients for Cumulative Gas Production

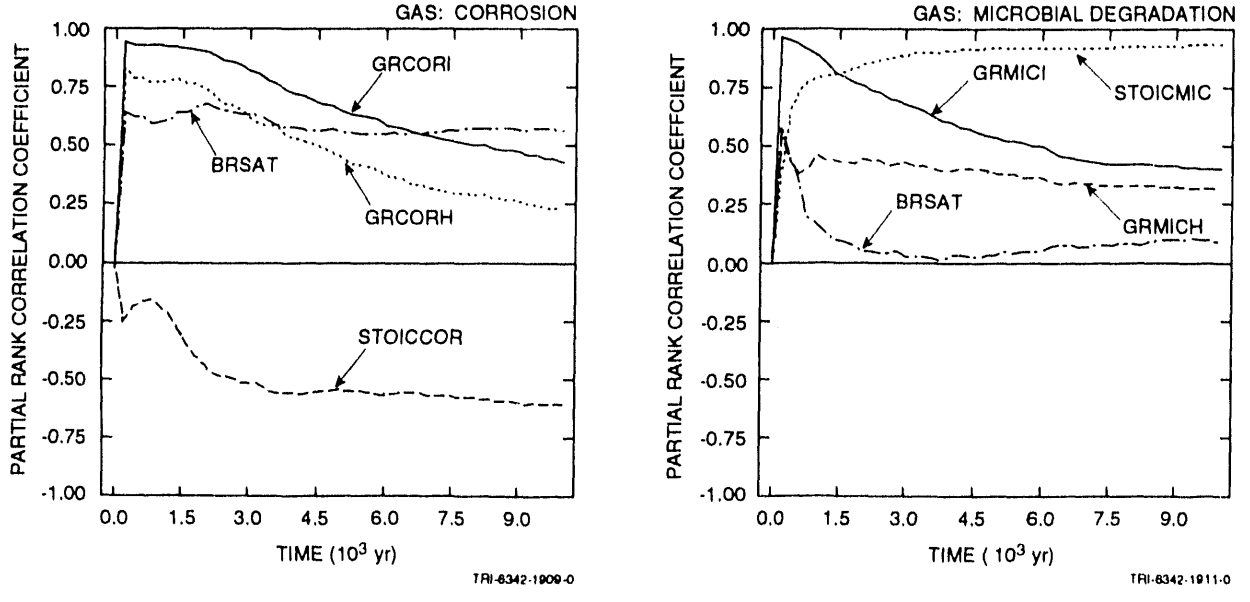

Figure 2-6. Uncertainty and sensitivity analysis results for gas generation due to corrosion of steel and microbial degradation of cellulosics.

Table 2-5. Stepwise Regression Analysis with Rank-Transformed Data for Total Gas Production Due to Corrosion and Total Gas Generation Due to Microbial Degradation.

Total Gas Production over 10,000 yr (Corrosion)				Total Gas Production over 10,000 yr (Microbial Degradation)			
Step[a]	Variable[b]	SRC[c]	R^{2d}	Step[a]	Variable[b]	SRC[c]	R^{2d}
1	STOICCOR	-0.48	0.21	1	STOICMIC	0.89	0.79
2	BRSAT	0.43	0.38	2	VWOOD	0.17	0.82
3	GRCORI	0.31	0.48	3	GRMICI	0.14	0.84
4	VMETAL	0.24	0.53				
5	MBPRES	0.21	0.58				

[a] Steps in stepwise regression analysis
[b] Variables listed in order of selection in regression analysis
[c] Standardized regression coefficients in final regression model
[d] Cumulative R^2 value with entry of each variable into regression model

steel), BRSAT (initial brine saturation), GRCORI (gas-generation rate for corrosion of steel under inundated conditions), VMETAL (fraction of total waste volume that is occupied by IDB metals and glass waste category) and MBPRES (pressure in Marker Bed 139 under undisturbed conditions), with STOICCOR having a negative effect on gas production and BRSAT, GRCORI, VMETAL and MBRPES having positive effects on gas production. However, the resolution in the regression model is low, with all five variables accounting for only 58% of the variability in gas production due to corrosion. This low resolution probably results from noise introduced into the analysis by sample elements in which the corrosion process stops in individual computational cells before 10,000 yr due to the depletion of brine.

To provide additional insight, Figure 2-7 presents selected scatterplots displaying the relationships between individual sampled variables and total gas production over 10,000 yr due to corrosion. As examination of the upper two frames shows, gas production tends to decrease as STOICCOR (stoichiometric factor for corrosion of steel) increases and tends to increase as BRSAT (initial brine saturation) increases. However, there is a large amount of variability around these trends. These patterns are consistent with the signs of the regression coefficients and low R^2 values in Table 2-5. The scatterplots for STOICCOR and BRSAT are particularly diffuse due to the almost random appearance of gas-production values of less than 6×10^7 m^3 over their ranges. As examination of the scatterplot for GRCORI (gas-generation rate for corrosion of steel under inundated conditions) in the lower left frame of Figure 2-7 shows, these

small gas production values tend to be associated with small values of GRCORI. Total gas production increases almost linearly with GRCORI until a value of 2×10^{-9} mol/m^{2}s is reached, after which there appears to be no relationship between GRCORI and total gas production. The scatterplot for SALPERM (Salado halite permeability) in the lower right frame of Figure 2-7 shows an interesting pattern, with there being wide variability in the total gas production associated with values of SALPERM less than 1.5×10^{-20} m^2 and a substantially reduced amount of variability for values of SALPERM greater than 1.5×10^{-20} m^2. The superposition of the effects of GRCORI and SALPERM on the effects of STOICCOR and BRSAT results in a pattern of relationships that cannot be easily captured by a simple regression model.

The regression analysis in Table 2-5 for gas production due to microbial degradation is considerably more successful in accounting for the observed variability in gas production than is the corresponding regression analysis for gas production due to corrosion. In particular, STOICMIC (stoichiometric coefficient for microbial degradation of cellulosics) was found to account for 79% of the observed variability and small additional effects were indicated for VWOOD (fraction of total waste volume occupied by IDB combustible waste category) and GRMICI (gas-generation rate due to microbial degradation of cellulosics under inundated conditions). The regression model with STOICMIC, VWOOD and GRMICI was able to account for 84% of the variability in gas production due to microbial degradation of cellulosics.

The cumulative gas production due to corrosion and to microbial degradation can be combined to produce total gas production, as shown in the upper frame of Figure 2-8. Most sample elements result in a total gas production over 10,000 yr between 5×10^7 mol and 1.2×10^8 mol. Also, most sample elements show a period of rapid gas production in the first few thousand years, with considerably reduced rates of gas production at later times. As examination of the two upper frames in Figure 2-9 shows, the inventory of steel and cellulosics is often exhausted or significantly depleted after the first few thousand years.

The lower frame in Figure 2-8 presents sensitivity analysis results based on partial rank correlation coefficients. At early times, total gas production is dominated by GRCORI (gas-generation rate for corrosion of steel under inundated conditions), GRCORH (scale factor used in definition of gas-generation rate for corrosion of steel under humid conditions), GRMICI (gas-generation rate for microbial degradation of cellulosics under

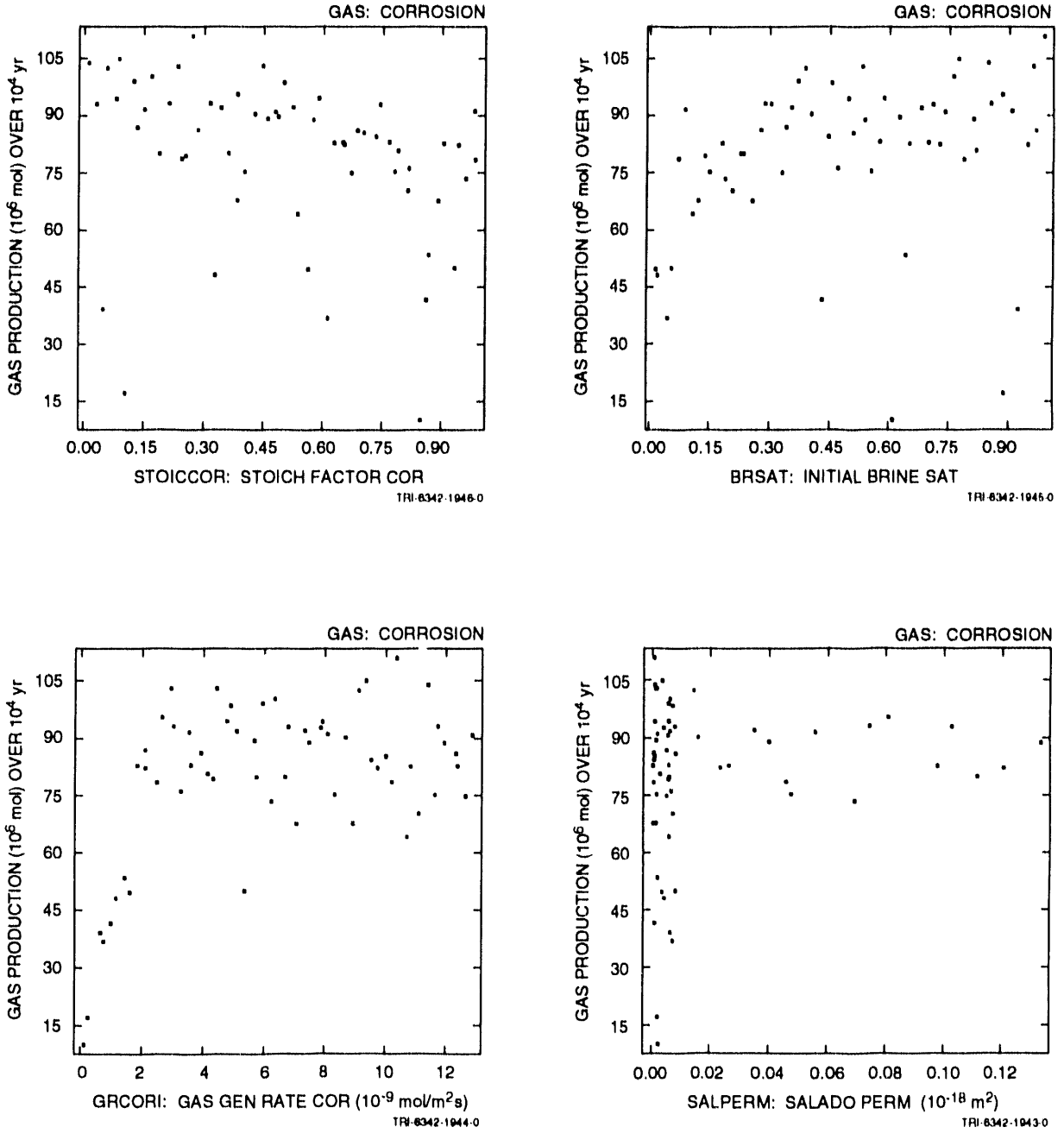

Figure 2-7. Scatterplots relating cumulative gas production over 10,000 yr due to corrosion to STOICCOR (stoichiometric factor for corrosion of steel), BRSAT (initial brine saturation), GRCORI (gas generation rate due to corrosion of steel under inundated conditions) and SALPERM (Salado halite permeability).

Cumulative Gas Production

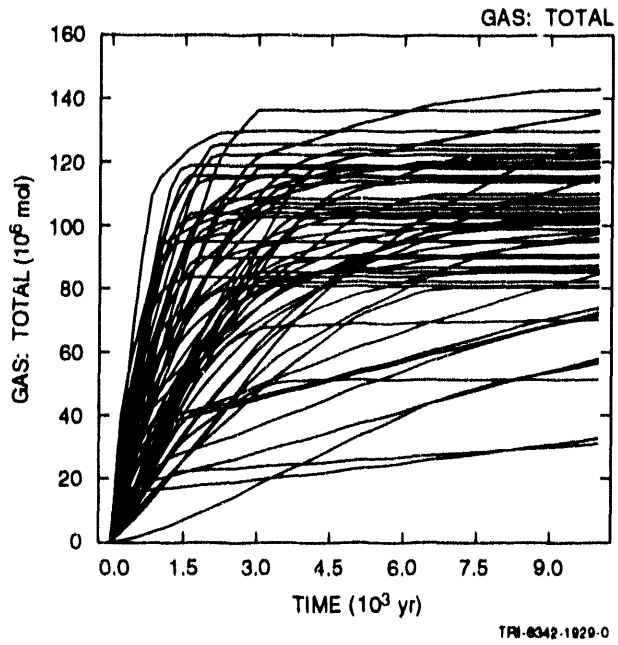

Partial Rank Correlation Coefficients for Cumulative Gas Production

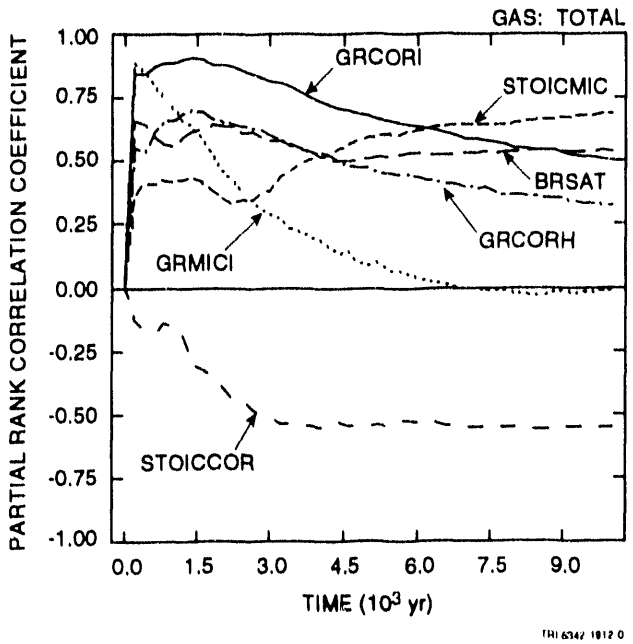

Figure 2-8. Uncertainty and sensitivity analysis results for total gas production (i.e., both corrosion of steel and microbial degradation of cellulosics).

Steel and Cellulosic Inventories

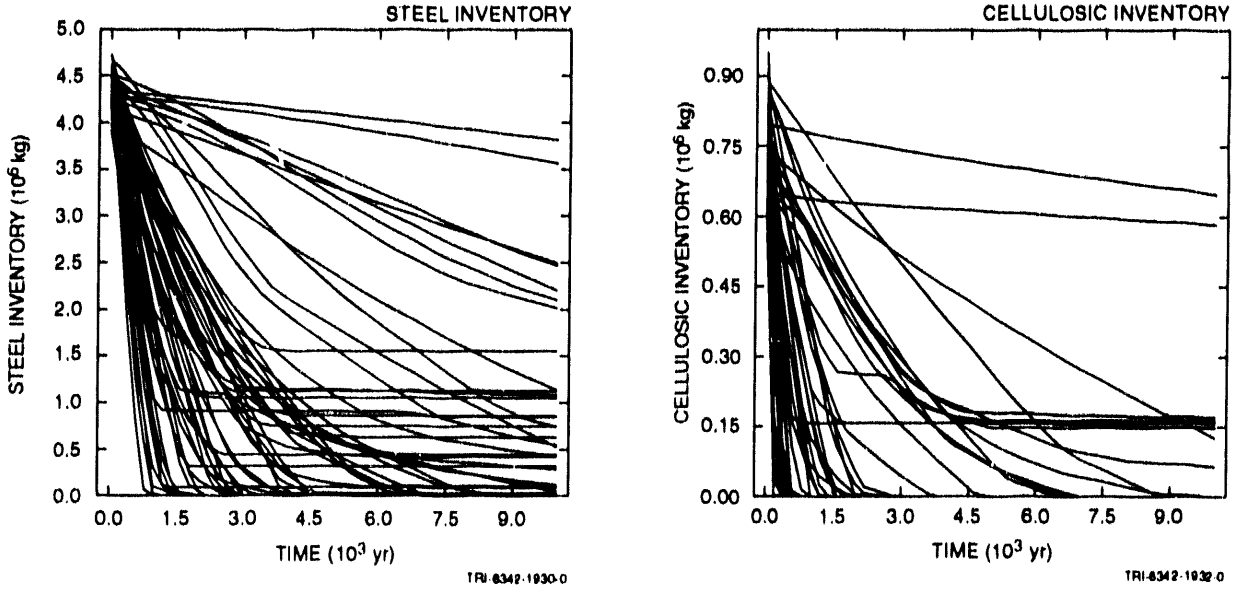

Partial Rank Correlation Coefficients for Steel and Cellulosic Inventories

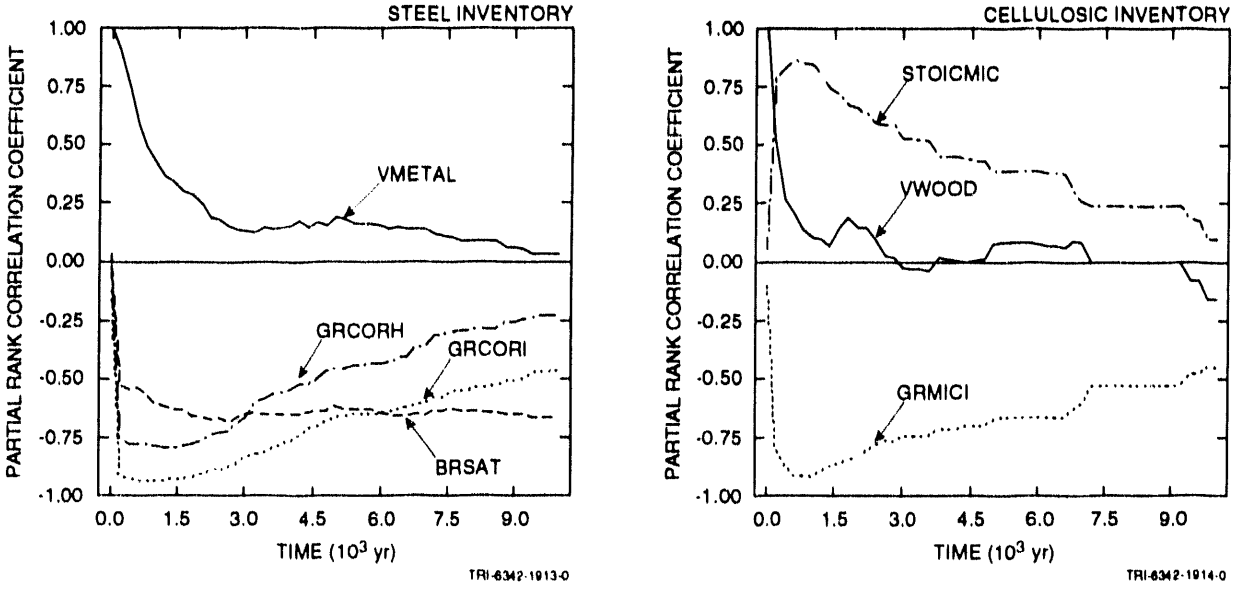

Figure 2-9. Uncertainty and sensitivity analysis results for steel and cellulosic inventories in waste panel.

inundated conditions) and BRSAT (initial brine saturation), with total gas generation tending to increase as each of these variables increases. As time increases, GRMICI, GRCORH and GRCORI become less important. In contrast, STOICMIC (stoichiometric coefficient for microbial degradation of cellulosics) and STOICCOR (stoichiometric factor for corrosion of steel) are unimportant at early times but are the dominant variables influencing gas production at later times, with gas production tending to increase as STOICMIC increases and tending to decrease as STOICCOR increases.

The regression analysis in Table 2-6 is for cumulative gas production over 10,000 yr due to both corrosion and microbial degradation. The first variable selected in the analysis is STOICMIC (stoichiometric coefficient for microbial degradation of cellulosics), which has a positive regression coefficient and can account for 27% of the variability in total gas production. The indicated effect for STOICMIC is consistent with its dominant influence on gas generation due to microbial degradation as indicated in Figure 2-6 and Table 2-5. The next variable selected in the regression analysis is STOICCOR (stoichiometric factor for corrosion of steel), with gas production tending to decrease as STOICOR increases. The selection of STOICMIC and STOICCOR as the first two variables in the stepwise regression analysis is consistent with the effects indicated for them in the partial correlation analysis in Figure 2-8 for total gas production. After STOICMIC and STOICCOR, the regression analysis selects GRCORI (gas-generation rate for corrosion of steel under inundated conditions) and BRSAT (initial brine saturation). The positive regression coefficients for GRCORI and BRSAT and the negative regression coefficient for STOICCOR are consistent with the effects of these variables on gas generation due to corrosion already seen in Figures 2-6 and 2-7 and Table 2-2. Collectively, STOICMIC, STOICCOR, BRSAT and GRCORI can account for 59% of the variability in total gas production over 10,000 yr. As shown by the scatterplots in Figure 2-10, no single variable identified in the regression analysis in Table 2-6 (i.e., STOICMIC, STOICCOR, BRSAT and GRCORI) plays a dominant role in the determination of cumulative gas production over 10,000 yr due to both corrosion and microbial degradation.

As previously indicated, the upper two frames in Figure 2-9 show the time-dependent steel and cellulosic inventories associated with the individual sample elements. The lower two frames present sensitivity analyses based on partial rank correlation coefficients. The steel inventory is initially dominated by VMETAL (fraction of total waste volume occupied by IDB metals and glass category), with the importance of this variable decreasing with time. The variables GRCORI (gas-generation rate for corrosion of steel under inundated conditions), GRCORH (scale factor

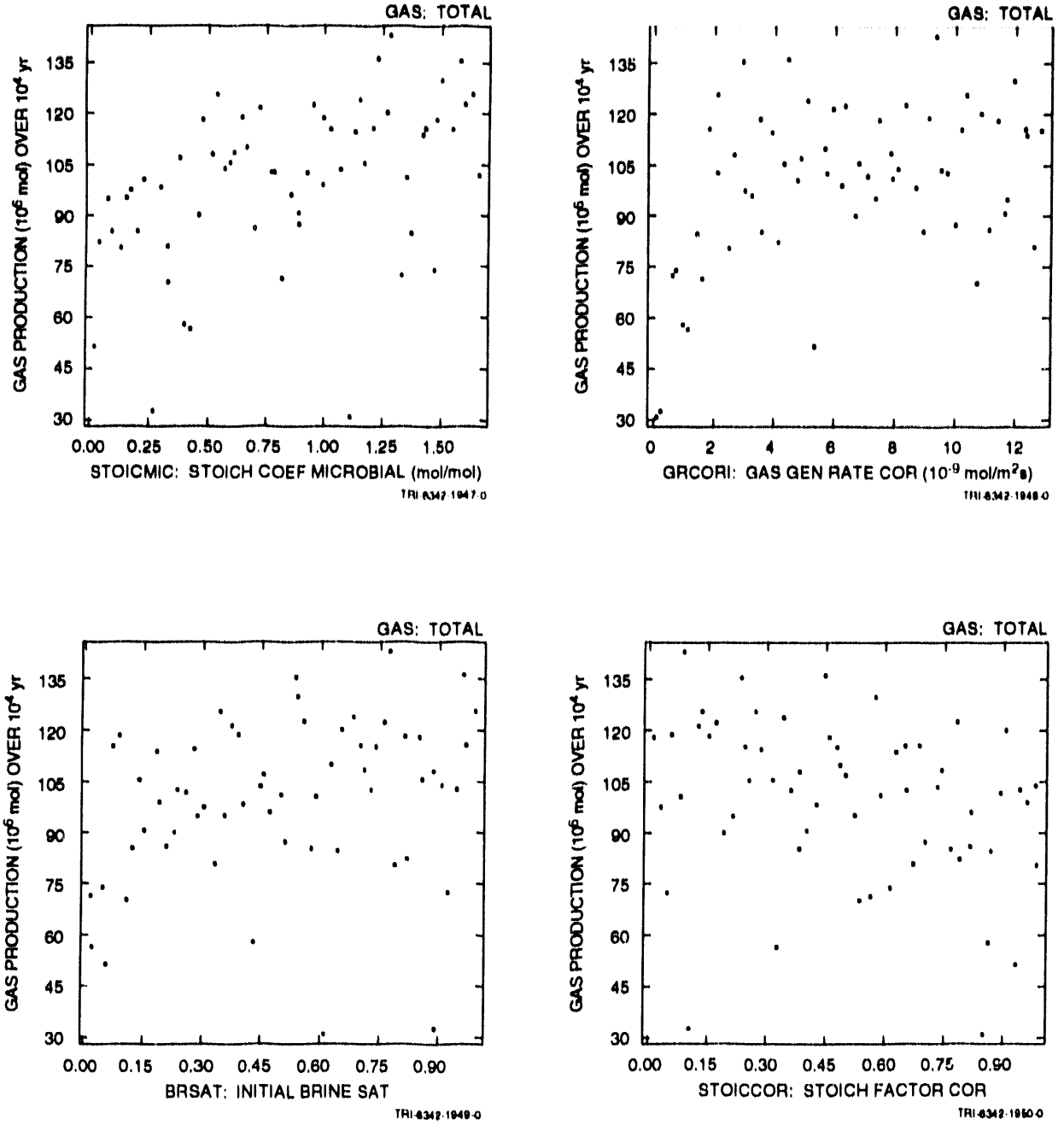

Figure 2-10. Scatterplots relating cumulative gas production over 10,000 yr due to both corrosion and microbial degradation to STOICMIC (stoichiometric coefficient for microbial degradation of cellulosics), GRCORI (gas-generation rate due to corrosion of steel under inundated conditions), BRSAT (initial brine saturation) and STOICCOR (stoichiometric factor for corrosion of steel).

Table 2-6. Stepwise Regression Analysis with Rank-Transformed Data for Total Gas Production Over 10,000 yr Due to Both Corrosion and Microbial Degradation.

	Total Gas Production over 10,000 yr (Corrosion and Biodegradation)		
Step[a]	Variable[b]	SRC[c]	R^{2d}
1	STOICMIC	0.51	0.27
2	STOICCOR	-0.35	0.38
3	BRSAT	0.34	0.49
4	GRCORI	0.33	0.59

[a] Steps in stepwise regression analysis
[b] Variables listed in order of selection in regression analysis
[c] Standardized regression coefficients in final regression model
[d] Cumulative R^2 value with entry of each variable into regression model

used in definition of gas-generation rate for corrosion of steel under humid conditions) and BRSAT (initial brine saturation) have negative effects on the steel inventory. As with VMETAL, the importance of GRCORI and GRCORH tends to decrease with time; in contrast, the importance of BRSAT remains relatively fixed. The negative relationships involving GRCORI, GRCORH and BRSAT result from their effects in increasing the rate of corrosion. The cellulosic inventory is initially dominated by VWOOD (fraction of total waste volume that is occupied by IDB combustible waste category), with the importance of this variable decreasing rapidly with time. The variable GRMICI (gas-generation rate due to microbial degradation of cellulosics under inundated conditions) shows a strong negative effect on cellulosic inventory due to its effect in increasing the rate at which cellulosics are consumed. The positive effect indicated for STOICMIC (stoichiometric coefficient for microbial degradation of cellulosics) probably results because increased values for STOICMIC lead to increased rates of gas generation, which in turn lead to humid conditions and thus lower rates of microbial degradation of cellulosics.

2.3.4 Gas Saturation and Pressure in Waste Panel

Time-dependent values for average gas saturation in the waste (i.e., averaged over entire waste panel) and gas pressure in the waste are presented in the two upper frames of Figure 2-11. As shown in the upper left frame, gas saturation often decreases in the first one thousand years and then steadily increases to an asymptote. This behavior happens because

Gas Saturation and Gas Pressure in Waste Panel

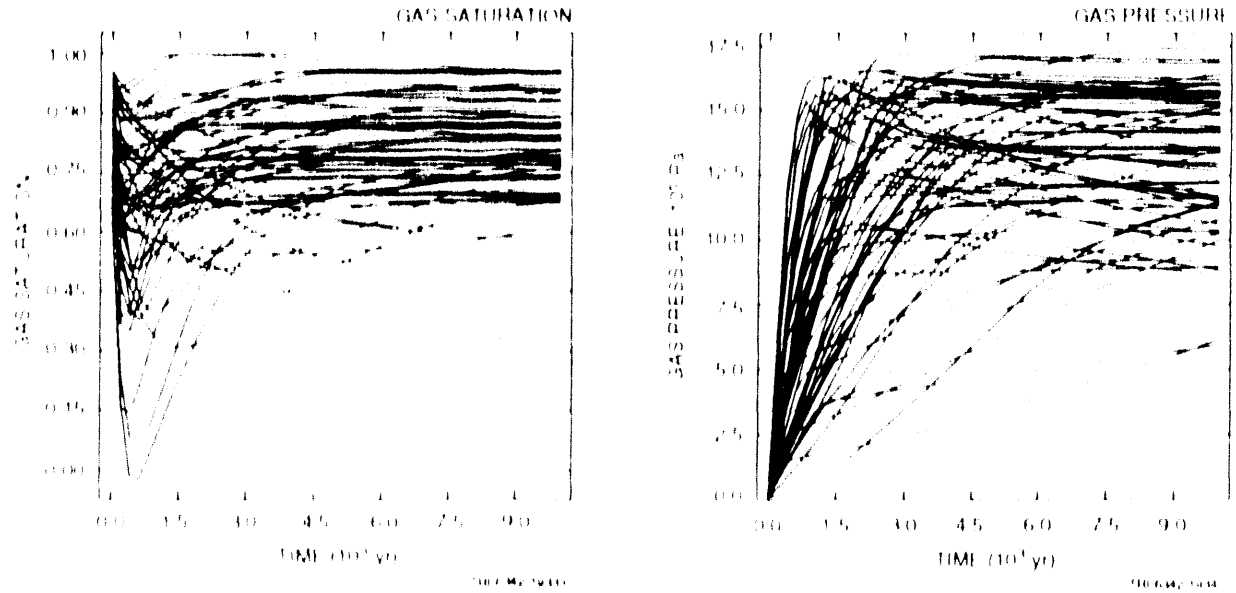

Partial Rank correlation coefficients for Gas Saturation and Gas Pressure in Waste Panel

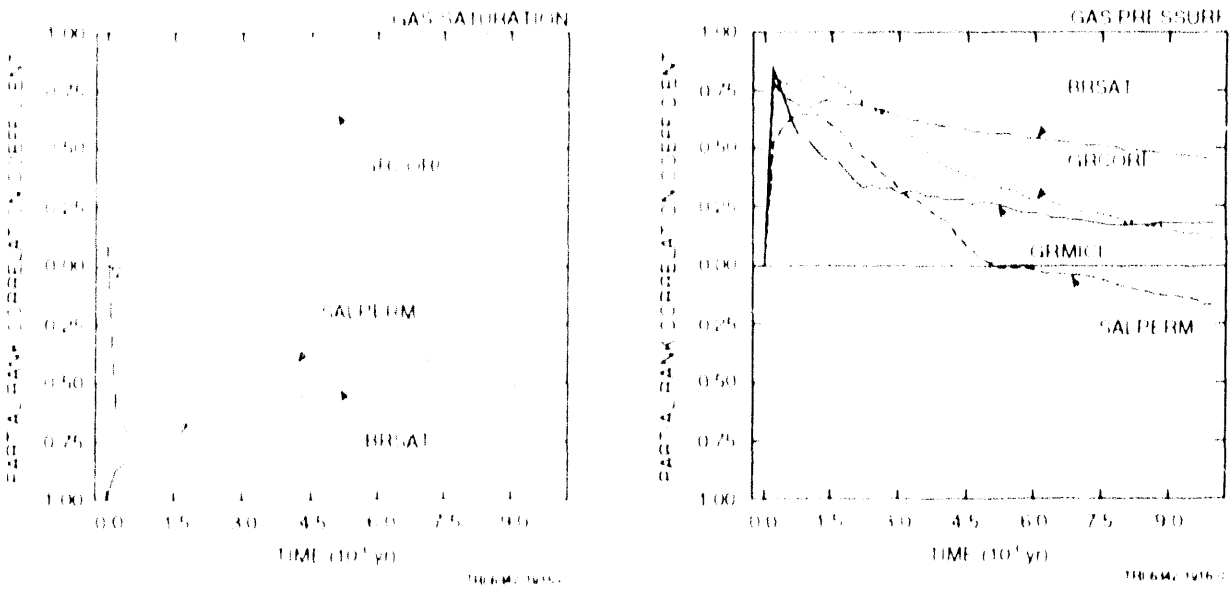

Figure 7.11 Uncertainty and sensitivity analysis results for average gas saturation and gas pressure in waste panel

brine initially flows into the waste panel and reduces the fraction of the pore space occupied by gas; then, as gas pressure increases, brine is forced out of the waste panel and gas saturation increases. This pattern of behavior can be seen in the two upper frames of Figure 2-12, which show total brine flow into the repository and net brine flow into the repository. In addition, brine is consumed during the corrosion of steel, with most of this consumption taking place during the first 3000 yr (Figure 2-9). As the partial rank correlation coefficients for gas saturation in the lower left frame of Figure 2-11 show, increasing GRCORI (gas-generation rate for corrosion of steel under inundated conditions) tends to increase gas saturation and increasing each of BRSAT (initial brine saturation) and SALPERM (Salado halite permeability) tends to decrease gas saturation, with these effects resulting because increasing GRCORI increases the amount of gas in the panel and increasing each of BRSAT and SALPERM increases the amount of brine in the panel. The dominant effect of BRSAT and SALPERM on net brine flow into the waste panel is indicated by the partial correlation coefficients shown in the lower right frame of Figure 2-12.

As shown in the upper right frame of Figure 2-11, time-dependent gas pressure in the waste panel displays three patterns of behavior: (1) a strictly monotonic increase in pressure, (2) a monotonic increase in pressure until an asymptote is reached, and (3) a monotonic increase in pressure until a maximum is reached and then a monotonic decrease in pressure. The largest gas pressures are approximately 2 MPa above the lithostatic pressure of 14.8 MPa. The partial rank correlation coefficients for gas pressure in the lower right frame of Figure 2-11 indicate that GRCORI (gas-generation rate for corrosion of steel under inundated conditions), GRMICI (gas-generation rate due to microbial degradation of cellulosics under inundated conditions), BRSAT (initial brine saturation of waste) and SALPERM (Salado halite permeability) have positive effects on gas pressure at early times. However, the importance of these variables decreases with time, and no single variable appears to have a large effect on the gas pressure at 10,000 yr. A stepwise regression analysis with rank-transformed data for gas pressure at 10,000 yr selected the variables BRSAT and MBPRES (pressure in Marker Bed 139 under undisturbed conditions) with an R^2 value of 0.30. This poor performance probably results from different variables being important in each of the three patterns of time-dependent gas pressure indicated at the beginning of this paragraph. Examination of scatterplots did not reveal a strong relationship between gas pressure at 10,000 yr and any of the sampled variables.

As previously indicated, the 1991 WIPP preliminary performance assessment did not directly model closure of the waste panels. However, possible interaction of gas generation and panel closure was incorporated

Total and Net Brine Inflow to Waste Panel

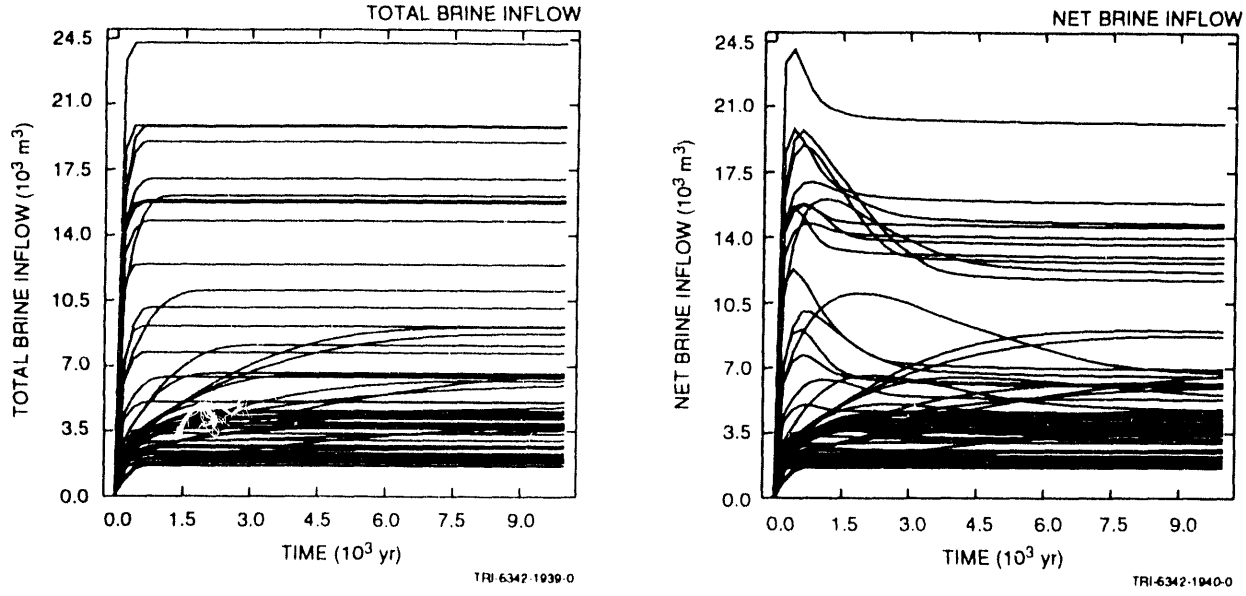

Partial Rank Correlation Coefficients for Total and Net Brine Inflow to Waste Panel

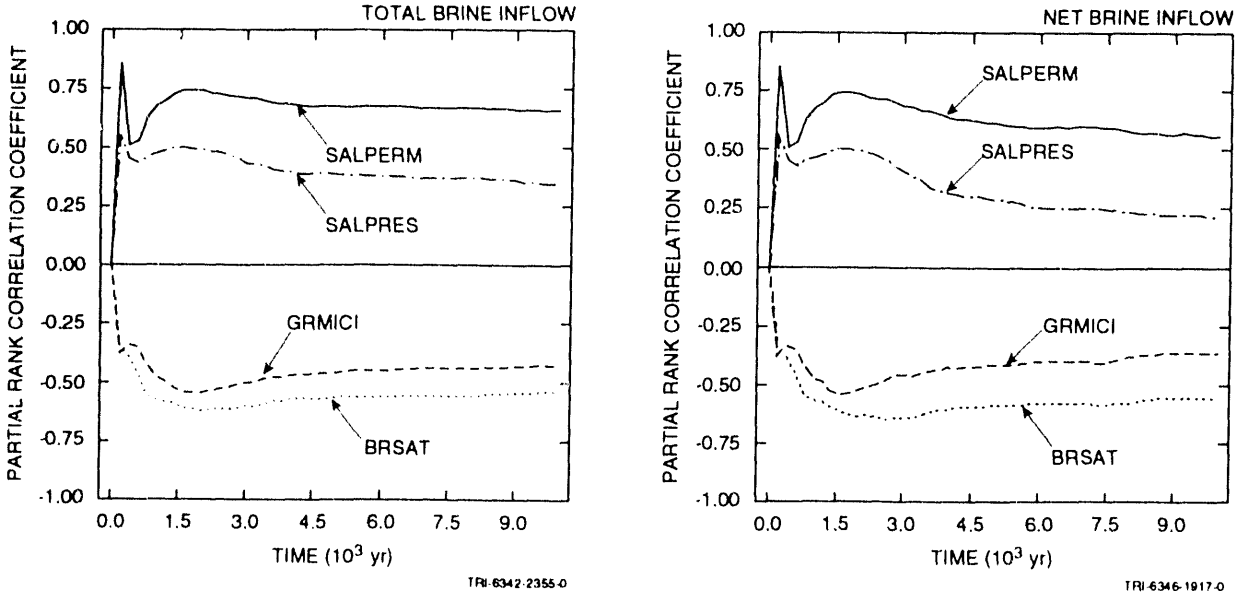

Figure 2-12. Uncertainty and sensitivity analysis results for total and net brine inflow to waste panel.

into the analysis by setting the initial pore volume in a waste panel to the volume necessary to contain all waste-generated gas at lithostatic pressure (i.e., 14.8 MPa) in a brine-free panel. As a result, initial pore volume is a function of STOICCOR (stoichiometric factor for corrosion of steel), STOICMIC (stoichiometric coefficient for microbial degradation of cellulosics), VMETAL (fraction of total waste volume occupied by IDB metals and glass waste category) and VWOOD (fraction of total waste volume occupied by IDB combustible waste category). As shown by the upper frame in Figure 2-13, pore volume remains essentially fixed at its initial volume, although there is a small response to changing gas pressures through rock compressibility effects. Further, the partial rank correlation coefficients in the lower frame of Figure 2-13 indicate that pore volume is indeed a function of STOICCOR, STOICMIC, VMETAL and VWOOD.

2.3.5 Lateral Gas Migration

A primary focus of the studies contained in this report is the migration of gas away from the waste panels. For Case 1, this means gas migration into the anhydrite marker beds in the Salado Formation. Due to gravity drainage of brine to the bottom of a waste panel, gas migration is more likely to occur into Anhydrite Layers A and B above the waste panels than into Marker Bed 139 below the waste panels. Of the 60 sample elements used in this study, 13 resulted in gas migration into Anhydrite Layers A and B and only 7 of these 13 resulted in gas migration into Marker Bed 139. Thus, a natural question to address is what controls gas migration into the marker beds rather than how much gas enters the marker beds or how far this gas travels.

Gas enters the marker beds from the disturbed rock zone surrounding a waste panel (Figure 2-2). Further, gas will enter the marker beds only if the gas pressure in the last computational cell of the disturbed rock zone exceeds the gas barrier pressure (i.e., brine pressure plus threshold displacement pressure if gas saturation is below residual, and gas pressure if gas saturation is above residual) in the adjacent computational cell of the undisturbed marker bed. To investigate these pressures, the time-dependent gas pressures in the computational cell of the disturbed rock zone adjacent to Anhydrite Layers A and B (i.e., Cell (10,5) shown in Figure 2-2) and the time-dependent gas barrier pressures in the adjoining computational cell containing undisturbed anhydrite in Anhydrite Layers A and B (i.e., Cell (11,5)) were plotted as shown in the two upper frames of Figure 2-14. No gas reaches Computational Cell (10,5) for 31 sample elements, as shown by the presence of only 29 nonzero gas pressure plots in the upper left frame of Figure 2-14. Further, as comparison of the upper two frames in Figure 2-14 shows, the gas barrier pressure in Computational

Total Pore Volume in Waste Panel

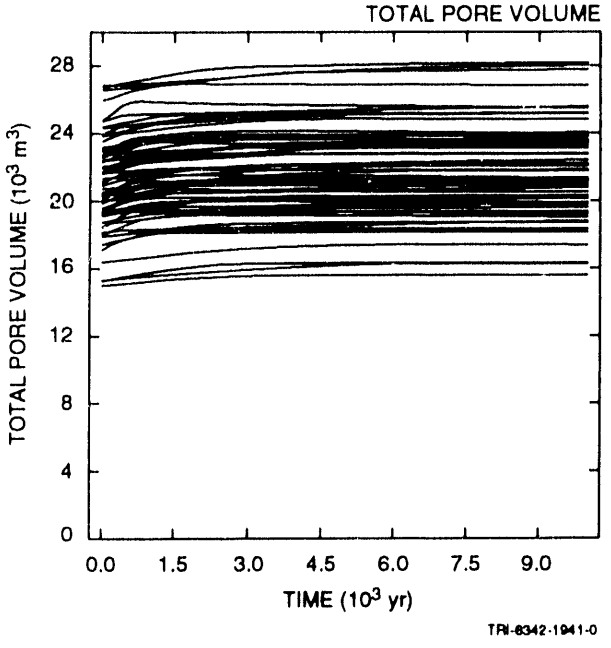

Partial Rank Correlation Coefficients for Total Pore Volume in Waste Panel

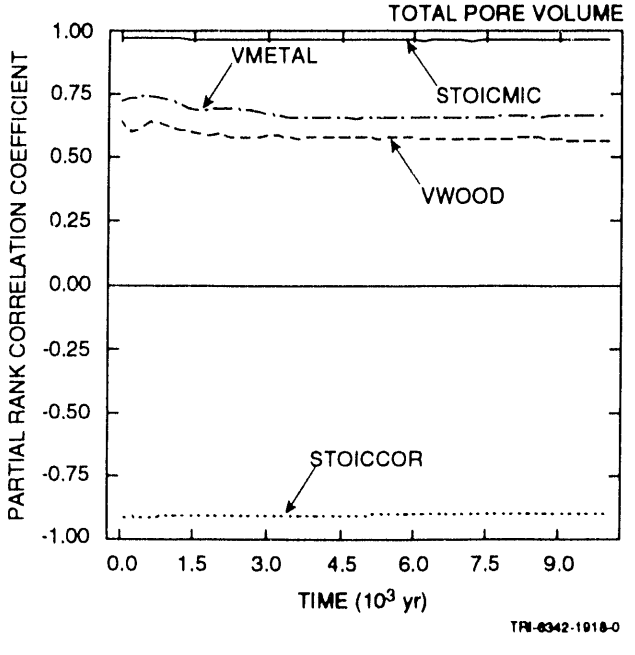

Figure 2-13. Uncertainty and sensitivity analysis results for total pore volume in waste panel.

Gas Pressure and Gas Barrier Pressure in Adjacent Computational Cells

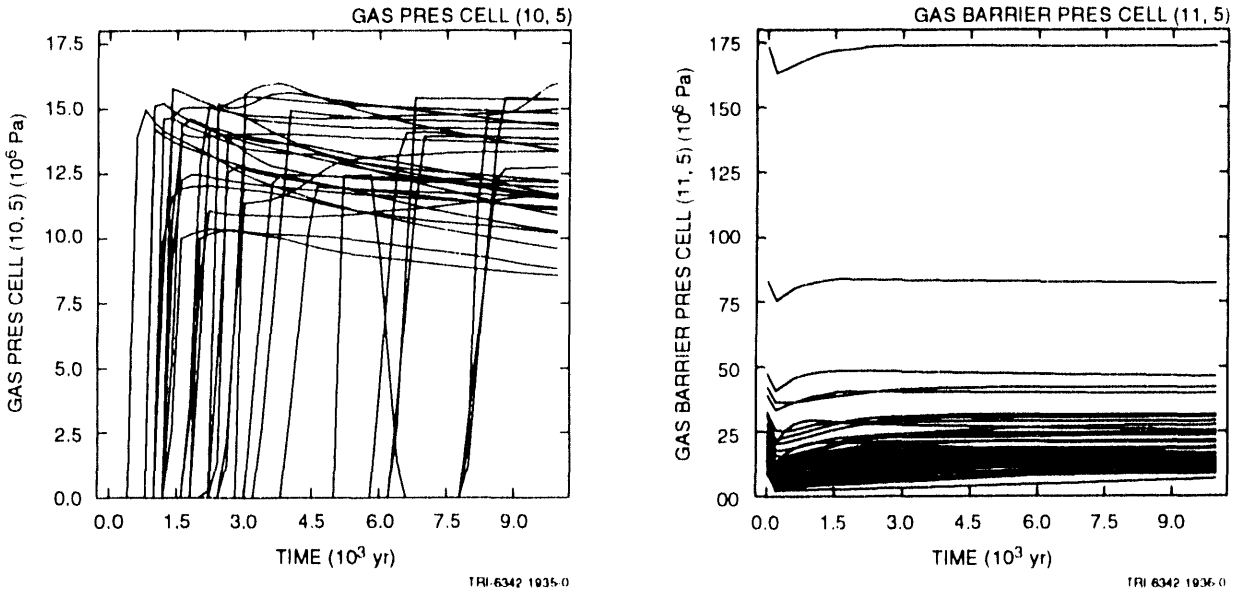

Partial Rank Correlation Coefficients for Gas Pressure and Gas Barrier Pressure in Adjacent Computational Cells

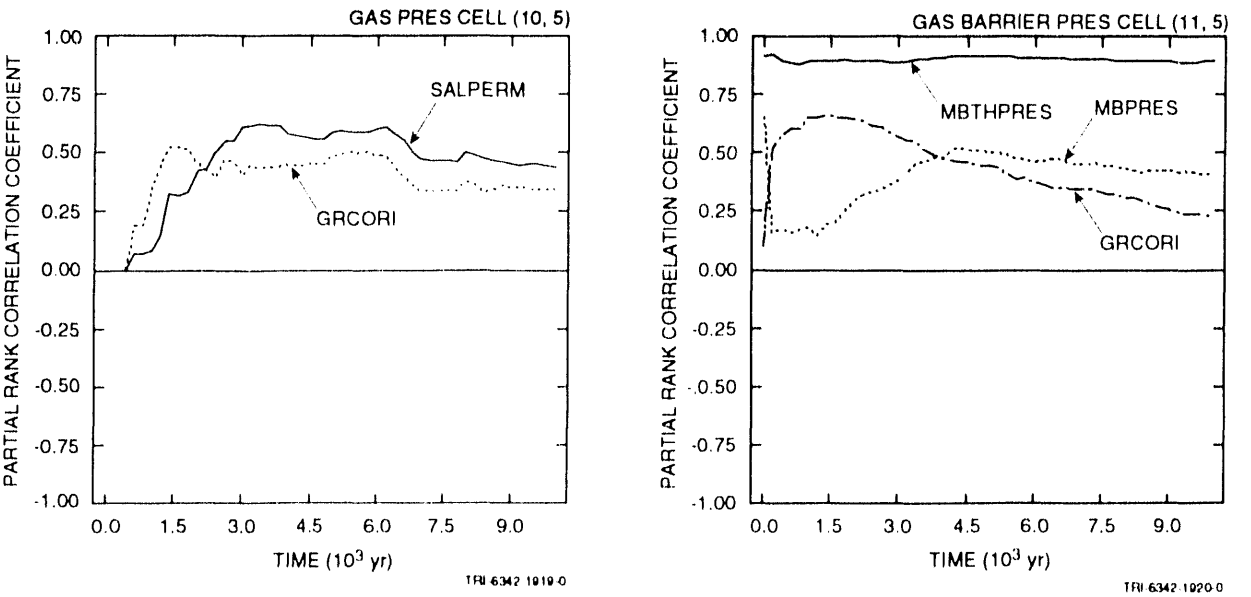

Figure 2-14. Uncertainty and sensitivity analysis results for gas pressure in computational cell of disturbed rock zone adjacent to Anhydrite Layers A and B (i.e., Cell (10,5) and gas barrier pressure in adjacent computational cell containing undisturbed anhydrite in Anhydrite Layers A and B (i.e., Cell (11,5)).

Cell (11,5) often exceeds the gas pressure in Computational Cell (10,5), with the result that no gas flow takes place into the undisturbed portion of Anhydrite Layers A and B (Note: the scale on the ordinate of upper right frame in Figure 2-14 is greater than the corresponding scale on the upper left frame by a factor of 10).

The partial rank correlation results in the lower right frame of Figure 2-14 indicate that the gas barrier pressure in Computational Cell (11,5) is dominated by MBTHPRES (threshold displacement pressure in anhydrite marker beds in Salado Formation), with smaller effects for GRCORI (gas-generation rate for corrosion of steel under inundated conditions) and MBPRES (pressure in Marker Bed 139 under undisturbed conditions). Increasing each of MBTHPRES, GRCORI and MBPRES tends to increase the gas barrier pressure in Computational Cell (11,5) and, hence, reduce the likelihood that gas will move from Computational Cell (10,15) in the disturbed rock zone to Computational Cell (11,5) in the undisturbed region of Anhydrite Layers A and B. The weak influence indicated for GRCORI probably results from the 13 sample elements in which gas penetrates Anhydrite Layers A and B, in which case the gas barrier pressure in Computational Cell (11,5) becomes the actual gas pressure once residual gas saturation is exceeded. The partial rank correlation results in the lower left frame of Figure 2-14 indicate that gas pressure in Computational Cell (10,5) tends to increase as SALPERM (Salado halite permeability) and GRCORI (gas generation rate due to corrosion under inundated conditions) increase. However, with only 29 nonzero gas pressure curves and these curves switching from zero to nonzero gas pressures at different times, partial correlation coefficients are not a particularly revealing analysis tool for the study of gas pressure in Computational Cell (10,5).

As shown by the scatterplot in Figure 2-15, SALPERM (Salado halite permeability) has a complex pattern of effects on gas pressure in Computational Cell (10,5) at 10,000 yr. All sample elements for which no gas reaches Computational Cell (10,5) have a value of SALPERM that is less than 1×10^{-20} m^2. The result is a positive relationship between SALPERM and gas pressure that is consistent with the partial correlation analysis shown in the lower left frame of Figure 2-14. However, for values of SALPERM above 1×10^{-20} m^2, a negative relationship exists between SALPERM and gas pressure in Computational Cell (10,5), with gas pressure tending to decrease as SALPERM increases. The patterns appearing in Figure 2-15 result primarily from the permeabilities used in the disturbed rock zone, with the halite and anhydrite permeabilities being set to values an order of magnitude above the permeabilities used for undisturbed halite and anhydrite (i.e., to 10 • SALPERM and 10 • MBPERM). Further, halite permeability (SALPERM) and anhydrite permeability (MBPERM) were sampled

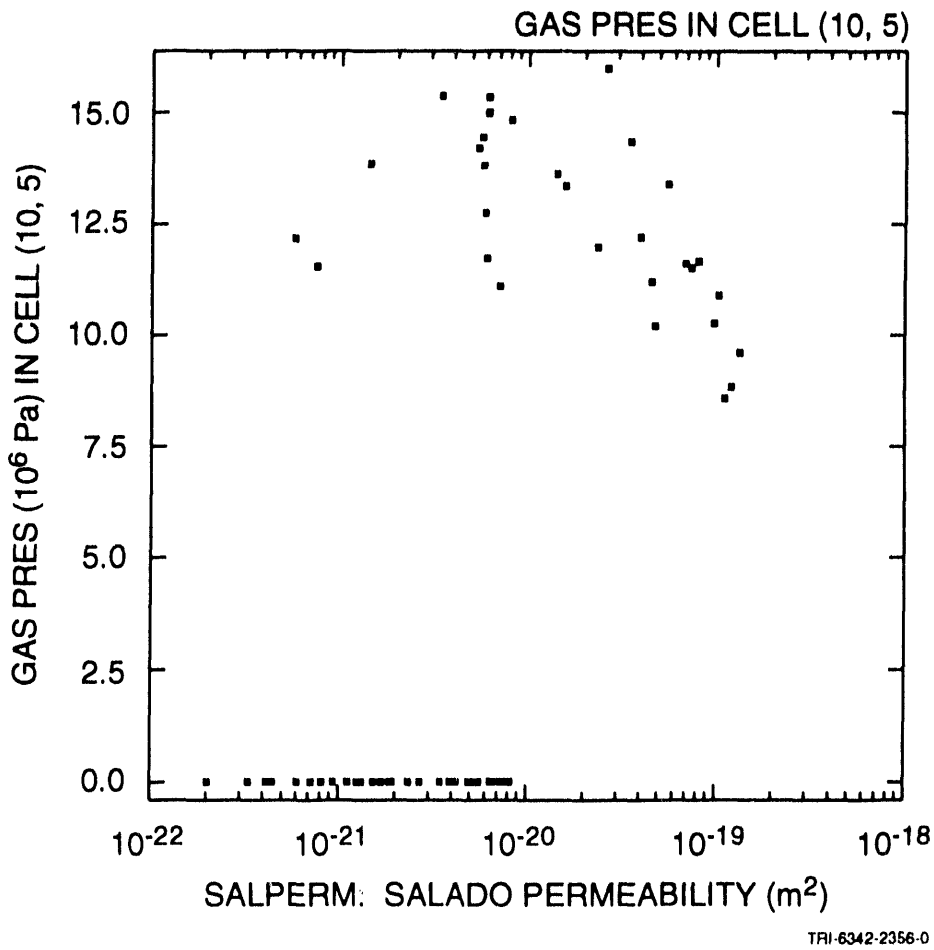

Figure 2-15. Scatterplot for gas pressure in Computational Cell (10,5) versus SALPERM (Salado halite permeability).

with a rank correlation of 0.8. When SALPERM is small (i.e., $< 1 \times 10^{-20}$ m^2), the resistance to gas and brine flow in the disturbed rock zone is increased, with the result that gas is less likely to reach Computational Cell (10,5) than when SALPERM has larger values. As shown in Figure 2-2, a layer of halite separates Computational Cell (10,5) from the repository, with the result that SALPERM is more important than MBPERM in determining whether or not gas reaches Computational Cell (10,5). As SALPERM increases above 1×10^{-21} m^2, brine begins to flow out of Computational Cell (10,5), with brine outflow increasing and brine pressure decreasing with increasing values for SALPERM. As a consequence of this tendency for brine pressures in Computational Cell (10,5) to decrease as brine flows out for values of SALPERM above 1×10^{-21} m^2, the pressures for the inflowing gas will also decrease, which is the pattern shown in Figure 2-15.

A more direct comparison of gas pressure and gas barrier pressure can be made by plotting the difference between gas barrier pressure in Computational Cell (11,5) and gas pressure in Computational Cell (10,5) as shown in the upper left frame of Figure 2-16. A positive difference indicates that the gas barrier pressure exceeds the gas pressure and thus that gas flow will not take place into undisturbed regions in anhydrites A and B. Further, the magnitude of this difference shows the amount of additional pressure rise that is needed to initiate gas flow into undisturbed regions in Anhydrite Layers A and B. The partial rank correlation results in the lower left frame of Figure 2-16 indicate that MBTHPRES (threshold displacement pressure in anhydrite marker beds in Salado Formation) is the most important variable in determining the difference between gas barrier pressure and gas pressure in Computational Cells (11,5) and (10,5), with smaller effects indicated for GRCORI (gas-generation rate for corrosion of steel under inundated conditions) and MBPRES (pressure in Marker Bed 139 under undisturbed conditions). The two right frames in Figure 2-16 present similar results for the difference between the gas barrier pressure in Computational Cell (11,5) and the gas pressure in the waste panel itself. Again, this difference is dominated by MBTHPRES, with smaller effects indicated for several additional variables.

2.4 Discussion

The primary purpose of the analyses presented in this chapter was to evaluate the factors influencing gas migration away from the repository. Little gas migration was observed. Of the 60 sample elements used in the analysis, only 7 resulted in gas migration into both Anhydrite Layers A and B and Marker Bed 139, and an additional 6 resulted in gas migration into Anhydrite Layers A and B but not Marker Bed 139; the remaining sample elements resulted in no gas migration into the anhydrite marker beds. The

Differences between Gas Barrier Pressure and Gas Pressure

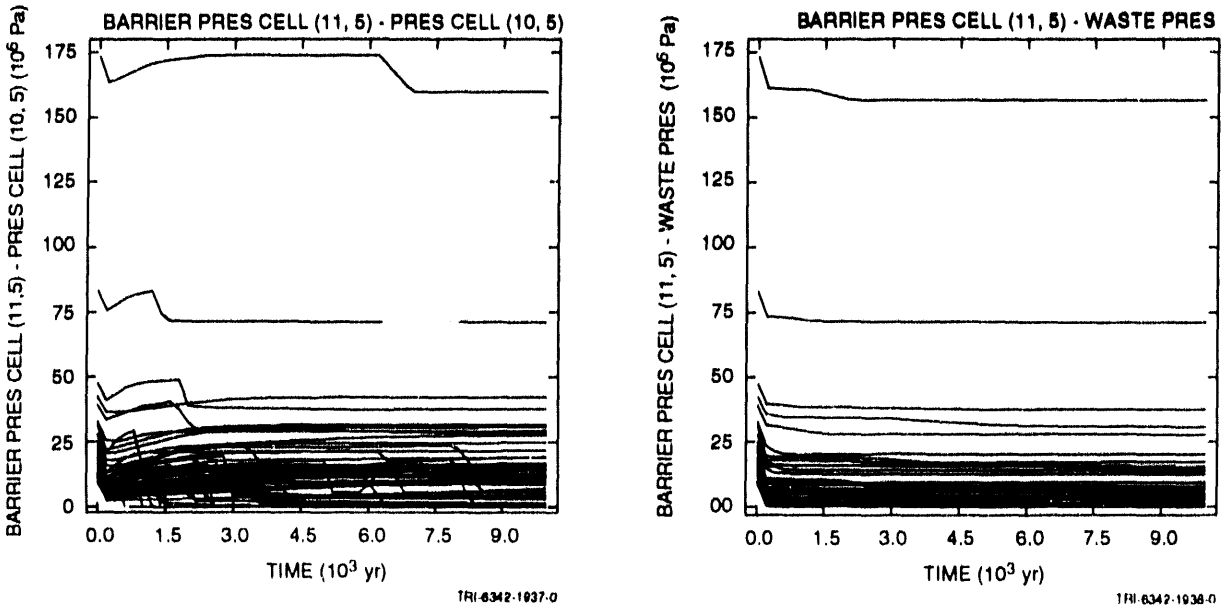

Partial Rank Correlation Coefficients for Differences between Gas Barrier Pressure and Gas Pressure

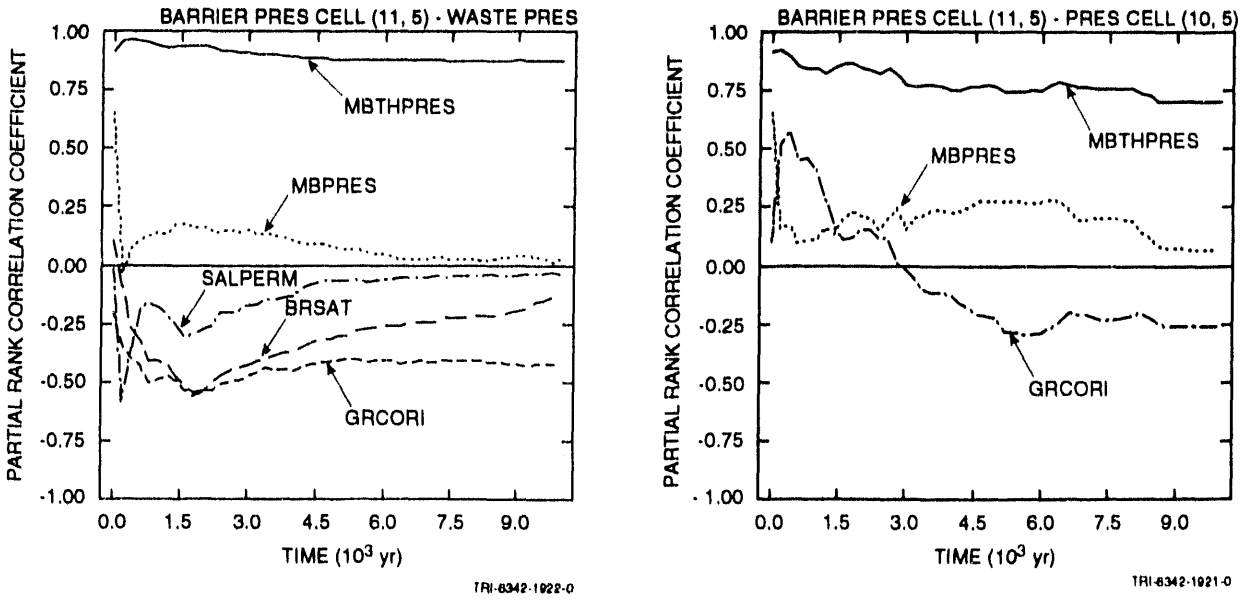

Figure 2-16. Uncertainty and sensitivity analysis results for differences between gas barrier pressure in Computational Cell (11,5) and gas pressure in Computational Cell (10,5) and the waste panel, respectively.

dominant variable in determining whether or not gas migration into the anhydrite marker beds occurs is the threshold displacement pressure. For most sample elements, gas pressures in the waste panel and the surrounding disturbed rock zone never reached values that exceeded the gas barrier pressure (i.e., brine pressure plus threshold displacement pressure if gas saturation is below residual, and gas pressure if gas saturation is above residual) for undisturbed anhydrite, with the result that waste-generated gas could not overcome the resistance to entry into the anhydrite marker beds.

For 31 of the 60 sample elements, no gas reached the boundary between the disturbed rock zone and Anhydrite Layers A and B. The sample elements for which no gas reached this boundary were strongly associated with small values for halite permeability. This pattern occurred because small values for halite permeability resulted in little brine outflow from the disturbed rock zone, with the result that brine pressures in the disturbed rock zone were sufficiently high to prevent the inflow of gas.

Gas pressures in the waste panel typically remained below the assumed lithostatic pressure of 14.8 MPa. The role of lithostatic pressure as an approximate bound on waste-panel gas pressure resulted from an adjustment to waste-panel pore volume that was made to incorporate the competing effects of pore-volume expansion due to waste-generated gas and pore-volume reduction due to waste compaction.

Most of the steel and cellulosic inventories were consumed over the 10,000-yr period under consideration. Thus, although parameters related to rates of corrosion and microbial degradation affect the time at which gas is generated, they did not have a large effect on the total amount of gas generated. Under the assumptions of this analysis, the total amount of waste-generated gas is determined by the steel and cellulosic inventories, the stoichiometric terms, and the amount of available brine. Gas production due to corrosion was approximately twice the gas production due to microbial degradation of cellulosics. However, it should be recognized that this comparison results from assumptions about stoichiometry and the steel and cellulosic inventories rather than from a mechanistic modeling of the underlying chemical and biological processes.

Brine saturation drops below residual brine saturation in many computational cells associated with the waste panel, with the result that no brine flow can occur through these cells. This depletion of brine in the presence of gas generation is potentially important with respect to radionuclide transport away from the repository. If brine cannot flow through parts of a waste panel, then the associated radionuclides are not available for transport.

Uncertainty and sensitivity analysis techniques of the type employed in this study provide a powerful tool for model verification. Due to the concurrent variation of many input variables, the opportunity to examine a variety of predicted variables and the capability to identify the effects of many input variables for each predicted variable, greater assurance with respect to the correct operation of a model can be obtained than results from simply examining a few selected calculations. The analysis for Case 1 employed the same formulation of BRAGFLO that was used in the 1991 WIPP performance assessment. The extensive analyses performed for Case 1 did not reveal any errors in the implementation of BRAGFLO, which helps provide assurance that the BRAGFLO component of the 1991 WIPP performance assessment was implemented correctly.

3. CASE 2: PERMEABLE SHAFT WITH PANEL SEALS

3.1 Summary Description*

Unlike the single isolated waste panel of Case 1, the entire repository is modeled in Case 2. Further, Case 2 explicitly incorporates the repository shafts and uses a more detailed characterization of the waste and its surroundings by representing the repository as a sequence of waste, panel seal, backfill and shaft regions through which gas and brine flow can occur in both the vertical and horizontal (i.e., north-south) directions.

As shown in Figure 3-1, the computational implementation of Case 2 with BRAGFLO is based on a rectangular grid aligned north-south through the repository. This grid is a simplification of the three-dimensional structure of the repository and involves several assumptions. The storage regions (i.e., waste panels) of the repository are grouped into the following three blocks on the basis of number of drift and panel seals between the waste and the nearest shaft: Waste Block A, which corresponds to the single waste panel that is separated from the waste and exhaust shafts by two sets of panel seals (i.e, the Northern Panel in Figure 2-3), Waste Block B, which corresponds to the five waste panels separated from the waste and exhaust shafts by three sets of panel seals (i.e., Panels 1, 2, 7 and 8 and the Southern Panel in Figure 2-3), and Waste Block C, which corresponds to the four waste panels separated from the waste and exhaust shafts by four sets of panel seals (i.e., Panels 3, 4, 5 and 6 in Figure 2-3). Each waste block contains the storage volume of the corresponding waste panels and drifts. The four shafts are combined into a single shaft at the location of the Waste Shaft, which is the shaft nearest the waste-disposal panels (Figure 2-3), and this single shaft is subdivided vertically into four segments. Stratigraphic layers are assumed to be parallel and horizontal. The marker beds within the Salado Formation are actually slightly undulatory, with a dip of less than 1° to the southeast at the WIPP. Because the repository is being excavated at a constant stratigraphic horizon rather than at a constant elevation, this dip results in a drop in floor elevation of about 7 m between the Waste Shaft and the Southern Panel. The computational gridding for BRAGFLO does not include this change in elevation.

The computational grid shown in Figure 3-1 extends vertically 645 m from the bottom of the Salado Formation to the top of the Culebra Dolomite Member of the Rustler Formation and extends horizontally for approximately 29 km. Stratigraphic units included in the grid are the intact halite of

*Adapted from Section 2.3 of WIPP PA, 1992.

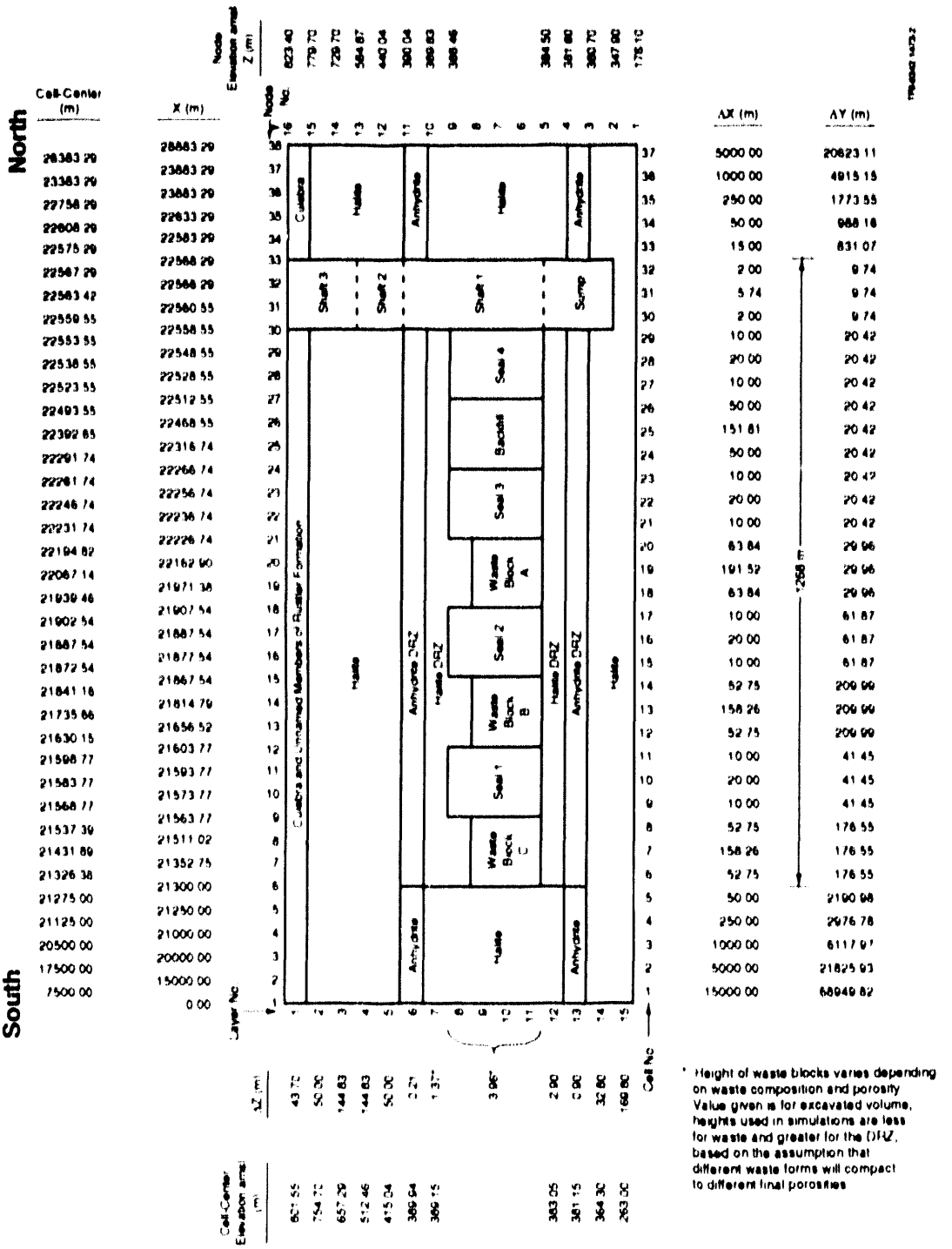

Figure 3-1. Gridding scheme employed with BRAGFLO for the two-dimensional vertical cross-section model of the full repository used for Case 2.

the Salado Formation, Marker Bed 139, Anhydrite Layers A and B, which are represented as a single anhydrite layer, and the lower unnamed member of the Rustler Formation and the Culebra Dolomite, which are represented as a single layer. The computational grid also includes a disturbed rock zone, which extends vertically around the repository and includes parts of Marker Bed 139 and Anhydrite Layers A and B. The permeability of the disturbed rock zone was assumed to be sufficiently low (i.e., 2.41×10^{-20} m^2, which is an order of magnitude above the assumed permeability of 2.41×10^{-21} m^2 for halite in the Salado Formation) to prevent significant gas flow around the panel seals.

The computational cells used with BRAGFLO represent two-dimensional projections of three-dimensional features with different volumes. The width of the computational cells (i.e., distance measured in the direction of the y coordinate in Figure 3-1, which is perpendicular to the page) varies significantly before projection to two dimensions, from as little as 9.74 m at the location of the shaft to as much as 69 km in the intact Salado Formation. This dimension of the grid does not vary vertically; thus, where the grid is thin near the shaft because of the small excavated volume, all grid elements, including the disturbed rock zone, the intact Salado Formation and the Culebra Dolomite, are given the same value for the y-dimension. Figures 2-5 and 2-6 of WIPP PA, 1992 show enlarged representations of the grid in the horizontal plane containing the repository.

The third dimension (i.e., the y coordinate, which is perpendicular to the page in Figure 3-1) is included in the construction of the computational grid to allow for different storage volumes for brine and gas in each cell. Flow is not modeled in the third dimension and occurs only in the plane of Figure 3-1 (i.e., in the directions of the x and z coordinates). Flow from Waste Block C to the Culebra Dolomite, for example, would occur horizontally through the other waste blocks and the panel seals, and then vertically up the shaft.

The ends of the grid, south of Waste Block C and north of the shaft, require additional explanation. The intent was to simulate some three-dimensional behavior with a two-dimensional grid. With the repository or shaft acting as sources or sinks, fluid flow will be primarily horizontal, and mostly through the anhydrite layers. Close to the repository, flow paths will have complex orientations because of the variable geometry of the excavations. Further away from the repository, at a distance perhaps several times the maximum horizontal dimension of the repository (about 1.3 km), flow will be nearly radial either toward or away from the sink or source. This cylindrical flow pattern can be approximated with a two-dimensional model if the width of grid blocks (i.e., the y-dimension of Figure 3-1) increases away from the source or sink by a factor of $2\pi r$,

where r is the distance from the source or sink at the center of the grid (Voss, 1974). In a strict sense, this relationship is valid only if the entire grid is set up this way, starting from one side. Such a grid represents a vertical cylinder, and the resulting two-dimensional model will simulate radial flow in a three-dimensional cylinder. In the grid used here, only the north and south ends were treated in this fashion, and the results are not exact in modeling all flow outward from the repository/shaft region. However, as a first approximation, this procedure accounts for the radial increase in pore volume away from the central region. This radial increase in pore volume is potentially important because brine and gas flow away from the repository will not be restricted to two dimensions (vertically and in one dimension horizontally). Rather, at a distance of a few kilometers from the repository (approximately the disposal-unit boundary), flow will be radial into an increasing pore volume.

Waste Blocks A, B and C are separated by seal blocks that preserve both the total length and the total volume of the seals located between the panels. Thus, Seals 3 and 4 contain the composite volume of the drift seals north of the waste (Figure 2-3). Seal 2 contains the composite volume of the 12 panel seals separating Waste Block A from Waste Block B, and Seal 3 contains the volume of the 8 panel seals separating Waste Block B from Waste Block C. Seals are assumed to have a height equal to that of a newly excavated room, approximately 4 m. Actual heights of seals may vary, depending on location. Seals are assumed to occupy only the original volume of the drifts in which they are emplaced, and no correction is made for possible additional excavation, such as downward into Marker Bed 139 during seal construction. All panel and drift seals are assumed to have the same properties.

The single composite shaft is divided into four sections: a sump and three arbitrarily divided higher sections, each having different material properties. The three upper sections are used to represent different degrees of consolidation of the halite seals and backfill at different depths, with the deeper sections having lower permeability. The first shaft section above the sump, labeled Shaft 1 in Figure 3-1, extends from the bottom of the waste blocks upward to the top of the Anhydrite Layers A and B. The middle shaft section, labeled Shaft 2 in Figure 3-1, extends halfway to the top of the Salado Formation, and the upper section, labeled Shaft 3, extends to the top of the Culebra Dolomite. The lower most portion of the shaft, the sump, is assumed to be backfilled, and has been included in the model because of its possible role as a brine sink. The modeled sump extends downward 36.6 m from the repository floor, resulting in a modeled volume larger than that of the actual sumps. Two of the four shafts have no sumps, and depths in the other two are 38.4 m (Waste Shaft)

and 33.5 m (Salt Handling Shaft) (Nowak et al., 1990). However, the pore volume of the sump is small relative to the volume in the entire shaft. The disturbed rock zone is modeled only above and below the waste, drift and panel seal, and backfill blocks.

No mass is allowed to cross the far-field outer boundary of the grid except for the northern- and southernmost cells of the Culebra Dolomite. Fixed-pressure boundaries are defined for those locations to approximate the observed head in the Culebra. The initial pressure throughout the Culebra, including the lateral boundary cells, was set at 1.053 MPa. Initial brine saturation in the Culebra was set to 1.0 (i.e., there is no initial gas in the Culebra). Any gas that does eventually appear in the Culebra must come from the waste or from gas initially in the shaft or drift blocks.

Initial far-field pressures in the Salado Formation, including halite and anhydrite layers, was varied hydrostatically relative to a specified value at the level of Marker Bed 139, with the assumption of a brine density of 1230 kg/m^3. Initial pressure in Marker Bed 139 is one of the imprecisely-known variables considered in the uncertainty/sensitivity analysis for Case 2. Initial pressure in the waste, seals and backfill was assumed to be atmospheric (0.101 MPa). Initial pressure was assumed to be constant horizontally throughout any given layer in all of its constituent materials. The Salado Formation halite, the anhydrite, and the disturbed rock zone were assumed to be initially fully brine saturated.

Initial conditions in the shafts and drifts are uncertain, and two sets of calculations were carried out to evaluate the effects of assuming initial full brine saturation and initial full gas saturation. In the first set, the shaft seals, drift seals and backfill were assumed to be gas saturated, and initial pressure was atmospheric, 0.101 MPa. In the second set, these regions were assumed to be fully brine saturated, with the initial pressure in the drift seals and backfill equal to atmospheric. The initial brine pressure in the shaft was hydrostatic, varying with depth relative to the sampled value for the pressure in Marker Bed 139. In both sets of calculations, the initial shaft pressure extends to the top of the Salado Formation, with the result that a difference exists between the shaft and the Culebra pressures. For the gas-saturated shaft, this initial pressure difference was -0.95 MPa, compared to a range from 3.9 to 4.5 MPa for the brine-saturated shaft. This difference in gradient could cause different early-time behavior in the calculations for gas-saturated and brine-saturated shafts. Because the shaft was brine-saturated in either case within about 150 yr, results over 10,000 yr were relatively insensitive to the initial gas saturation of the drifts and shafts. The Case 2 results presented in this report were obtained with the assumption

of an initially gas-saturated shaft; results obtained with the assumption of an initially brine-saturated shaft are given in WIPP PA, 1992.

3.2 Sampled Variables

The 16 imprecisely-known variables listed in Table 3-1 were used as input to BRAGFLO for the Case 2 uncertainty and sensitivity studies. As is the case for Table 3-1, the distributions indicated in Table 3-1 for the individual variables are characterizing subjective uncertainty. The Case 2 calculations used a Latin hypercube sample of size 22 from the 16 variables in Table 3-1, which was generated in the same manner as the sample for Case 1. The resultant sample is listed in Table 3.2-2b of WIPP PA, 1992.

A widely-used guide for selecting the sample size to use in an uncertainty/sensitivity study based on Latin hypercube sampling is that the number of elements in the sample should equal 4 nV/3, where nV is the number of variables in the sample. This rule was used for Case 2 and resulted in the choice of 22 as the sample size. However, the actual basis for this rule is the size of the sample needed for the successful numerical implementation of the Iman/Conover restricted-pairing technique (Imar and Conover, 1982) that is used to control the correlation structure within the sample. To the best of the authors' knowledge, a rule for the optimum size of a Latin hypercube sample for use in uncertainty and sensitivity analysis is not known.

The variables BFPERMF, BRSATF, GRCORHF, GRMICHF, SH2PERMF and SH3PERMF in Table 3-1 are scale factors that are used in constructing the variable values that are actually used in the analysis. Associated with each of these scale factors in Table 3-1 is the definition of the variable that is actually used by BRAGFLO. The sensitivity analyses presented in Section 3.3 use the actual BRAGFLO inputs (i.e., BFPERM, BRSAT, GRCORH, GRMICH, SH2PERM and SH3PERM) rather than the corresponding scale factors. In contrast, the sensitivity analyses for Cases 1 and 3 use the sampled variables rather than the actual BRAGFLO inputs. The transformed variables (i.e., actual BRAGFLO inputs) are used in Case 2 because of the relatively complex relationships involving BFPERMF, SH2PERMF and SH3PERMF.

In addition to the 16 sampled variables listed in Table 3-1, the calculations for Case 2 also required values for a number of additional variables that were fixed at their best-estimate values. These variables and their values are listed in Tables 3.1-1b and 3.2-1a of WIPP PA, 1992. Further, additional discussion of the BRAGFLO input for Case 2 is available in Section 3.2 of WIPP PA, 1992.

Table 3-1. Imprecisely Known Variables Used in BRAGFLO for Case 2 to Determine the Effects of Seal Permeabilities and Gas Generation Parameters on Gas Flow through the Repository and up the Shaft to the Culebra Dolomite.

Variable	Definition
BFPERMF	Scale factor used in definition of permeability of backfill in waste panels (dimensionless). Range: 0 to 1. Median: 0.5. Distribution: Normal. Actual backfill permeability, BFPERM, is defined by $\log BFPERM = \log SEALPERM + (-14 - \log SEALPERM)\ BFPERMF$ Additional information: Section 3.2.2, WIPP PA, 1992. Variable 13 in Latin hypercube sample.
BRSATF	Scale factor used in definition of initial brine saturation of waste (dimensionless). Range: 0 to 1. Median: 0.5. Distribution: Uniform. Actual value for initial brine saturation of waste, BRSAT, is $BRSAT = 0.276\ BRSATF.$ Additional information: Section 3.4.9, WIPP PA, 1991c. Variable 1 in Latin hypercube sample.
GRCORHF	Scale factor used in definition of gas generation rate for corrosion of steel under humid conditions (dimensionless). Range: 0 to 5×10^{-1}. Median: 1×10^{-1}. Distribution: Piecewise uniform. Actual gas generation rate, GRCORH, is $GRCORH = GRCORHF \cdot GRCORI.$ Additional information: Memo from Brush, July 8, 1991, contained in Appendix A, Vol. 3; Section 3.3.8, WIPP PA, 1991c. Variable 3 in Latin hypercube sample.
GRCORI	Gas-generation rate for corrosion of steel under inundated conditions (mol/m^2 surface area steel • s). Range: 0 to 1.3×10^{-8} mol/m^2 s. Median: 6.3×10^{-9} mol/m^2 s. Distribution: Piecewise uniform. Additional information: Same as GRCORHF. Variable 4 in Latin hypercube sample.
GRMICHF	Scale factor used in definition of gas-generation rate due to microbial degradation of cellulosics under humid conditions (dimensionless). Range: 0 to 2×10^{-1}. Median: 1×10^{-1}. Distribution: Piecewise uniform. Actual gas-generation rate , GRMICH, is $GRMICH = GRMICHF \cdot GRMICI.$ Additional information: Same as GRCORHF. Variable 5 in Latin hypercube sample.

Table 3-1. Imprecisely Known Variables Used in BRAGFLO for Case 2 to Determine the Effects of Seal Permeabilities and Gas Generation Parameters on Gas Flow through the Repository and up the Shaft to the Culebra Dolomite (continued).

Variable	Definition
GRMICI	Gas-generation rate due to microbial degradation of cellulosics under inundated conditions (mol/kg cellulosics•s). Range: 0 to 1.6×10^{-8} mol/kg s. Median: 3.2×10^{-9} mol/kg s. Distribution: Piecewise uniform. Additional information: Same as GRCORHF. Variable 6 in Latin hypercube sample.
MBPERM	Permeability (k) in anhydrite marker beds in Salado Formation under undisturbed conditions (m^2). Range: 8.5×10^{-21} to 1.8×10^{-18} m^2. Median: 7.8×10^{-20} m^2. Distribution: Piecewise uniform. Additional information: Memo from Beauheim, June 14, 1991, contained in Appendix A, WIPP PA, 1991c; Section 2.4.5, WIPP PA, 1991c. Variable 11 in Latin hypercube sample.
MBPRES	Pressure (p) in anhydrite marker beds in Salado Formation under undisturbed conditions (Pa). Range: 8.21×10^6 to 1.48×10^7 Pa. Median: 1.28×10^7 Pa. Distribution: Piecewise uniform. Additional information: Memos from Beauheim, June 14, 1991, and Howarth, June 12, 1991, contained in Appendix A, WIPP PA, 1991c; Section 2.4.6, WIPP PA, 1991c. Variable 10 in Latin hypercube sample.
SEALPERM	Permeability (k) of seals between waste blocks in repository (m^2). Range: 3.3×10^{-21} to 1×10^{-14} m^2. Median: 5.7×10^{-18} m^2. Distribution: Lognormal. Additional information: Section 3.2.2, WIPP PA, 1992; Section 3.2.2, WIPP PA, 1991c. Variable 12 in Latin hypercube sample.
SH1PERM	Permeability (k) of lower shaft section (m^2). Range: 3.3×10^{21} to 1×10^{-14} m^2. Median: 5.7×10^{-18} m^2. Distribution: Lognormal. Additional information: Section 3.2.2, WIPP PA, 1992. Variable 14 in Latin hypercube sample.
SH2PERMF	Scale factor used in definition of permeability of middle shaft section. Range: 0 to 1. Median: 0.5. Distribution: Normal. Actual permeability of middle shaft section, SH2PERM, is defined by $\log \text{SH2PERM} = \log \text{SH1PERM} + (-14 - \log \text{SH1PERM})\ \text{SH2PERMF}.$ Additional information: Section 3.2.2, WIPP PA, 1992. Variable 15 in Latin hypercube sample.

Table 3-1. Imprecisely Known Variables Used in BRAGFLO for Case 2 to Determine the Effects of Seal Permeabilities and Gas Generation Parameters on Gas Flow through the Repository and up the Shaft to the Culebra Dolomite (concluded).

Variable	Definition
SH3PERMF	Scale factor used in definition of permeability of upper shaft section. Range = 0 to 1. Median: 0.5. Distribution: Normal. Actual permeability of upper shaft section, SH3PERM, is defined by log SH3PERM = log SH2PERM + (-14 - log SH2PERM) SH3PERMF. Additional information: Section 3.2.2, WIPP PA, 1992. Variable 16 in Latin hypercube sample.
STOICCOR	Stoichiometric factor for corrosion of steel (dimensionless). Defines proportion of two different chemical reactions that take place during the corrosion process. Range: 0 to 1. Median: 5×10^{-1}. Distribution: Uniform. Additional information: Brush and Anderson in Lappin et al., 1989, p. A-6; Section 3.3.8, WIPP PA, 1991c. Variable 2 in Latin hypercube sample.
STOICMIC	Stoichiometric coefficient for microbial degradation of cellulosics (mol gas/mol CH_2O). Range: 0 to 1.67 mol/mol. Median: 8.35×10^{-1} mol/mol. Distribution: Uniform. Additional information: Brush and Anderson in Lappin et al., 1989, p. A-10; Section 3.3.9, WIPP PA, 1991c. Variable 9 in Latin hypercube sample.
VMETAL	Fraction of total waste volume that is occupied by IDB (Integrated Data Base) metals and glass waste category (dimensionless). Range: 2.76×10^{-1} to 4.76×10^{-1}. Median: 3.76×10^{-1}. Distribution: Normal. Additional information: Section 3.4.1, WIPP PA, 1991c. Variable 7 in Latin hypercube sample.
VWOOD	Fraction of total waste volume that is occupied by IDB combustible waste category (dimensionless). Range: 2.84×10^{-1} to 4.84×10^{-1}. Median: 3.84×10^{-1}. Distribution: Normal. Additional information: Section 3.4.1, WIPP PA, 1991c. Variable 8 in Latin hypercube sample.

3.3 Uncertainty and Sensitivity Analysis Results

Gas flow through the repository and up the shaft to the Culebra Dolomite is the outcome of greatest interest for Case 2. Thus, as for Case 1, a natural starting point is an exploration of gas generation. Uncertainty and sensitivity analysis results related to corrosion, microbial degradation and total gas production are presented in Sections 3.3.1, 3.3.2 and 3.3.3. Then, gas saturation and gas pressure in the individual waste blocks are investigated in Section 3.3.4. Finally, gas migration through the shaft to the Culebra Dolomite is considered in Section 3.3.5.

3.3.1 Gas Generation Due to Corrosion

A summary of the results for gas generation due to corrosion is given in Figure 3-2. The two upper frames in Figure 3-2 show cumulative gas generation as a function of time due to corrosion under humid conditions (upper left frame) and corrosion under inundated conditions (upper right frame). Each curve in the upper two frames results from a single Latin hypercube sample element (i.e., each frame has 22 curves, one for each sample element). Overall, the range of gas production under humid conditions is similar to the range of gas production under inundated conditions.

Formal sensitivity analysis techniques based on partial rank correlation can be used to investigate the variation in cumulative gas production shown in the upper two frames of Figure 3-2. The analyses in this chapter use the variables BRSAT, GRCORH, GRMICH, BFPERM, SH2PERM and SH3PERM defined in Table 3-1 rather than the scale factors BRSATF, GRCORHF, GRMICHF, BFPERMF, SH2PERMF and SH3PERMF generated in the Latin hypercube sample. As indicated by the (rank) correlation matrix

SEALPERM	1.00					
BFPERM	0.54	1.00				
SH1PERM	0.00	0.04	1.00			(3-1)
SH2PERM	-0.03	-0.01	0.64	1.00		
SH3PERM	0.05	0.11	0.52	0.80	1.00	
	SEALPERM	BFPERM	SH1PERM	SH2PERM	SH3PERM	

the transformations given in Table 3-1 result in substantial correlations between SEALPERM and BFPERM and also between SH1PERM, SH2PERM and SH3PERM. In initial analyses based on partial rank correlation coefficients, these correlations tended to produce unstable and ambiguous results. In particular, with 16 sampled variables, a sample size of 22 and correlations between variables, there is often little information left to characterize with a partial correlation coefficient after the correction is made for the effects of the other variables (e.g., see Sections IX.1, IX.2, Beyer, 1968; David, 1938). To reduce the problems resulting from correlated input, the variables BFPERM, SH1PERM and SH3PERM were dropped from the analysis. Rank correlations also exist between GRCORH and GRCORI (i.e., 0.64) and between GRMICH and GRMICI (i.e., 0.68). However, these correlations did not seem to cause the misleading results that derived from the correlations between SEALPERM and BFPERM and also between SH1PERM, SH2PERM, and SH3PERM; thus, the transformed variables GRCORH and GRMICH were left in the partial correlation analysis. As a result, the following 13 variables were used in the calculation of the partial rank correlation coefficients presented in

Cumulative Gas Production Due to Corrosion of Steel

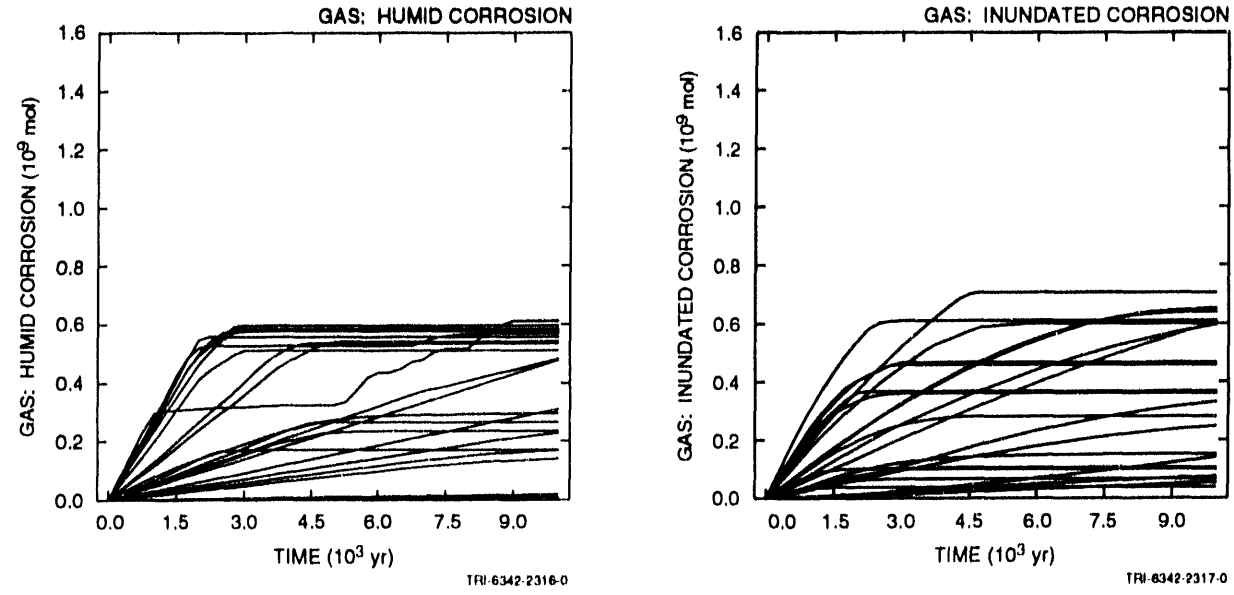

Partial Rank Correlation Coefficients for Cumulative Gas Production Due to Corrosion of Steel

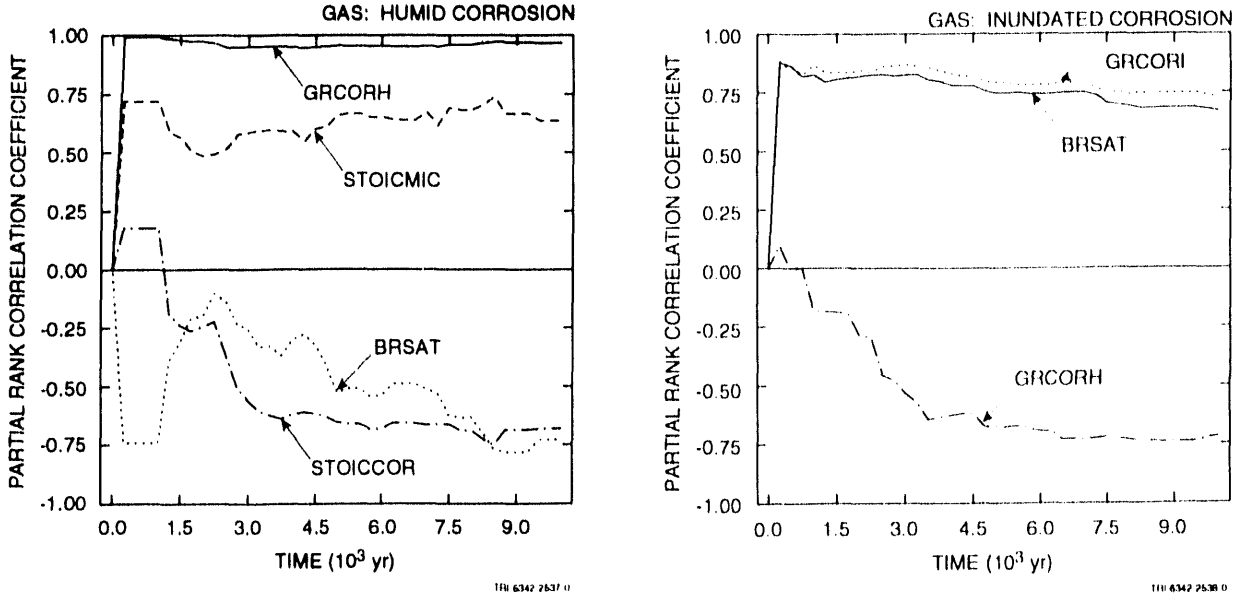

Figure 3-2. Uncertainty and sensitivity analysis results for gas generation due to corrosion of steel.

this chapter: BRSAT, GRCORH, GRCORI, GRMICH, GRMICI, MBPERM, MBPRES, SEALPERM, SH2PERM, STOICCOR, STOICMIC, VMETAL and VWOOD.

The lower two frames in Figure 3-2 show time-dependent plots of partial rank correlation coefficients between cumulative gas production and individual variables. The coefficients in Figure 3-2 and other similar figures in this chapter are calculated on the basis of vertical slices through the corresponding curves in the upper half of the figure. Due to the relatively small sample size in use (i.e., 22 observations for 13 independent variables), an absolute value cutoff of 0.7 is used for the selection of partial rank correlation coefficients for presentation in this chapter. As a reminder, a positive rank correlation coefficient indicates that two variables tend to increase and decrease together, and a negative rank correlation coefficient indicates that, as one variable increases, the other tends to decrease.

As shown by the partial correlation results in the lower left frame of Figure 3-2, cumulative gas production due to corrosion under humid conditions is dominated by GRCORH (gas-generation rate for corrosion of steel under humid conditions), with cumulative gas production showing a strong tendency to increase as GRCORH increases. In addition, cumulative gas production due to corrosion under humid conditions tends to increase as STOICMIC (stoichiometric coefficient for microbial degradation of cellulosics) increases and tends to decrease as BRSAT (initial brine saturation of waste) and STOICCOR (stoichiometric factor for corrosion of steel) increase. The positive effect for STOICMIC results from increased gas generation due to microbial degradation of cellulosics, with a resultant increase in the amount of repository pore space that is filled with gas (i.e., humid conditions) rather than with brine (i.e., inundated conditions). The negative effect for STOICCOR results because increasing STOICCOR increases the proportion of low-gas-producing reactions in the corrosion process. The negative effect for BRSAT results because there is a fixed amount of steel in the repository for each sample element. Increasing BRSAT increases the amount of this steel that will be consumed by corrosion under inundated conditions, with the result that the amount of gas that can be produced by corrosion under humid conditions is reduced. The partial correlation coefficients for GRCORH are very close to 1, with the result that STOICMIC, STOICCOR and BRSAT are actually making relatively small contributions to the uncertainty in gas generation due to corrosion under humid conditions.

As shown by the partial correlation results in the lower right frame of Figure 3-2, cumulative gas production due to corrosion under inundated conditions tends to increase as GRCORI (gas-generation rate for corrosion of steel under inundated conditions) and BRSAT (initial brine saturation of

waste) increase and tends to decrease as GRCORH (gas-generation rate for corrosion of steel under humid conditions) increases. The positive effects for GRCORI and BRSAT result because increasing GRCORI increases the rate at which gas is produced by corrosion under inundated conditions and increasing BRSAT increases the amount of steel that will be consumed by corrosion under inundated conditions. The negative effect for GRCORH results because the increased consumption of steel and brine by corrosion under humid conditions reduces the amount of gas that can be produced by the corrosion of steel under inundated conditions.

Stepwise regression analysis can also be used to analyze the cumulative gas production results shown in Figure 3-2. The two regression analyses shown in Table 3-2 are for cumulative gas production over 10,000 yr due to corrosion under humid and inundated conditions, respectively. Thus, these two regression analyses are for the gas production values appearing above 10,000 yr in the two upper frames of Figure 3-2. The regression analysis for gas production under humid conditions indicates a positive effect (i.e., a positive regression coefficient) for GRCORH (gas-generation rate for corrosion of steel under humid conditions), with this variable accounting for 81% of the uncertainty in gas production.

The regression analysis in Table 3-2 for gas production under inundated conditions did not identify any variables that satisfy the minimum condition to enter the regression model (i.e., an α-value of at least 0.02). Scatterplots of cumulative gas production over 10,000 yr due to corrosion under inundated conditions versus the individual variables in Table 3-2 show no obvious relationships.

Table 3-2. Stepwise Regression Analyses with Rank-Transformed Data for Cumulative Gas Production over 10,000 yr Due to Corrosion under Humid and Inundated Conditions.

Total Gas Production over 10,000 yr (Humid Corrosion)				Total Gas Production over 10,000 yr (Inundated Corrosion)			
Step[a]	Variable[b]	SRC[c]	R^{2d}	Step[a]	Variable[b]	SRC[c]	R^{2d}
1	GRCORH	0.90	0.81		No variables selected		

[a] Steps in stepwise regression analysis
[b] Variables listed in order of selection in regression analysis
[c] Standardized regression coefficients in final regression model
[d] Cumulative R^2 value with entry of each variable into regression model

3.3.2 Gas Generation Due to Microbial Degradation

A summary of the analysis results for gas generation due to microbial degradation is given in Figure 3-3. The upper two frames in Figure 3-3 show cumulative gas generation due to microbial degradation under humid and inundated conditions, respectively. As comparison with the corresponding plots in Figure 3-2 shows, gas generation due to microbial degradation is approximately 50% or less of gas generation due to corrosion. The range of cumulative gas generation shown in Figure 3-3 is slightly larger for inundated than for humid conditions.

The lower two frames in Figure 3-3 present sensitivity analysis results based on partial rank correlation coefficients as in Figure 3-2. For cumulative gas production under humid conditions, increasing each of STOICMIC (stoichiometric coefficient for microbial degradation of cellulosics), GRMICH (gas-generation rate due to microbial degradation of cellulosics under humid conditions) and VWOOD (fraction of total waste volume occupied by IDB combustible waste category) increases gas production and increasing BRSAT (initial brine saturation) decreases gas production. The positive effects for STOICMIC, GRMICH and VWOOD result because increasing STOICMIC increases the amount of gas produced per unit of cellulose consumed, increasing GRMICH increases the rate of microbial degradation under humid conditions, and increasing VWOOD increases the amount of cellulose available for microbial degradation. In contrast, increasing BRSAT decreases the amount of gas produced under humid conditions by increasing the amount of cellulosics that will be consumed under inundated conditions.

For cumulative gas production under inundated conditions, increasing each of STOICMIC (stoichiometric coefficient for microbial degradation of cellulosics), BRSAT (initial brine saturation) and GRMICI (gas-generation rate due to microbial degradation of cellulosics under inundated conditions) increases gas production. Increasing STOICMIC increases the amount of gas produced per unit of cellulose consumed; increasing BRSAT increases the amount of cellulose that will be consumed under inundated conditions, and increasing GRMICI increases the rate of microbial degradation under inundated conditions.

The two regression analyses in Table 3-3 are for cumulative gas production over 10,000 yr due to microbial degradation under humid and inundated conditions, respectively. Thus, these two regression analyses are for the gas-production values appearing above 10,000 yr in the two upper frames of Figure 3-3. For gas production under humid conditions, the variables STOICMIC (stoichiometric coefficient for microbial degradation of cellulosics) and GRMICH (gas generation rate due to microbial degradation

Cumulative Gas Production Due to Microbial Degradation of Cellulosics

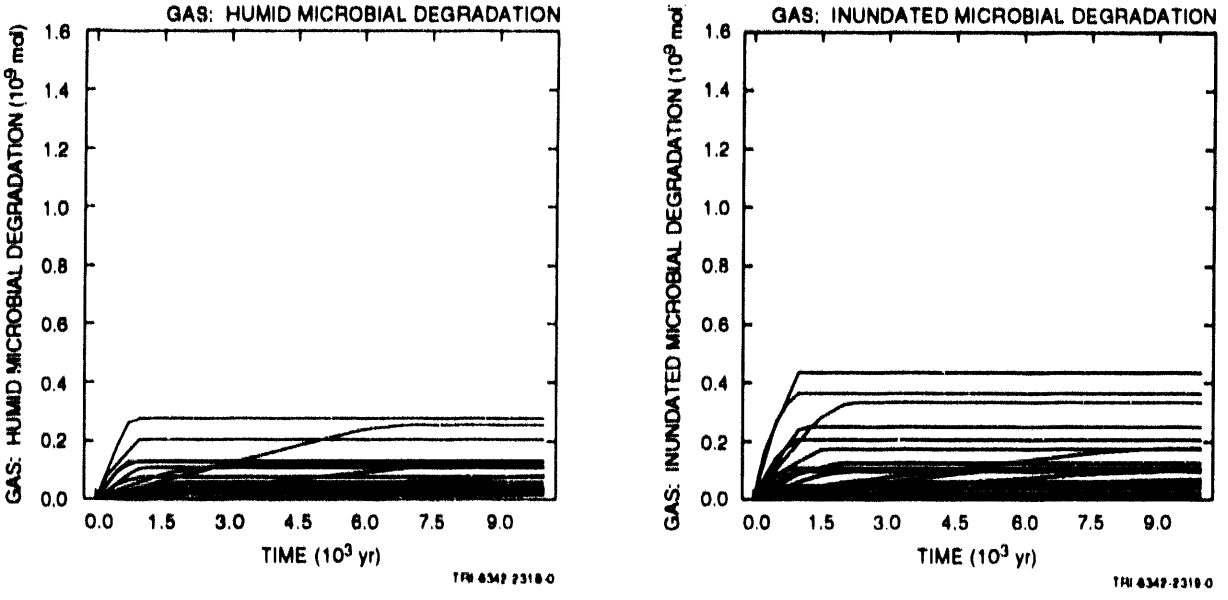

Partial Rank Correlation Coefficients for Cumulative Gas Production Due to Microbial Degradation of Cellulosics

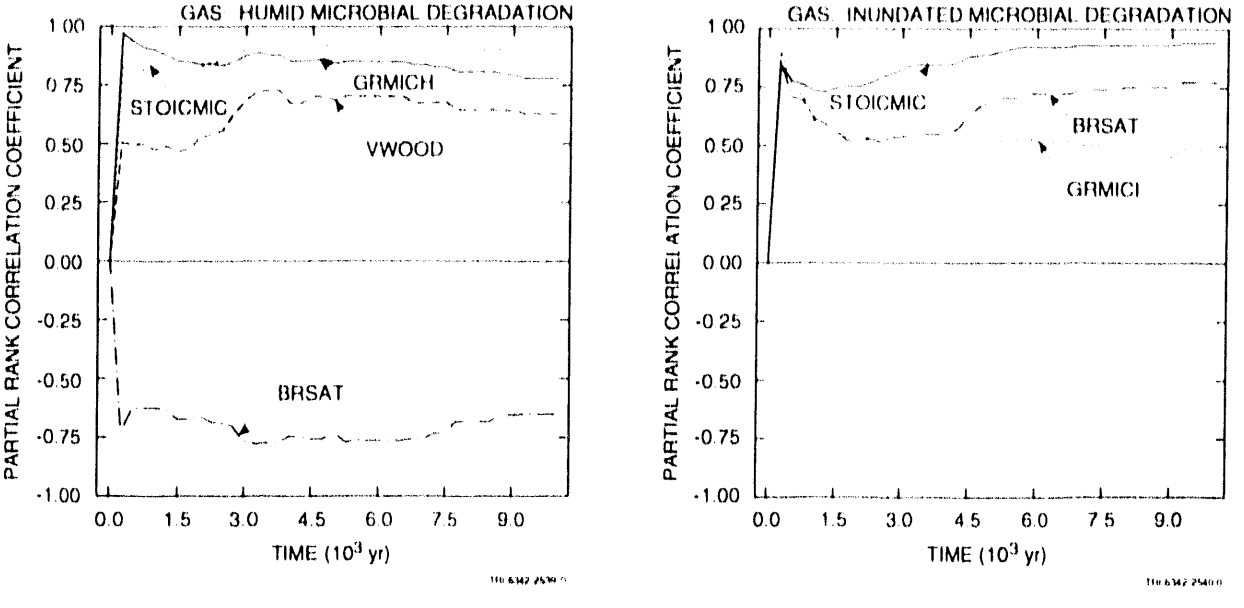

Figure 3-3. Uncertainty and sensitivity analysis results for gas generation due to microbial degradation of cellulosics under humid and inundated conditions.

Table 3-3. Stepwise Regression Analyses with Rank-Transformed Data for Cumulative Gas Production over 10,000 yr Due to Microbial Degradation under Humid and Inundated Conditions.

Total Gas Production over 10,000 yr (Humid Degradation)				Total Gas Production over 10,000 yr (Inundated Degradation)			
Step[a]	Variable[b]	SRC[c]	R^{2d}	Step[a]	Variable[b]	SRC[c]	R^{2d}
1	STOICMIC	0.69	0.57	1	STOICMIC	0.79	0.68
2	GRMICH	0.34	0.68	2	BRSAT	0.33	0.79
				3	GRCORH	-0.24	0.85

[a] Steps in stepwise regression analysis
[b] Variables listed in order of selection in regression analysis
[c] Standardized regression coefficients in final regression model
[d] Cumulative R^2 value with entry of each variable into regression model

of cellulosics under humid conditions) can account for 68% of the observed variability in gas production, with gas production tending to increase with increasing values for STOICMIC and GRMICH. For gas production under inundated conditions, the variables STOICMIC and BRSAT (initial brine saturation) can account for 79% of the observed variability in gas production, with gas production tending to increase as each of these variables increases. When the additional variable GRCORH (gas-generation rate for corrosion of steel under humid conditions) is added to the regression model, 85% of the variability in gas production can be accounted for, with gas production tending to decrease as GRCORH increases because increased gas production tends to decrease the fraction of the pore volume that is filled with brine and hence reduce the amount of microbial degradation that takes place under inundated conditions.

3.3.3 Total Gas Production

The upper two frames in Figure 3-4 show total gas production due to corrosion and microbial degradation and were obtained by combining the corresponding results in Figures 3-2 and 3-3 for gas production under humid and inundated conditions. Typically, low gas production under humid conditions is associated with higher gas production under inundated conditions and vice versa. As a result, the gas-production curves in Figure 3-4 tend to lie farther above the abscissa than many of the individual curves in Figures 3-2 and 3-3 Overall, the gas production due to corrosion tends to be about twice the gas production due to microbial degradation. Gas production due to microbial degradation has more curves

Cumulative Gas Production

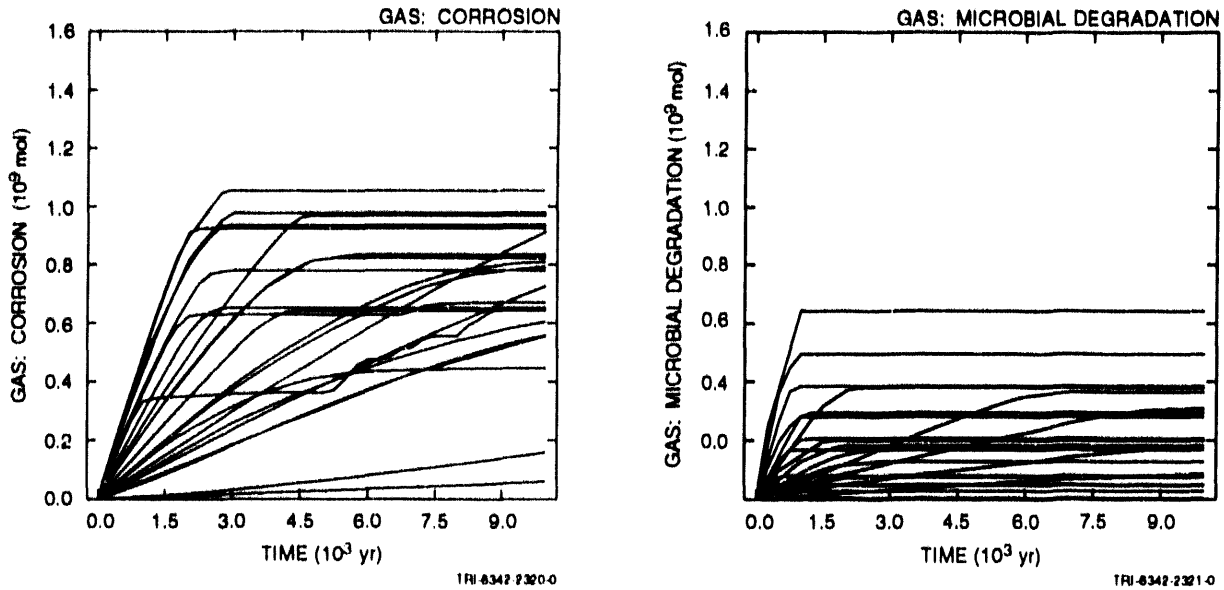

Partial Rank Correlation Coefficients for Cumulative Gas Production

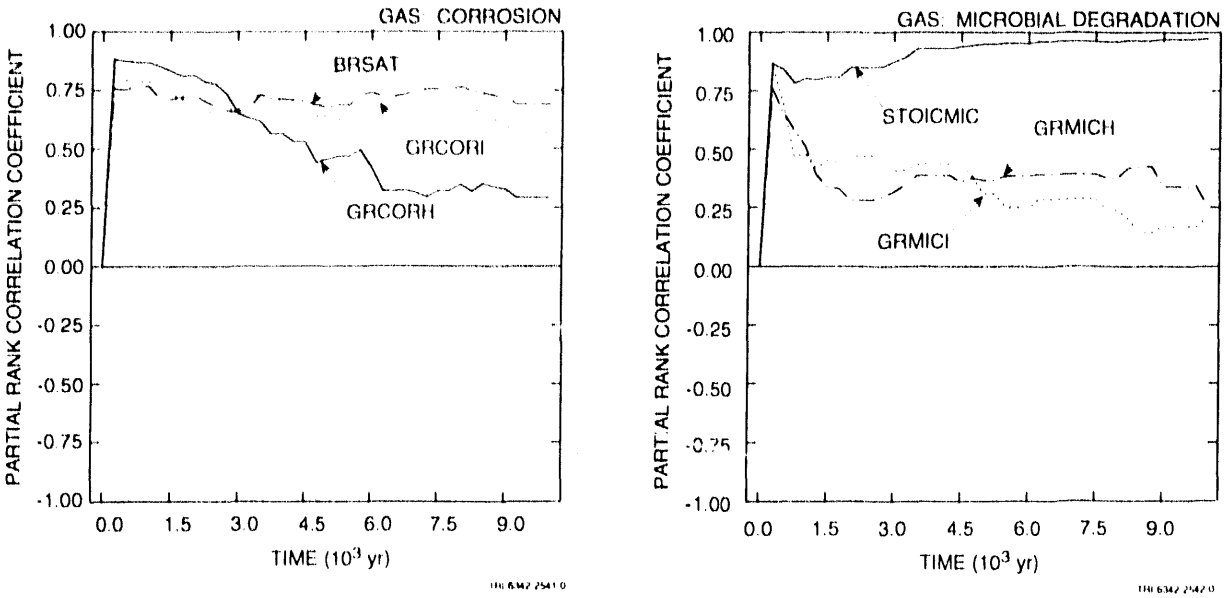

Figure 3-4. Uncertainty and sensitivity analysis results for gas generation due to corrosion of steel and microbial degradation of cellulosics.

close to zero than gas production due to corrosion due to the assignment of a range of possible values for STOICMIC (stoichiometric coefficient for microbial degradation of cellulosics) that extends to zero, which results in no gas generation due to microbial degradation.

The lower two frames in Figure 3-4 present sensitivity analysis results based on partial rank correlation coefficients as in Figure 3-2. For cumulative gas production due to corrosion, increasing each of GRCORI (gas-generation rate for corrosion of steel under inundated conditions), GRCORH (gas-generation rate for corrosion of steel under humid conditions) and BRSAT (initial brine saturation) tends to increase gas production. Increasing GRCORI, GRCORH and BRSAT tends to increase the rate of gas production and hence cumulative gas production, with this effect becoming less important at later times due to exhaustion of either steel or brine in the waste panels.

The dominant variable for cumulative gas production due to microbial degradation is STOICMIC (stoichiometric coefficient for microbial degradation of cellulosics), which has an increasingly important positive effect with time and ultimately dominates the variability in cumulative gas production. The variables GRMICI (gas-generation rate due to microbial degradation of cellulosics under inundated conditions) and GRMICH (gas-generation rate due to microbial degradation of cellulosics under humid conditions) also have positive effects at early times and then decrease in importance.

The two regression analyses in Table 3-4 are for cumulative gas production over 10,000 yr due to corrosion and microbial degradation, respectively. Thus, these two regression analyses are for the gas production values appearing above 10,000 yr in the two upper frames of Figure 3-4. The regression analysis for gas production due to corrosion selected the variables GRCORI (gas-generation rate for corrosion of steel under inundated conditions) and BRSAT (initial brine saturation), with GRCORI and BRSAT each having a positive effect on gas production. However, the resolution in the regression model is low, with GRCORI and BRSAT accounting for only 55% of the variability in gas production due to corrosion.

To provide additional insight, Figure 3-5 presents selected scatterplots displaying the relationships between individual sampled variables and total gas production over 10,000 yr due to corrosion. As examination of these plots shows, gas production tends to increase as BRSAT (initial brine saturation) and GRCORI (gas generation rate due to corrosion

Table 3-4. Stepwise Regression Analysis with Rank-Transformed Data for Total Gas Production Due to Corrosion and Total Gas Generation Due to Microbial Degradation.

Total Gas Production over 10,000 yr (Corrosion)				Total Gas Production over 10,000 yr (Microbial-Degradation)			
Step[a]	Variable[b]	SRC[c]	R^{2d}	Step[a]	Variable[b]	SRC[c]	R^{2d}
1	GRCORI	0.56	0.32	1	STOICMIC	0.95	0.91
2	BRSAT	0.48	0.55				

[a] Steps in stepwise regression analysis
[b] Variables listed in order of selection in regression analysis
[c] Standardized regression coefficients in final regression model
[d] Cumulative R^2 value with entry of each variable into regression model

of steel under inundated conditions) increase and tends to decrease as STOICCOR (stoichiometric factor for corrosion of steel) increases. However, there is a large amount of variability around these trends. These patterns are consistent with the signs of the regression coefficients and low R^2 values for GRCORI and BRSAT in Table 3-4. The plots in Figure 3-5 show the best-defined patterns of the 16 scatterplots associated with total gas production over 10,000 yr due to corrosion (i.e., one scatterplot for each variable in Table 3-1). Thus, no one variable is exerting a dominant influence on total gas production due to corrosion. However, the actual uncertainty in total gas production due to corrosion is rather small in this analysis, with most values falling between 0.4×10^9 and 1.0×10^9 mol.

The regression analysis in Table 3-4 for gas production due to microbial degradation identified only the variable STOICMIC (stoichiometric coefficient for microbial degradation of cellulosics). However, STOICMIC was able to account for 91% of the observed variability.

The cumulative gas production due to corrosion and to microbial degradation can be combined to produce total gas production as shown in the upper frame of Figure 3-6. Most sample elements result in a total gas production over 10,000 yr between 5×10^8 and 1.2×10^9 mol. Also, most sample elements show a period of rapid gas production in the first few thousand years, with considerably reduced rates of gas production at later times. As examination of the two upper frames in Figure 3-7 shows, the

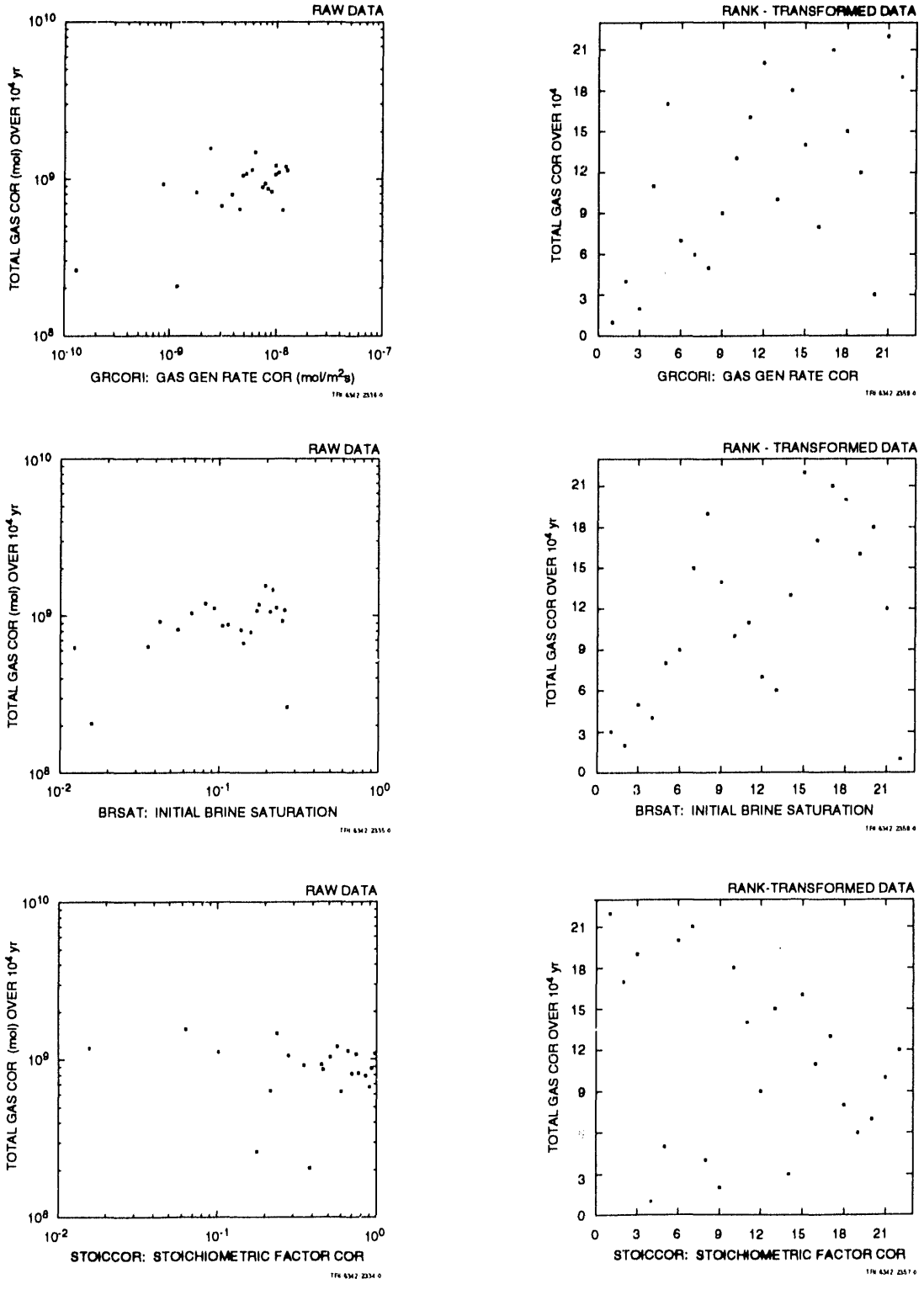

Figure 3-5. Scatterplots relating cumulative gas production over 10,000 yr due to corrosion to GRCORI (gas-generation rate due to corrosion of steel under inundated conditions), BRSAT (initial brine saturation) and STOICCOR (stoichiometric factor for corrosion of steel).

Cumulative Gas Production

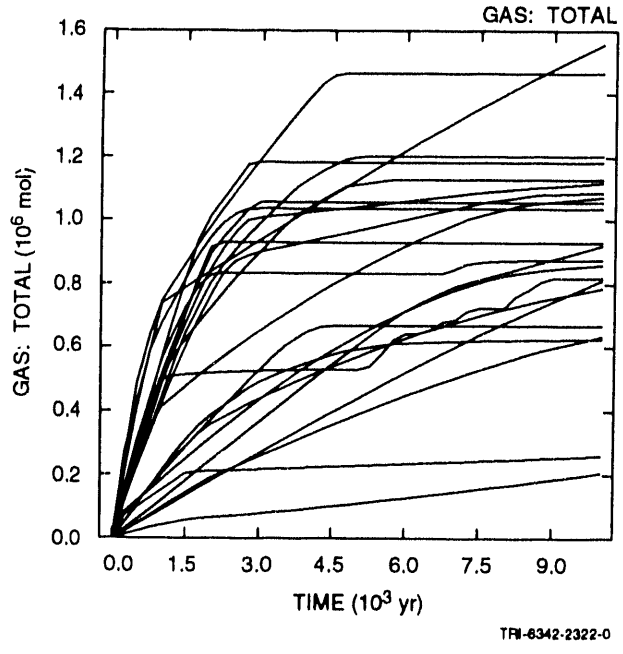

Partial Rank Correlation Coefficients for Cumulative Gas Production

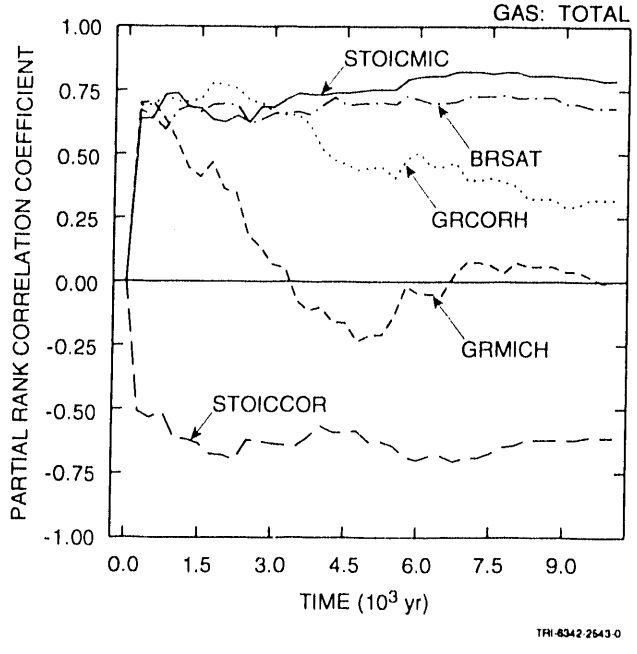

Figure 3-6. Uncertainty and sensitivity analysis results for total gas production (i.e., both corrosion of steel and microbial degradation of cellulosics).

Steel and Cellulosic Inventories

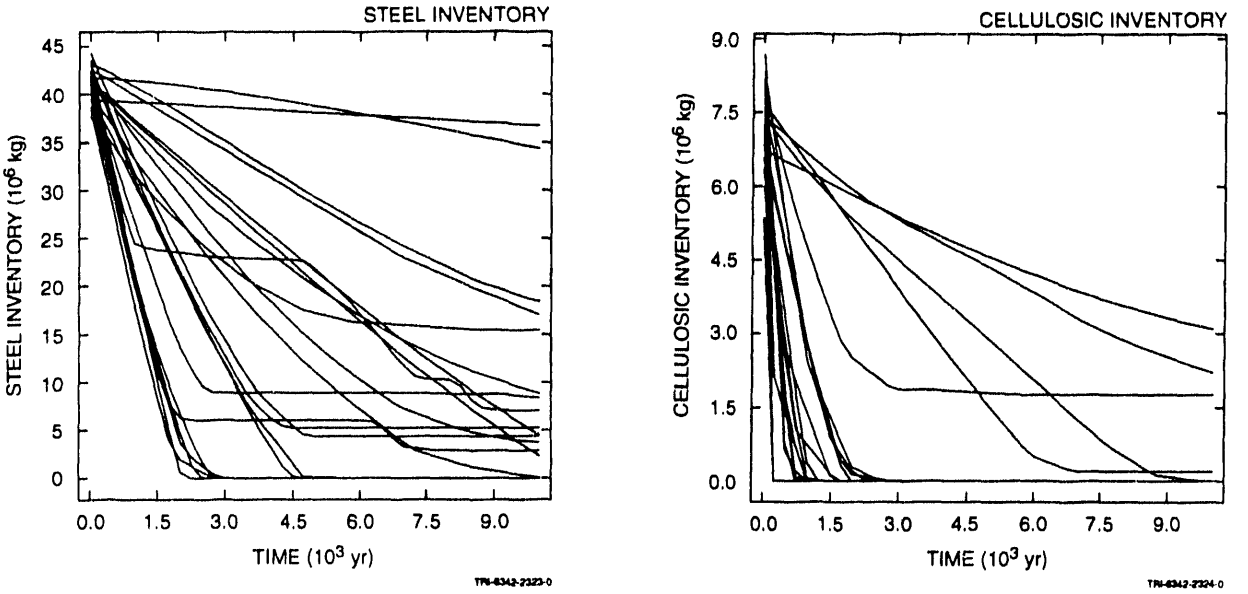

Partial Rank Correlation Coefficients for Steel and Cellulosic Inventories

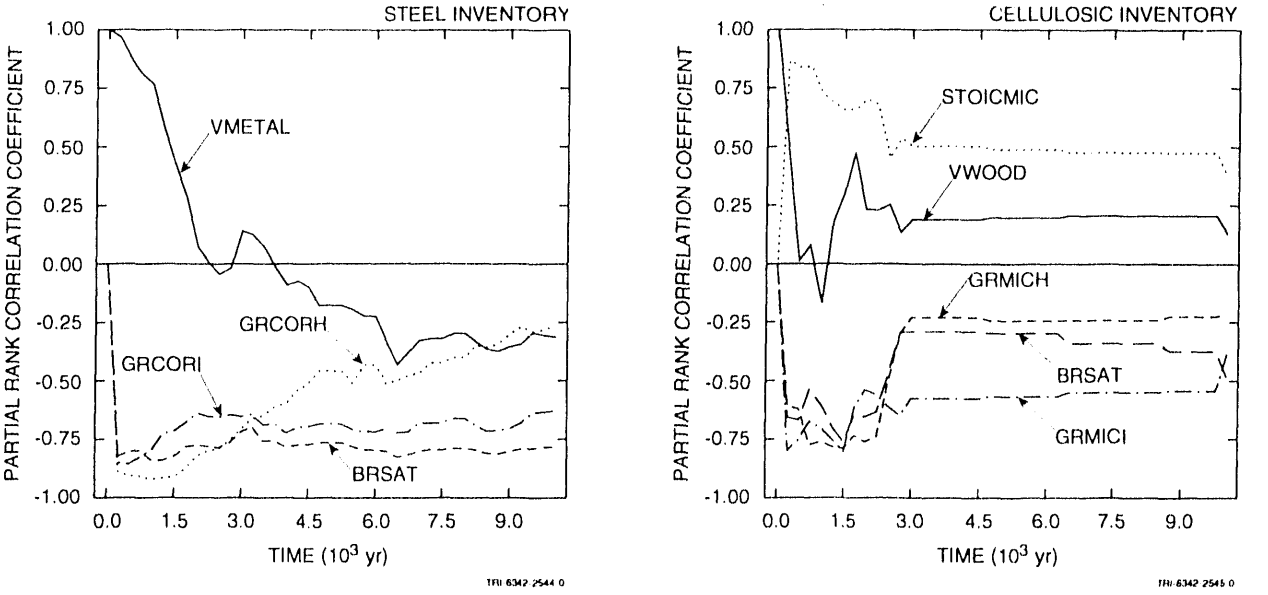

Figure 3-7. Uncertainty and sensitivity analysis results for steel and cellulosic inventories in waste panel.

inventory of steel and cellulosics is often exhausted or significantly depleted after the first few thousand years.

The lower frame in Figure 3-6 presents sensitivity analysis results based on partial rank correlation coefficients for total gas production. Positive effects are indicated for GRCORH (gas-generation rate for corrosion of steel under humid conditions), GRMICH (gas-generation rate for microbial degradation of cellulosics under humid conditions), STOICMIC (stoichiometric coefficient for microbial degradation of cellulosics) and BRSAT (initial brine saturation), and negative effects are indicated for STOICCOR (stoichiometric factor for corrosion of steel). For the entire 10,000-yr period, the most important variables are STOICMIC, BRSAT and STOICCOR.

The regression analysis in Table 3-5 is for cumulative gas production over 10,000 yr due to both corrosion and microbial degradation. The only variable selected in the analysis is STOICMIC (stoichiometric coefficient for microbial degradation of cellulosics), which has a positive regression coefficient and can account for 33% of the variability in total gas production. The indicated effect for STOICMIC is consistent with its dominant influence on gas generation due to microbial degradation as indicated in Figure 3-3 and Table 3-3. As for cumulative gas production over 10,000 yr due to corrosion, the examination of scatterplots indicates that no single variable exerts a dominant influence on cumulative gas production due to corrosion and microbial degradation.

As previously indicated, the upper two frames in Figure 3-7 show the time-dependent steel and cellulosic inventories associated with the individual sample elements. The lower two frames present sensitivity analyses based on partial rank correlation coefficients. The steel inventory is initially dominated by VMETAL (fraction of total waste volume occupied by IDB metals and glass category), with the importance of this variable decreasing with time. The variables GRCORI (gas-generation rate for corrosion of steel under inundated conditions), GRCORH (gas-generation rate for corrosion of steel under humid conditions) and BRSAT (initial brine saturation) have negative effects on the steel inventory. The negative relationships involving GRCORI, GRCORH and BRSAT result from their effects on increasing the rate of corrosion.

The cellulosic inventory is initially dominated by VWOOD (fraction of total waste volume that is occupied by IDB combustible waste category), with the importance of this variable decreasing rapidly with time. An additional positive effect is indicated for STOICMIC (stoichiometric coefficient for microbial degradation of cellulosics). Increasing STOICMIC tends to increase gas production and thus increase the fraction of the

Table 3-5. Stepwise Regression Analysis with Rank-Transformed Data for Total Gas Production Over 10,000 yr Due to Both Corrosion and Microbial Degradation.

	Total Gas Production over 10,000 yr (Corrosion and Biodegradation)		
Step[a]	Variable[b]	SRC[c]	R^{2d}
1	STOICMIC	0.57	0.33

[a] Steps in stepwise regression analysis
[b] Variables listed in order of selection in regression analysis
[c] Standardized regression coefficients in final regression model
[d] Cumulative R^2 value with entry of each variable into regression model

waste panel pore volume that is filled with gas; in turn, this reduces the rate at which cellulose is consumed by microbial degradation. Negative effects are indicated for GRMICI (gas-generation rate due to microbial degradation of cellulosics under inundated conditions), GRMICH (gas generation rate due to microbial degradation of cellulosics under humid conditions) and BRSAT (initial brine saturation), with increasing values for each of these variables tending to increase the rate at which cellulose is consumed by microbial degradation. At times greater than 3000 yr, the cellulose inventory is completely depleted for most sample elements, with the result that the calculated partial correlation coefficients have little meaning due to the large number (i.e., 17 out of 22) of zeros involved.

3.3.4 Gas Saturation and Pressure in Waste Panel

Time-dependent values for average gas saturation in the individual waste blocks (i.e., averaged over entire waste block) are presented in the left column of Figure 3-8. Although gas saturation initially decreases for some sample elements, the overall tendency is for gas saturation to increase towards an asymptote with increasing time. The gas saturations in Waste Block A tend to be lower than those in Waste Blocks C and B. As shown in Figure 3-1, Waste Block A is adjacent to the shaft and hence loses more gas by flow up the shaft than Waste Blocks C and B. As the partial rank correlation coefficients for gas saturation in the right column of Figure 3-8 show for all three waste blocks, increasing GRCORH (gas-generation rate for corrosion of steel under humid conditions) and GRMICI (gas generation rate due to microbial degradation of cellulosics under inundated conditions) tends to increase gas saturation and increasing BRSAT (initial brine saturation) tends to decrease gas saturation, with these

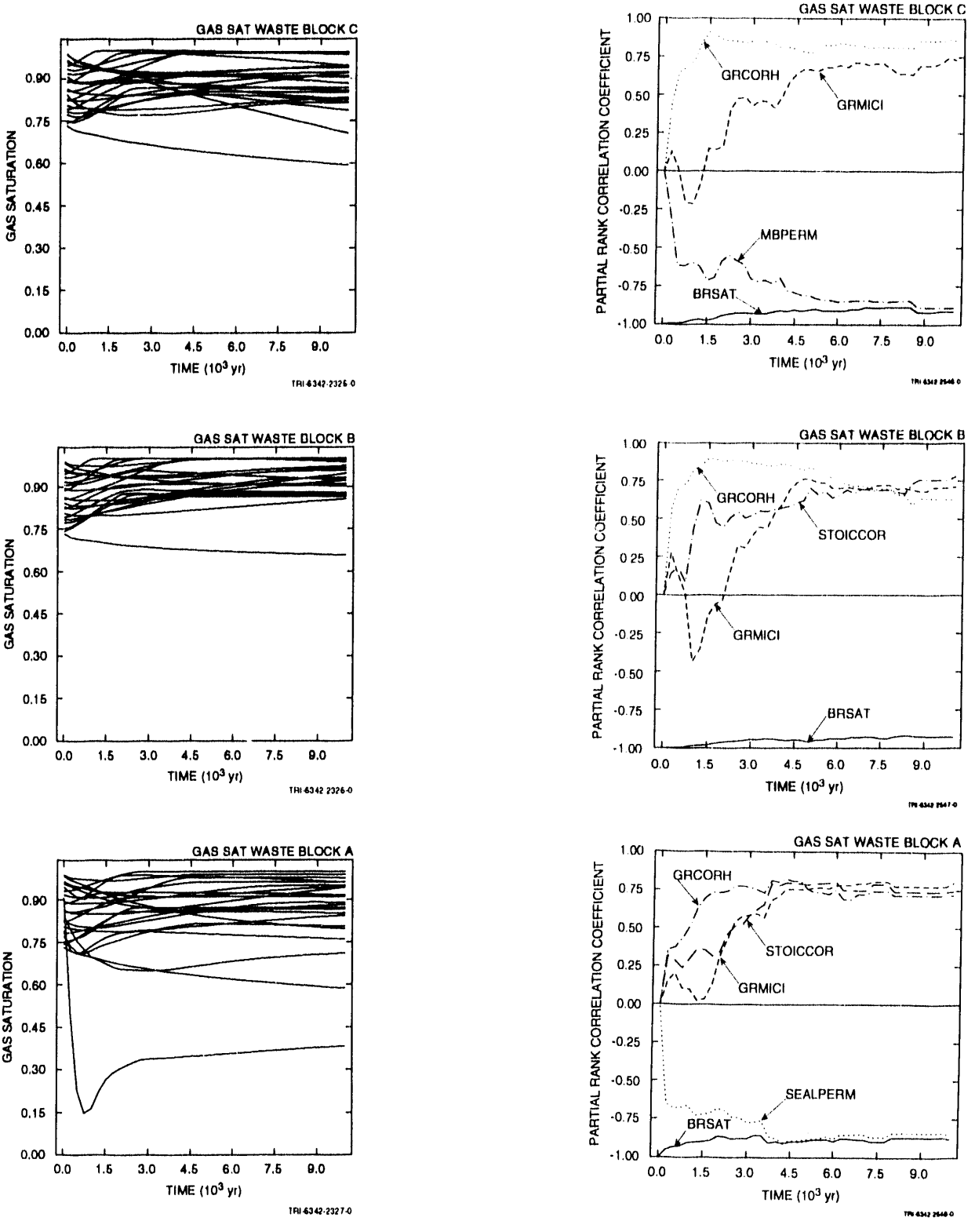

Figure 3-8. Uncertainty and sensitivity analysis results for gas saturation in individual waste blocks.

effects resulting because increasing GRCORH and GRMICI increases the amount of gas in the panel and increasing BRSAT increases the amount of brine in the panel.

For Waste Block C, a negative effect is also indicated for MBPERM (marker bed permeability), with this effect occurring because increasing MBPERM increases the rate at which brine flows into Waste Block C from anhydrite layers in the Salado Formation. Due to the structure of the computational grid shown in Figure 3-1, most inflowing brine enters the repository through Waste Block C. In addition, the variable STOICCOR (stoichiometric factor for corrosion of steel) appears in the analysis for gas saturation in Waste Block B. As discussed at the end of this section, increasing STOICCOR decreases the initial pore volume in the repository. Since the initial amount of brine is set as a fraction of the pore volume, increasing STOICCOR also reduces the amount of brine initially present in the pore space of the repository. Thus, as constant gas generation rates are assumed in this analysis, the total brine inventory can be depleted more rapidly when STOICCOR is large than when STOICCOR is small (i.e., because large values for STOICCOR result in less brine being initially present). This relationship between STOICCOR and amount of brine initially present in the repository is resulting in the positive correlations between STOICOR and gas saturation in Waste Block B and also in Waste Block A. This relationship is an artifact of the manner in which initial repository pore volume was set in an attempt to incorporate the competing effects of gas generation and waste panel closure due to salt creep.

As shown in the left column of Figure 3-9, time-dependent gas pressure in the individual waste blocks tends to increase monotonically until a maximum is reached and then undergoes a slower monotonic decrease. The largest gas pressures are approximately 2 MPa above the lithostatic pressure of 14.8 MPa. The gas pressures in the three waste blocks are quite similar. As comparison of the left column in Figures 3-8 and 3-9 shows, there is more variability in gas saturation between the waste blocks than in gas pressure. Thus, gas appears to be flowing between the waste blocks to a greater extent than brine.

The partial rank correlation coefficients for gas pressure in the right column of Figure 3-9 indicate that SEALPERM (permeability of seals between waste panels) and SH2PERM (middle shaft section permeability) are

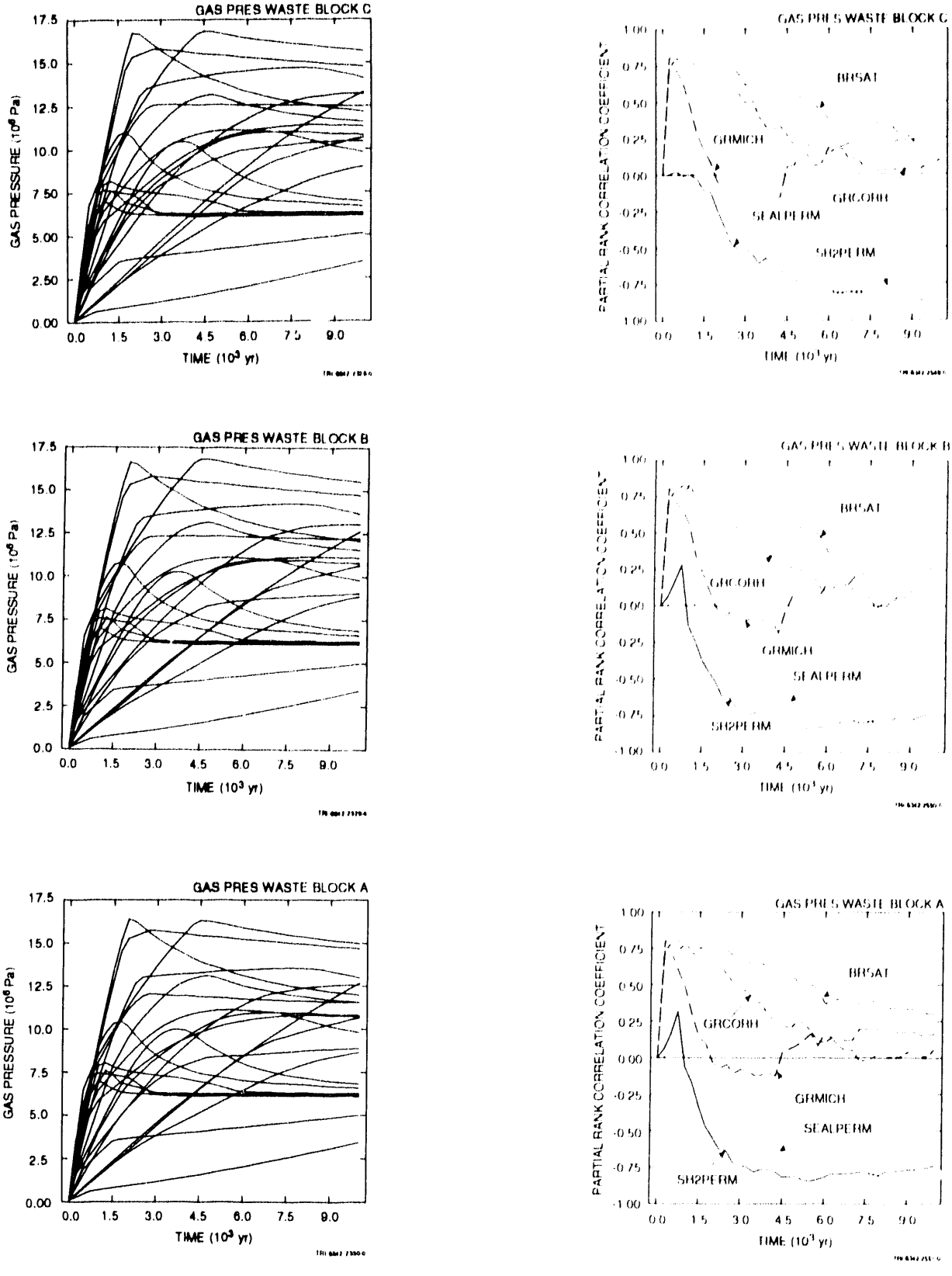

Figure 3-9. Uncertainty and sensitivity analysis results for gas pressure in individual waste blocks.

the two most important variables influencing gas pressure, with gas pressure tending to decrease as each of these variables increases. Prior to 5000 yr, gas pressure tends to increase as the variables GRCORH (gas-generation rate for corrosion of steel under humid conditions), GRMICH (gas-generation rate for microbial degradation of cellulosics under humid conditions) and BRSAT (initial brine saturation) increase due to the influence of these variables on increasing gas production. However, as shown in Figure 3-4, most gas production is over by 5000 yr, with the result that gas pressure is then controlled by variables such as SEALPERM and SH2PERM that influence gas flow out of the waste blocks.

The 1991 WIPP preliminary performance assessment did not directly model closure of the waste panels. However, possible interaction of gas generation and panel closure was incorporated into the analysis by setting the initial pore volume in a waste panel to the volume necessary to contain all waste-generated gas at lithostatic pressure (i.e., 14.8 MPa). As a result, initial pore volume is a function of STOICCOR (stoichiometric factor for corrosion of steel), STOICMIC (stoichiometric coefficient for microbial degradation of cellulosics), VMETAL (fraction of total waste volume occupied by IDB metals and glass waste category) and VWOOD (fraction of total waste volume occupied by IDB combustible waste category). As shown by the upper frame in Figure 3-10, pore volume remains essentially fixed at its initial volume, although there is a small response to changing gas pressures through rock compressibility effects. Further, the partial rank correlation coefficients in the lower frame of Figure 3-10 indicate that pore volume is indeed a function of STOICCOR, STOICMIC, VMETAL and VWOOD.

3.3.5 Gas Migration

A primary focus of the studies contained in this report is the migration of gas away from the waste panels. For Case 2, this means gas migration through the shaft to the Culebra Dolomite. As shown by the upper two frames in Figure 3-11, most gas leaving the repository does indeed flow up the shaft to the Culebra Dolomite.

Sensitivity analysis results based on partial rank correlation coefficients for cumulative gas flow out of the repository are given in the lower left frame of Figure 3-11. These results indicate that total gas flow out of the repository tends to increase with increasing gas generation and decreasing resistance to gas flow. In particular, gas outflow increases as BRSAT (initial brine saturation), GRCORI (gas-generation rate for corrosion of steel under inundated conditions) and GRCORH (gas-generation rate for corrosion of steel under humid conditions)

Total Pore Volume in Repository

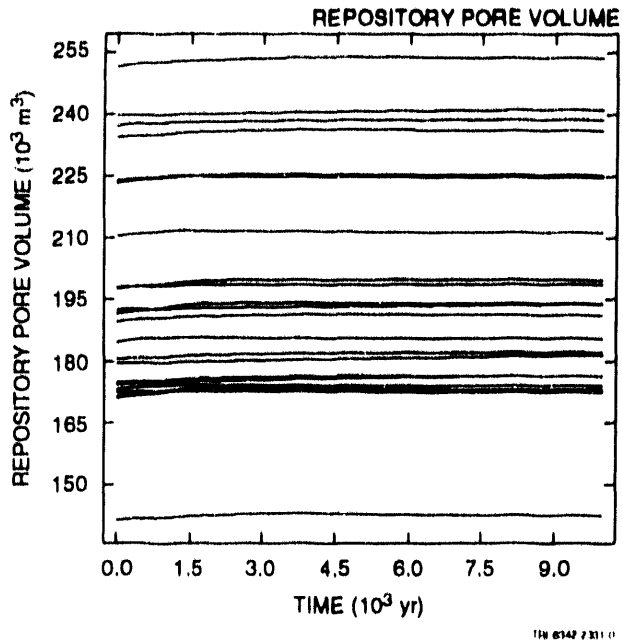

Partial Rank Correlation Coefficients for Total Pore Volume in Repository

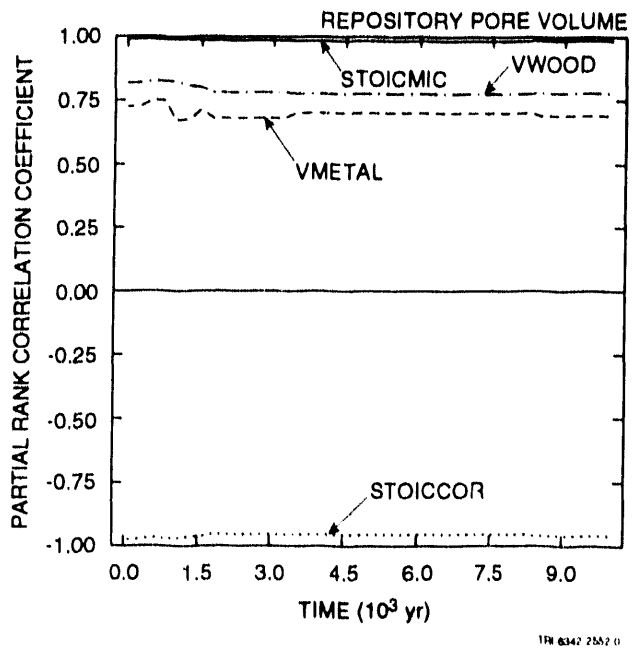

Figure 3-10. Uncertainty and sensitivity analysis results for total pore volume in repository.

Cumulative Gas Flows out of Repository and through Shaft to Culebra Dolomite.

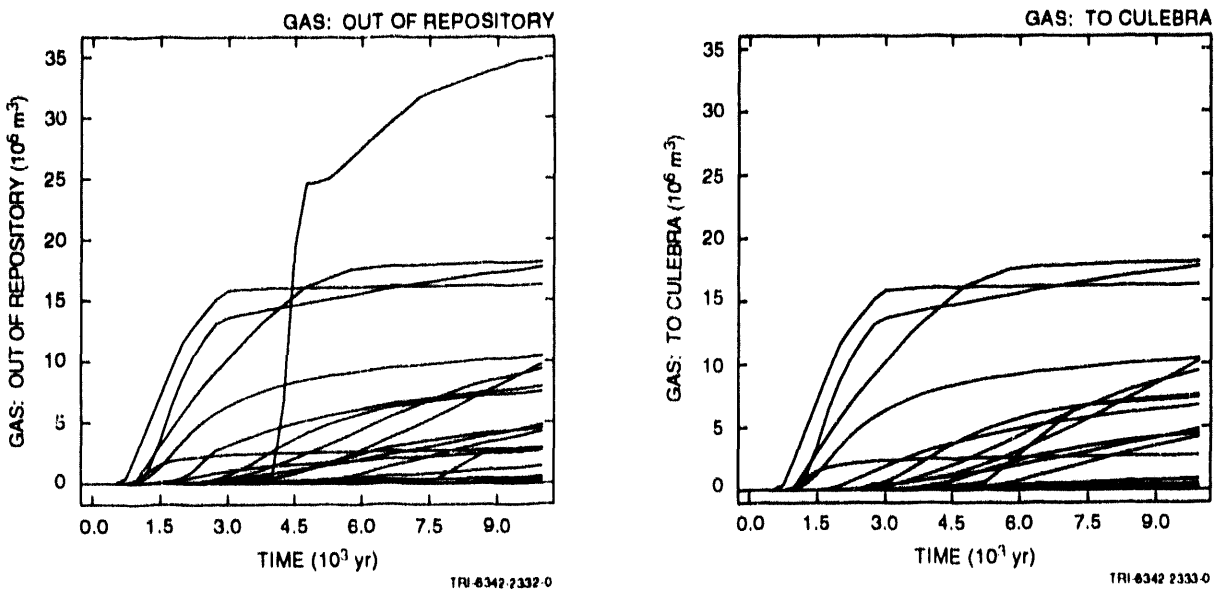

Partial Rank Correlation Coefficients for Cumulative Gas Flows out of Repository and through Shaft to Culebra Dolomite

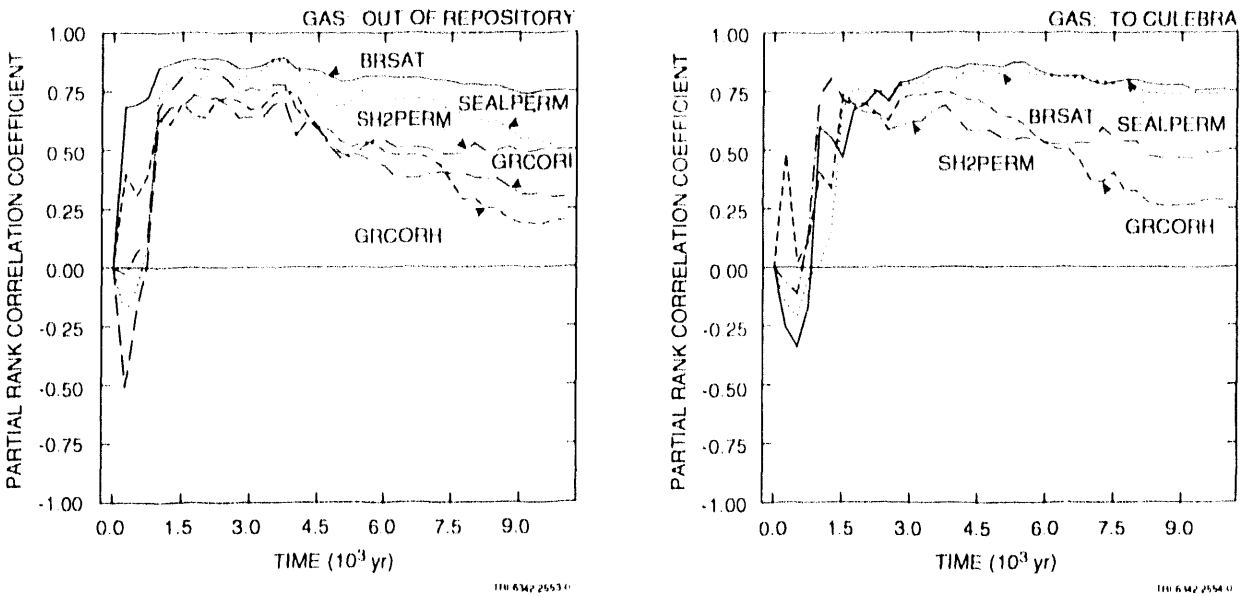

Figure 3-11. Uncertainty and sensitivity analysis results for cumulative gas flow out of repository and through shaft to Culebra Dolomite.

increase due to the effect of these variables on increasing gas generation, and gas outflow increases as SEALPERM (permeability of seals between waste panels) and SH2PERM (permeability of middle shaft section) increase due to decreased resistance to gas flow.

The sensitivity analysis results for cumulative gas flow through the shaft to the Culebra Dolomite appear in the lower right of Figure 3-11. As examination of the partial rank correlation coefficients in this frame shows, the analysis is initially unstable with wide swings in the values for these coefficients. This instability results from the fact that many of the releases to the Culebra Dolomite are 0 at early times (i.e., < 1500 yr), with the result that the analysis results are dominated by random noise for the first 1500 yr (e.g., changing from 19 zeros out of 22 observations to 18 zeros out of 22 observations can cause large, but meaningless, swings in the values for the partial correlation coefficients). After about 3000 yr, the effects of the individual variables are clearer, with positive effects indicated for variables that increase gas generation (i.e., BRSAT and GRCORH) and decrease resistance to gas flow (i.e., SEALPERM and SH2PERM). However, four sample elements result in no release to the Culebra, which tends to reduce the effectiveness of partial correlation coefficients in identifying the effects of individual variables.

When zero observations and possibly other patterns of behavior are present, the examination of scatterplots can help reveal the relationships between sampled and calculated variables. The scatterplots for cumulative gas flow through the shaft to the Culebra Dolomite over 10,000 yr versus five individual variables are shown in Figure 3-12. These variables were selected as having the strongest relationships with cumulative gas flow through the shaft to the Culebra Dolomite on the basis of a visual examination of the scatterplots for the 16 variables defined in Table 3-1. Although all the scatterplots show a positive relationship between the sampled variable and cumulative gas flow, none of the relationships are very tight. Further, the four zero releases are scattered over the range of each sampled variable. Thus, no single variable appears to dominate cumulative gas release to the Culebra. As shown in Eq. 3-1, the shaft seal permeabilities SH1PERM, SH2PERM and SH3PERM are correlated, and only the middle shaft permeability SH2PERM was included in the partial correlation analysis.

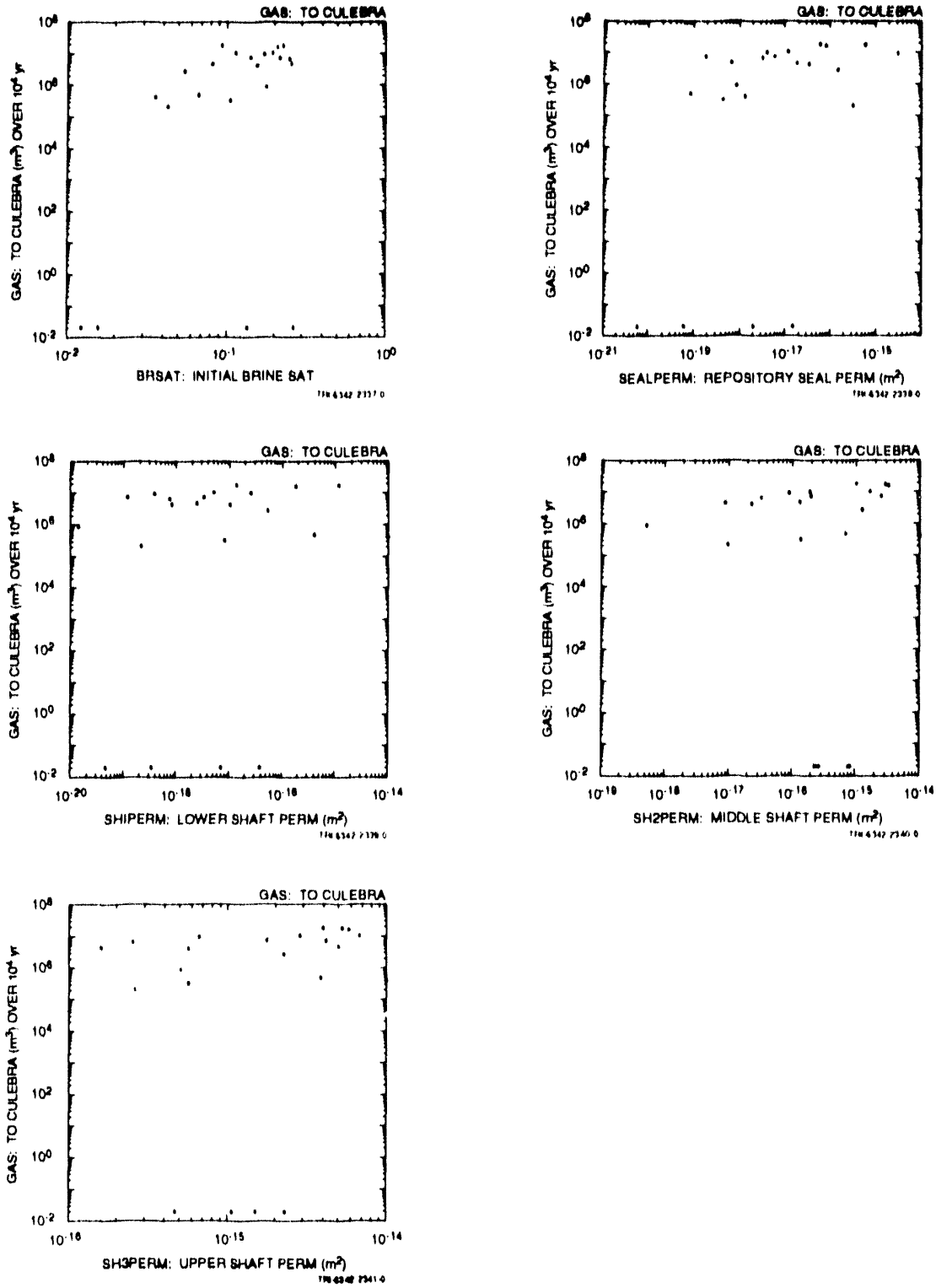

Figure 3-12. Scatterplots for cumulative gas flow over 10,000 yr through the shaft to the Culebra Dolomite for the following sampled variables: BRSAT (initial brine saturation), SEALPERM (permeability of seals between waste blocks in repository), SH1PERM (permeability of lower shaft section), SH2PERM (permeability of middle shaft section) and SH3PERM (permeability of upper shaft section).

Very little brine migration away from the waste panels occurred in this analysis case. Of the 22 sample elements used in this analysis, only 4 resulted in brine migration away from the waste panels.

As previously noted, the analysis results contained in this section were obtained under the assumption that the pore space in the shaft was initially gas-filled. The results obtained with this assumption are similar to, but not identical with, the results obtained under the assumption that the pore space in the shaft is initially brine-filled. For example. the scatterplot of cumulative gas flow to the culebra over 10,000 yr (on a linear scale) versus SH1PERM (permeability of lower shaft section) (on a logarithmic scale) for the initially gas-filled shaft is given in Figure 3-13. The corresponding scatterplot for the initially brine-filled shaft is given in Figure 5-1 of WIPP PA, 1992. As comparison of these two scatterplots shows, the two assumptions do indeed lead to similar, but not identical, results.

3.4 Discussion

The inventories of steel and cellulosics are substantially consumed by corrosion and microbial degradation for most sample elements. Variables affecting gas generation rates are important for gas production at early times but not for gas production over the entire 10,000 yr period under consideration. Overall, the most important variables for total gas production are the two stoichiometric terms and initial brine saturation.

The analyses often produce brine saturations that are below residual brine saturation when averaged over entire waste blocks. Thus, there are significant regions within the individual waste panels in which brine flow will not take place. Under such conditions, radionuclides cannot be transported from these regions by flowing brine.

Pressures in the waste blocks typically remained below lithostatic pressure (i.e., 14.8 MPa). However, this may be primarily due to an analysis assumption made to resolve the competing effects of gas pressurization of the waste panels and compaction of the waste due to overburden pressure.

Gas flow to the Culebra resulted for 18 of the 22 sample elements used in the analysis. Thus, the sealing system modeled in this analysis does not prevent gas flow to the Culebra. The dominant variables with respect to such flow were initial brine saturation in the waste, permeability of seals between waste blocks, and permeability of seals in the shaft. In contrast,

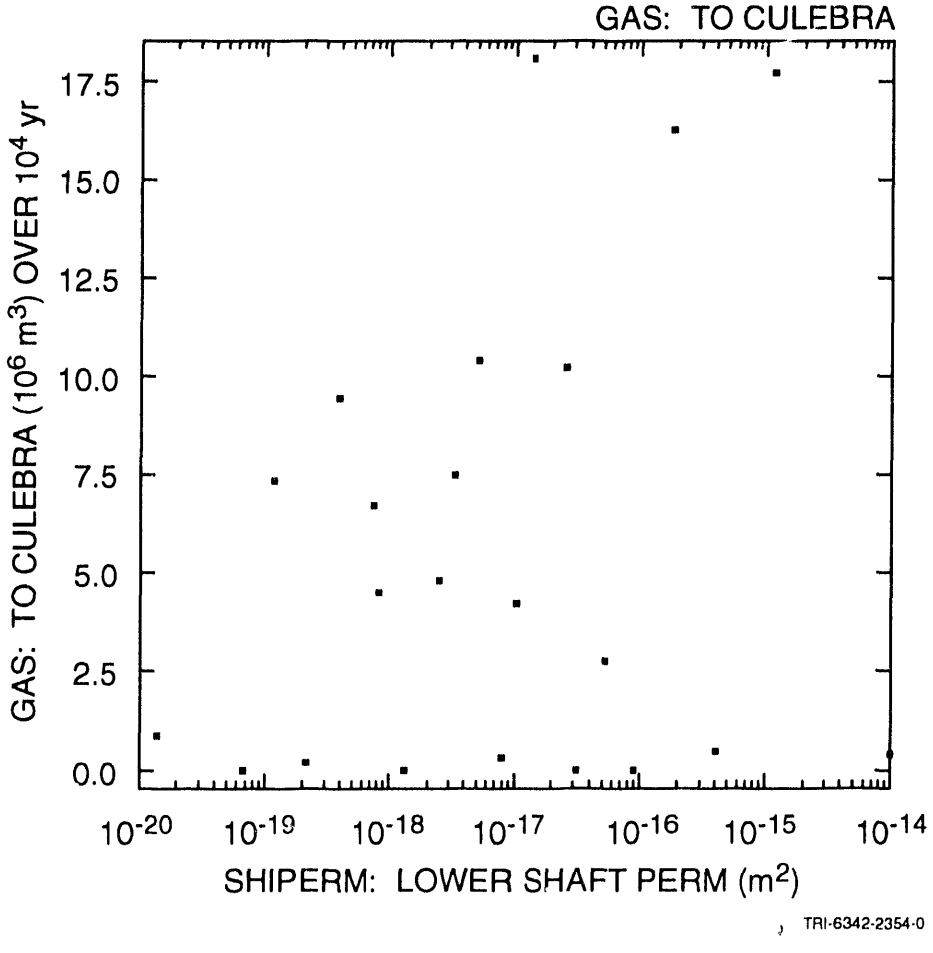

Figure 3-13. Scatterplot for cumulative gas flow over 10,000 yr through the shaft to the Culebra Dolomite versus SH1PERM (permeability of lower shaft section). The results in this figure and elsewhere in this section were generated with the assumption that the pore space in the shaft is initially gas-filled.

brine flow away from the waste panels occurred for only 4 of the 22 sample elements. The importance of panel seal permeability results in part from the assumption that the disturbed rock zone permeability is sufficiently low to prevent significant quantities of gas from bypassing the panel seals.

The analysis for Case 2 used a Latin hypercube sample of size 22 from 16 imprecisely known variables. Comparison of analysis results with those obtained with Case 1, which used a sample of size 60 from 14 variables, suggests that use of a somewhat larger sample size would have produced better-defined results. However, it is unlikely that any of the insights obtained in the analysis would change significantly.

No errors in the implementation or operation of BRAGFLO were observed.

4. CASE 3: PERMEABLE SHAFT WITHOUT PANEL SEALS

4.1 Summary Description*

Case 3 differs from Case 2 in the following aspects: (1) the inclusion of the experimental area north of the shaft to account for the additional volume available for gas storage, (2) the inclusion of anhydrite Marker Bed 138 above Anhydrite Layers A and B (see Figure 1-4 of WIPP PA, 1992), (3) the expansion of the disturbed rock zone to include the region around the experimental area, (4) the inclusion of a transition zone with material properties intermediate between those of the disturbed rock zone and the intact Salado Formation, (5) the definition of a single region containing the 10 waste panels and another region containing the seals and backfill, and (6) the inclusion of a single, 10-m shaft seal above Marker Bed 138. The shaft seal design was chosen jointly by the WIPP Performance Assessment Department and the Repository Isolation Systems Department at SNL and is included in the analysis to provide insights on the potential effectiveness of very high-quality, and hence expensive, low-permeability seals emplaced over short distances. The current concept for shaft seals relies on long regions of conventionally emplaced and compacted crushed salt, comparable to the system modeled for Case 2.

Several features of the model formulation for Case 3 are specific to investigating the effectiveness of short low permeability seals. For example, the region in the shaft above and below the 10-m seal is assumed to be backfill that offers limited flow resistance to fluid flow. In addition, the panel seals, drift seals and backfill are combined into a single region and no credit is taken for the low-permeability barriers that panel seals might provide. The permeability of these seals is assumed to be the same as the permeability of the waste, with the result that the primary effect panel and drift seals have on repository performance is to provide additional gas-storage volume. These assumptions were made to facilitate observations on the effectiveness of the shaft seal. Thus, although Case 3 uses a more detailed representation of the Salado Formation stratigraphy and the disturbed rock zone than Case 2, it is not intended to provide a more realistic approximation of the repository than Case 2.

*Adapted from Section 2.4 of WIPP PA, 1992.

The computational grid used for Case 3, which is shown in Figure 4-1, is similar to the grid used for Case 2. The grid extends 645 m vertically from the bottom of the Salado Formation to the top of the Culebra Dolomite, and approximately 39 km in the north-south direction. Stratigraphy is unchanged from Case 2 except for the addition of Marker Bed 138, which is 0.4 m of anhydrite located 6 m above Anhydrite Layers A and B. The disturbed rock zone extends horizontally 1.0 m from the waste, and a transition zone with intermediate material properties (Chapter 3, WIPP PA, 1992) is assumed to extend upward through Marker Bed 138 and to extend 1.0 m below Marker Bed 139 into the underlying halite. The shaft is divided into three segments, with a single seal separating two regions of backfill. The sump is assumed to be backfilled, and is included in the lower shaft segment. As previously indicated, the waste disposal region is divided into two regions, one containing the waste panels and the other containing the panel seals and associated backfill. Figures 2-8 and 2-9 of WIPP PA, 1992 provide enlarged representations of the horizontal plane through the repository horizon.

Boundary conditions are the same as for Case 2: there is no flow in the normal direction across all far-field boundaries except the lateral boundaries of the Culebra, where the initial pressure of 1.053 MPa is held constant throughout the simulations. Initial pressure in the shaft, drifts, waste, experimental region, the disturbed rock zone, and the transition zone is atmospheric (0.101 MPa). Initial far-field pressure in the Salado Formation is set as in Case 2 by hydrostatic variation from the sampled value for pressure in Marker Bed 139.

Initial brine saturation is assumed to be 1.00 for all undisturbed rock. Initial brine saturation in the shaft is assumed to be residual and is a sampled variable ranging from 0.0 to 0.4. (Section 2.3.1, WIPP PA, 1991c). Initial brine saturation within the waste is also a sampled variable. The initial brine saturations of the disturbed rock zone and transition zone are adjusted relative to the sampled values for disturbed rock zone and intact halite porosities so that total brine content in these zones is not changed from undisturbed halite. The initial saturation for the seals and backfill is set to the same sampled value used for the shaft.

4.2 Sampled Variables

The 20 imprecisely known variables listed in Table 4-1 are used as input to BRAGFLO for the Case 3 uncertainty and sensitivity studies. As for Cases 1 and 2, the distributions indicated in Table 4-1 characterize subjective uncertainty. The Case 3 calculations use a Latin hypercube sample of size 60 from the 20 variables in Table 4-1. The resultant sample is listed in Table 3.3-2b of WIPP PA, 1992.

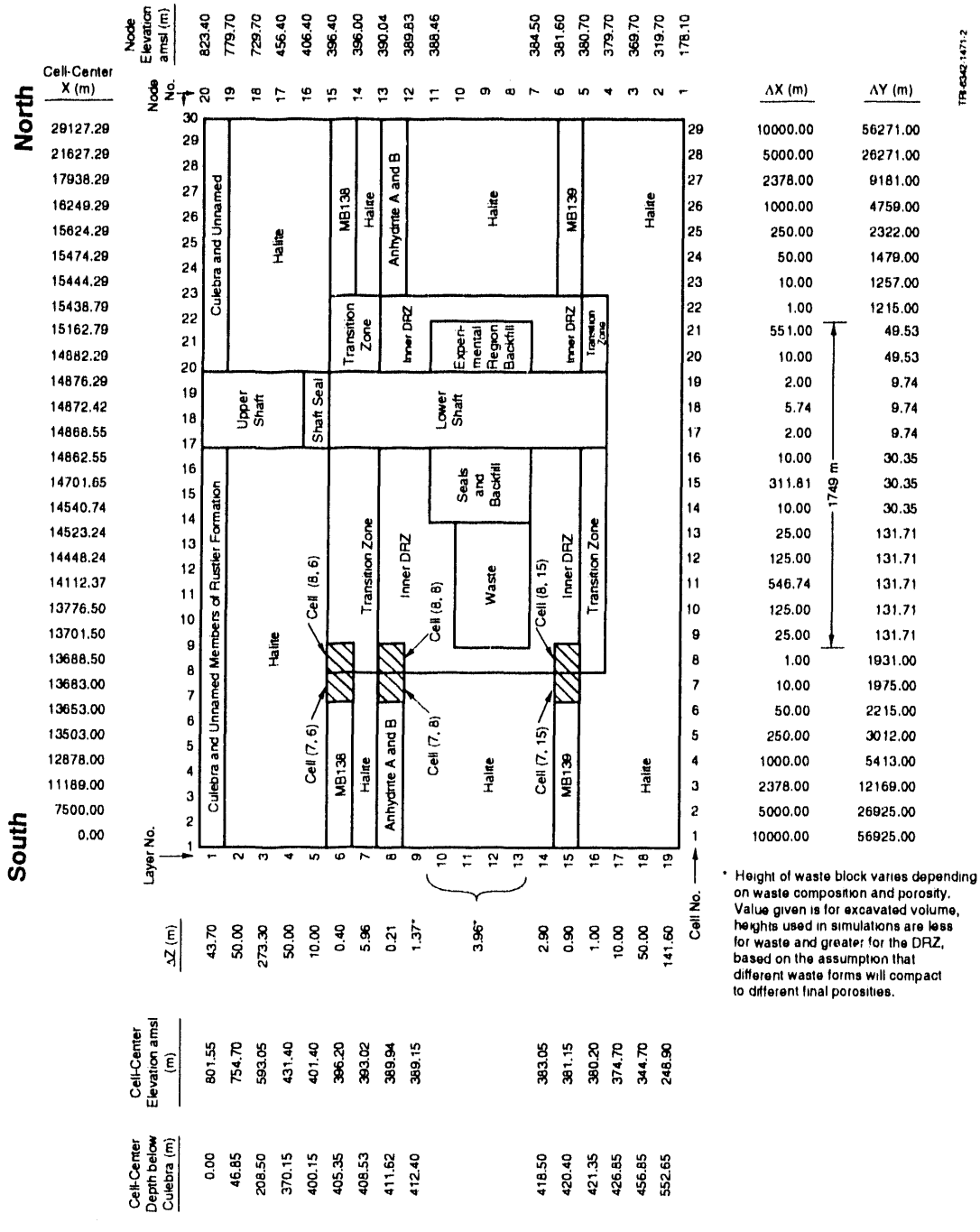

Figure 4-1. Gridding scheme employed with BRAGFLO for the two-dimensional vertical cross-section model used for Case 3. Individual computational cells are identified with an ordered pair (i,j) of integers, where i designates the horizontal coordinate and j designates the vertical coordinate.

Table 4-1. Imprecisely Known Variables Used in BRAGFLO in the Estimation of Gas Flow through a 10-m Shaft Seal

Variable	Definition
BCBRSAT	Brooks and Corey residual brine saturation ($S_{\ell r}$) (dimensionless). Range: 0.0 to 0.4. Median: 0.2. Distribution: Piecewise uniform. Additional information: Sect. 3.3.2, WIPP PA, 1992. Variable 12 in Latin hypercube sample.
BCEXP	Brooks and Corey exponent (η) (dimensionless). Range: 0.2 to 10. Median: 0.7. Distribution: Piecewise uniform. Additional information: Same as BCBRSAT. Variable 14 in Latin hypercube sample.
BCGSSAT	Brooks and Corey residual gas saturation (S_{gr}) (dimensionless). Range: 0.0 to 0.4. Median: 0.2. Distribution: Piecewise uniform. Additional information: Same as BCBRSAT. Variable 13 in Latin hypercube sample.
BRSAT	Initial fluid (brine) saturation of waste (dimensionless). Range: 0 to 2.76×10^{-1}. Median: 1.38×10^{-1}. Distribution: Uniform. Additional information: Section 3.4.9, WIPP PA, 1991c. Variable 1 in Latin hypercube sample is uniformly distributed on interval [0,1] and used to select value for BRSAT by preprocessor to BRAGFLO.
DRZPERM	Disturbed rock zone permeability (k) (m^2). Range: 1×10^{-18} to 1×10^{-13} m^2. Median: 3×10^{-16} m^2. Distribution: Piecewise loguniform. Additional information: Sect. 3.3.2, WIPP PA, 1992. Variable 17 in Latin hypercube sample.
GRCORH	Scale factor used in definition of gas-generation rate for corrosion of steel under humid conditions (dimensionless). Actual gas-generation rate is GRCORH • GRCORI. Range: 0 to 5×10^{-1}. Median: 1×10^{-1}. Distribution: Piecewise uniform. Additional information: Memo from Brush, July 8, 1991, contained in Appendix A, WIPP PA 1991c; Section 3.3.8, WIPP PA 1991c. Variable 3 in Latin hypercube sample.
GRCORI	Gas-generation rate for corrosion of steel under inundated conditions (mol/m^2 surface area steel • s). Range: 0 to 1.3×10^{-8} mol/m^2 s. Median: 6.3×10^{-9} mol/m^2 s. Distribution: Piecewise uniform. Additional information: Same as GRCORH. Variable 4 in Latin hypercube sample.
GRMICH	Scale factor used in definition of gas-generation rate due to microbial degradation of cellulosics under humid conditions (dimensionless). Actual gas-generation rate is GRMICH • GRMICI. Range: 0 to 2×10^{-1}. Median: 1×10^{-1}. Distribution: Piecewise uniform. Additional information: Same as GRCORH. Variable 5 in Latin hypercube sample.

Table 4-1. Imprecisely Known Variables Used in BRAGFLO in the Estimation of Gas Flow through a 10-m Shaft Seal (Continued)

Variable	Definition
GRMICI	Gas-generation rate due to microbial degradation of cellulosics under inundated conditions (mol/kg cellulosics • s). Range: 0 to 1.6×10^{-8} mol/kg s. Median: 3.2×10^{-9} mol/kg s. Distribution: Piecewise uniform. Additional information: Same as GRCORH. Variable 6 in Latin hypercube sample.
MBPERM	Permeability (k) in anhydrite marker beds in Salado Formation under undisturbed conditions (m^2). Range: 8.5×10^{-21} to 1.8×10^{-18} m^2. Median: 8×10^{-20} m^2. Distribution: Piecewise uniform. Additional information: Sect. 3.3.2, WIPP PA, 1992. Variable 19 in Latin hypercube sample.
MBPRES	Pressure (p) in anhydrite Marker Bed 139 under undisturbed conditions (Pa). Pressures at other elevations in Salado Formation were varied hydrostatically from sampled value for MBPRES. Pressures Range: 8.2×10^{6} to 1.5×10^{7} Pa. Median: 1.3×10^{-7} Pa. Distribution: Piecewise uniform. Additional information: Section 2.4.6, WIPP PA, 1991c. Variable 18 in Latin hypercube sample.
SALPERM	Permeability (k) in halite component of Salado Formation (m^2). Range: 1×10^{-25} to 1×10^{-21} m^2. Median: 2×10^{-24} m^2. Distribution: Piecewise loguniform. Additional information: Sect. 3.3.2, WIPP PA, 1992. Variable 10 in Latin hypercube sample.
SALPOR	Porosity (ϕ) in Salado Formation halite and anhydrite under undisturbed conditions (dimensionless). Range: 1×10^{-3} to 3×10^{-2}. Median: 1.55×10^{-2}. Distribution: Uniform. Additional information: Section 2.3.7, WIPP PA, 1991c. Variable 11 in Latin hypercube sample.
SEALPERM	Shaft Seal Permeability (k) (m^2). Range: 1×10^{-21} to 1×10^{-18} m^2. Median: 3.16×10^{-20} m^2. Distribution: Lognormal. Additional information: Sect. 3.3.2, WIPP PA, 1992. Variable 20 in Latin hypercube sample.
STOICCOR	Stoichiometric factor for corrosion of steel (dimensionless). Defines proportion of two different chemical reactions that take place during the corrosion process. Range: 0 to 1. Median: 5×10^{-1}. Distribution: Uniform. Additional information: Brush and Anderson in Lappin et al., 1989, p. A-6; Section 3.3.8, WIPP PA, 1991c. Variable 2 in Latin hypercube sample.
STOICMIC	Stoichiometric coefficient for microbial degradation of cellulosics (mol gas/mol CH_2O). Range: 0 to 1.67 mol/mol. Median: 8.35×10^{-1} mol/mol. Distribution: Uniform. Additional information: Brush and Anderson in Lappin et al., 1989, p. A-10; Section 3.3.9, WIPP PA, 1991c. Variable 9 in Latin hypercube sample.

Table 4-1. Imprecisely Known Variables Used in BRAGFLO in the Estimation of Gas Flow through a 10-m Shaft Seal (Concluded)

Variable	Definition
TZPERM	Transition zone permeability (k) (m^2). Range: 1×10^{-21} to 1×10^{-19} m^2. Median: 7×10^{-21} m^2. Distribution: Piecewise Loguniform. Additional information: Sect. 3.3.2, WIPP PA, 1992. Variable 16 in Latin hypercube sample.
TZPOR	Scale factor used in definition of transition zone and disturbed rock zone porosity (ϕ_z), with the transition zone and disturbed rock zone porosity defined by ϕ_z = SALPOR + (0.06 - SALPOR)•TZPOR. Range: 0 to 1. Median: 0.5. Distribution: Uniform. Additional information: Sect. 3.3.2, WIPP PA, 1992. Variable 15 in Latin hypercube sample.
VMETAL	Fraction of total waste volume that is occupied by IDB (Integrated Data Base) metals and glass waste category (dimensionless). Range: 2.76×10^{-1} to 4.76×10^{-1}. Median: 3.76×10^{-1}. Distribution: Normal. Additional information: Section 3.4.1, WIPP PA, 1991c. Variable 7 in Latin hypercube sample.
VWOOD	Fraction of total waste volume that is occupied by IDB combustible waste category (dimensionless). Range: 2.84×10^{-1} to 4.84×10^{-1}. Median: 3.84×10^{-1}. Distribution: Normal. Additional information: Section 3.4.1, WIPP PA, 1991c. Variable 8 in Latin hypercube sample.

Use of the 4/3 rule indicated in Section 3.2 to select the sample size for Case 3 results in a sample of size 27. However, the sample of size 22 used for Case 2 did not seem to be as revealing as the sample of size 60 used for Case 1. Therefore, the decision was made to use a larger sample size (i.e., 60), which results in both denser stratification across the range of each variable and a greater variety of variable combinations but at the price of greater computational cost.

In addition to the 20 sampled variables listed in Table 4-1, the calculations for Case 3 also required values for a number of additional variables that were fixed at their best-estimate values. These variables and their values are listed in Tables 3.1-1b and 3.3-1a of WIPP PA, 1992. Further, additional discussion of the BRAGFLO input for Case 3 is available in Section 3.3 of WIPP PA, 1992.

4.3 Uncertainty and Sensitivity Analysis Results

Gas flow through the repository and up the shaft to the Culebra Dolomite is the outcome of greatest interest for Case 3. Thus, as for Cases 1 and 2, a natural starting point is an exploration of the factors affecting gas generation. Uncertainty and sensitivity analysis results for corrosion, microbial degradation and total gas production are presented in Sections 4.3.1, 4.3.2 and 4.3.3. Then, results for gas saturation and gas pressure in the repository are presented in Section 4.3.4, followed by results for gas migration into the anhydrite marker beds in Section 4.3.5. Finally, gas and brine migration through the shaft to the Culebra Dolomite is considered in Section 4.3.6.

4.3.1 Gas Generation Due to Corrosion

A summary of the results for gas generation due to corrosion is given in Figure 4-2. The two upper frames in Figure 4-2 show cumulative gas generation as a function of time due to corrosion under humid conditions (upper left frame) and corrosion under inundated conditions (upper right frame). Each curve in the upper two frames results from a single Latin hypercube sample element (i.e., each frame has 60 curves, one for each sample element). Overall, the range of gas production under humid conditions is similar to the range of gas production under inundated conditions.

Formal sensitivity analysis techniques based on partial rank correlation can be used to investigate the variation in cumulative gas production shown in the upper two frames of Figure 4-2. Specifically, the lower two frames in Figure 4-2 show time-dependent plots of partial rank correlation coefficients between cumulative gas production and individual variables from Table 4-1. These coefficients were calculated on the basis of vertical slices through the cumulative gas production curves. As a reminder, a positive rank correlation coefficient indicates that two variables tend to increase and decrease together, and a negative rank correlation coefficient indicates that, as one variable increases, the other tends to decrease.

As shown by the partial correlation results in the lower left frame of Figure 4-2, cumulative gas production due to corrosion under humid conditions tends to increase as GRCORH (scale factor used in definition of gas-generation rate for corrosion of steel under humid conditions) and GRCORI (gas-generation rate for corrosion of steel under inundated conditions) increase. The positive effects for GRCORH and GRCORI result because the actual gas generation-rate due to corrosion under humid conditions is defined by GRCORH•GRCORI. As shown by the partial correlation

Cumulative Gas Production Due to Microbial Degradation of Cellulosics

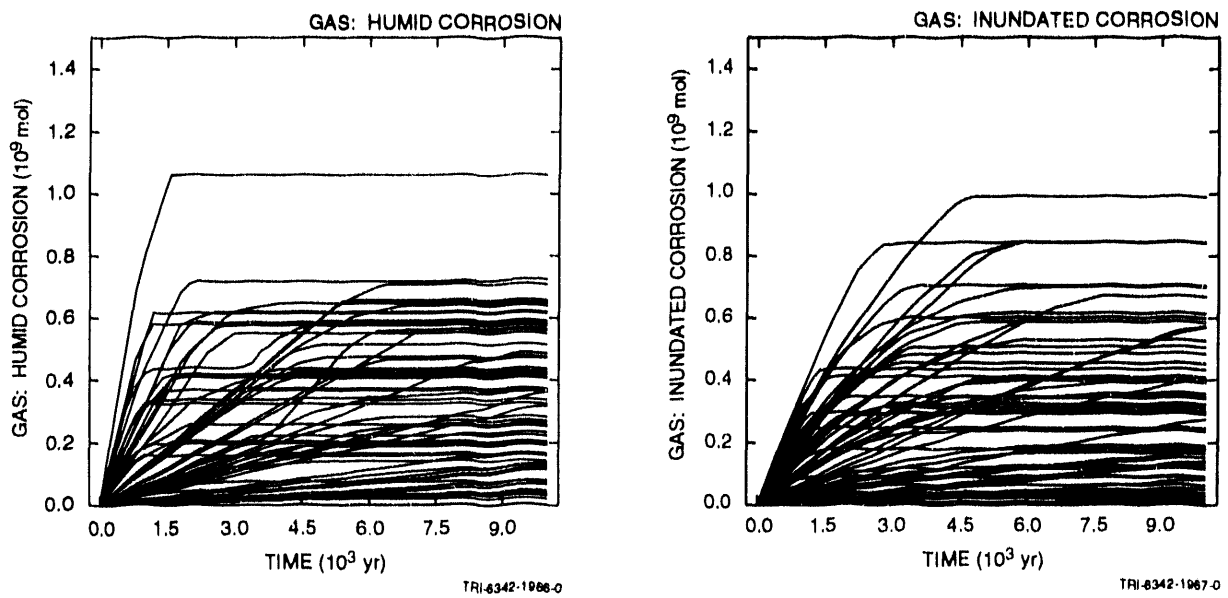

Partial Rank Correlation Coefficients for Cumulative Gas Production Due to Microbial Degradation of Cellulosics

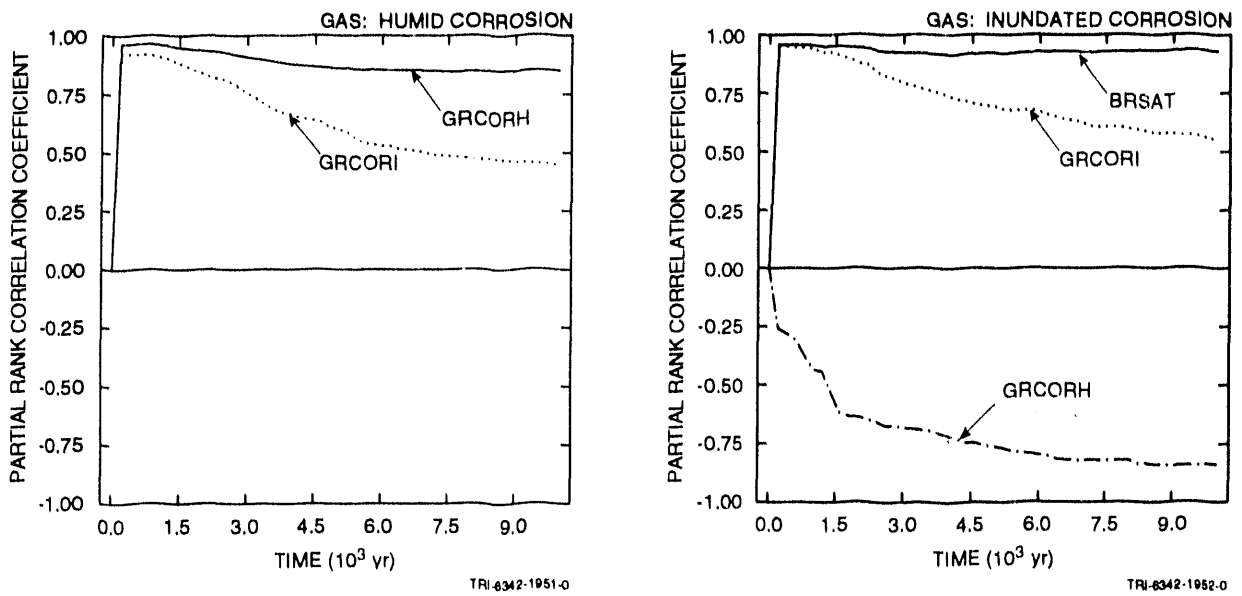

Figure 4-2. Uncertainty and sensitivity analysis results for gas generation due to microbial degradation of cellulosics.

results in the lower right frame of Figure 4-2, cumulative gas production due to corrosion under inundated conditions tends to increase as BRSAT (initial brine saturation of waste) and GRCORI (gas-generation rate for corrosion of steel under inundated conditions) increase and tends to decrease as GRCORH (scale factor used in definition of gas generation rate for corrosion of steel under humid conditions) increases. The positive effects for BRSAT and GRCORI result because increasing BRSAT increases the amount of steel that will be consumed by corrosion under inundated conditions and increasing GRCORI increases the rate which gas is produced by corrosion under inundated conditions. The negative effect for GRCORH results because the increased consumption of steel and brine by corrosion under humid conditions reduces the amount of gas that can be produced by the corrosion of steel under inundated conditions.

Stepwise regression analysis can also be used to analyze the cumulative gas production results shown in Figure 4-2. The two regression analyses shown in Table 4-2 are for cumulative gas production over 10,000 yr due to corrosion under humid and inundated conditions, respectively. Thus, these two regression analyses are for the gas production values appearing above 10,000 yr in the two upper frames of Figure 4-2. The regression analysis for gas production under humid conditions indicates positive effects (i.e., positive regression coefficients) for GRCORH (scale factor used in definition of gas-generation rate for corrosion of steel under humid conditions) and GRCORI (gas-generation rate for corrosion of steel under inundated conditions. As indicated earlier, the positive effects for GRCORH and GRCORI result because the gas-generation rate for the corrosion of steel under humid conditions is GRCORH•GRCORI. The scale factor GRCORH is the most important variable and accounts for 61% (i.e., $R^2 = 0.61$) of the variability in gas generation due to corrosion under humid conditions. Further, GRCORI accounts for an additional 6% of the variability (i.e., 67% - 61% = 6%).

The regression analysis in Table 4-2 for gas production under inundated conditions indicates positive effects for BRSAT (initial brine saturation of waste) and GRCORI (gas-generation rate for corrosion of steel under inundated conditions) and negative effects for GRCORH (scale factor used in definition of gas-generation rate for corrosion of steel under humid conditions) and STOICCOR (stochiometric factor for corrosion of steel). These effects result because increasing BRSAT increases the amount of steel exposed to corrosion under inundated conditions, increasing GRCORI increases the gas-generation rate under inundated conditions, increasing GRCORH decreases the amount of steel available for corrosion under inundated conditions, and increasing STOICCOR decreases the amount of gas produced per unit of steel consumed in the corrosion process. Initial brine saturation (BRSAT) is the most important variable and accounts for 58% of the

variability in gas generation due to corrosion under inundated conditions. Further, GRCORH, GRCORI and STOICCOR collectively account for an additional 28% of the variability.

4.3.2 Gas Generation Due to Microbial Degradation

A summary of the analysis results for gas generation due to microbial degradation is given in Figure 4-3. The upper two frames in Figure 4-3 show cumulative gas generation due to microbial degradation under humid and inundated conditions, respectively. As comparison with the corresponding plots in Figure 4-2 shows, gas generation due to microbial degradation is approximately 50% or less than gas generation due to corrosion. The ranges of cumulative gas generation shown in Figure 4-3 for inundated and humid conditions are similar.

Table 4-2. Stepwise Regression Analyses with Rank-Transformed Data for Cumulative Gas Production over 10,000 yr Due to Corrosion under Humid and Inundated Conditions

Total Gas Production over 10,000 yr (Humid Corrosion)				Total Gas Production over 10,000 yr (Inundated Corrosion)			
Step[a]	Variable[b]	SRC[c]	R^{2d}	Step[a]	Variable[b]	SRC[c]	R^{2d}
1	GRCORH	0.78	0.61	1	BRSAT	0.75	0.58
2	GRCORI	0.25	0.67	2	GRCORH	-0.47	0.80
				3	GRCORI	0.20	0.84
				4	STOICCOR	-0.14	0.86

[a] Steps in stepwise regression analysis
[b] Variables listed in order of selection in regression analysis
[c] Standardized regression coefficients in final regression model
[d] Cumulative R^2 value with entry of each variable into regression model

The lower two frames in Figure 4-3 present sensitivity analysis results based on partial rank correlation coefficients. For cumulative gas production under humid conditions, increasing each of GRMICH (scale factor used in definition of gas-generation rate due to microbial degradation of cellulosics under humid conditions), STOICMIC (stoichiometric coefficient for microbial degradation of cellulosics) and GRMICI (gas-generation rate due to microbial degradation of cellulosics under inundated conditions) increases gas production. Increasing STOICMIC increases the amount of gas

Cumulative Gas Production Due to Corrosion of Steel

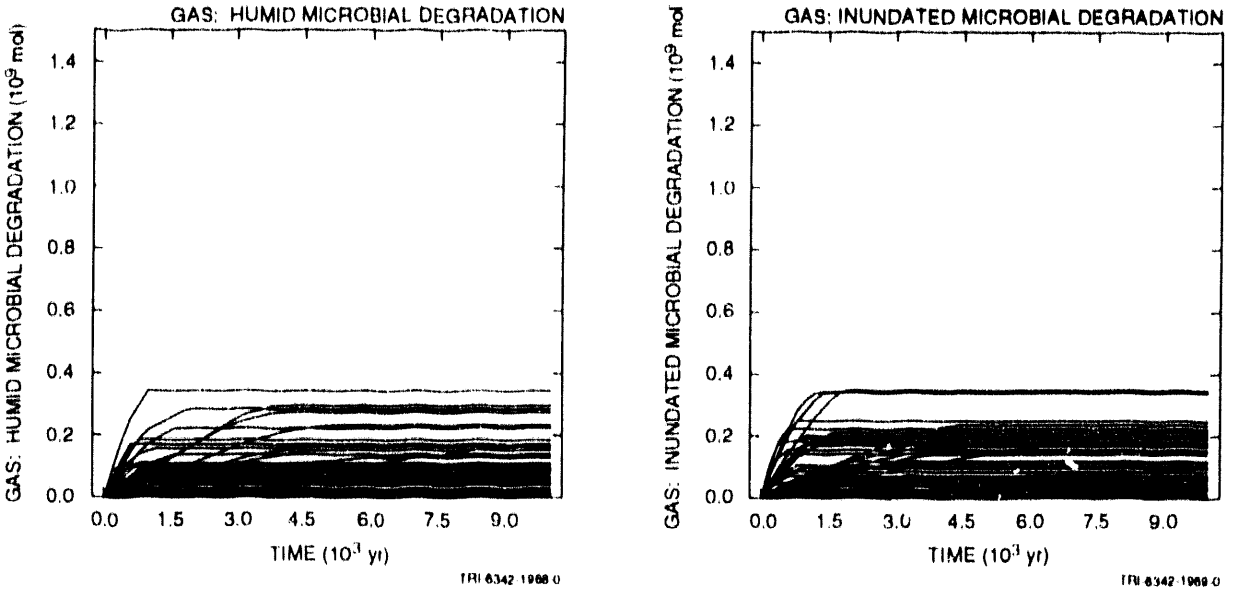

Partial Rank Correlation Coefficients for Cumulative Gas Production Due to Corrosion of Steel

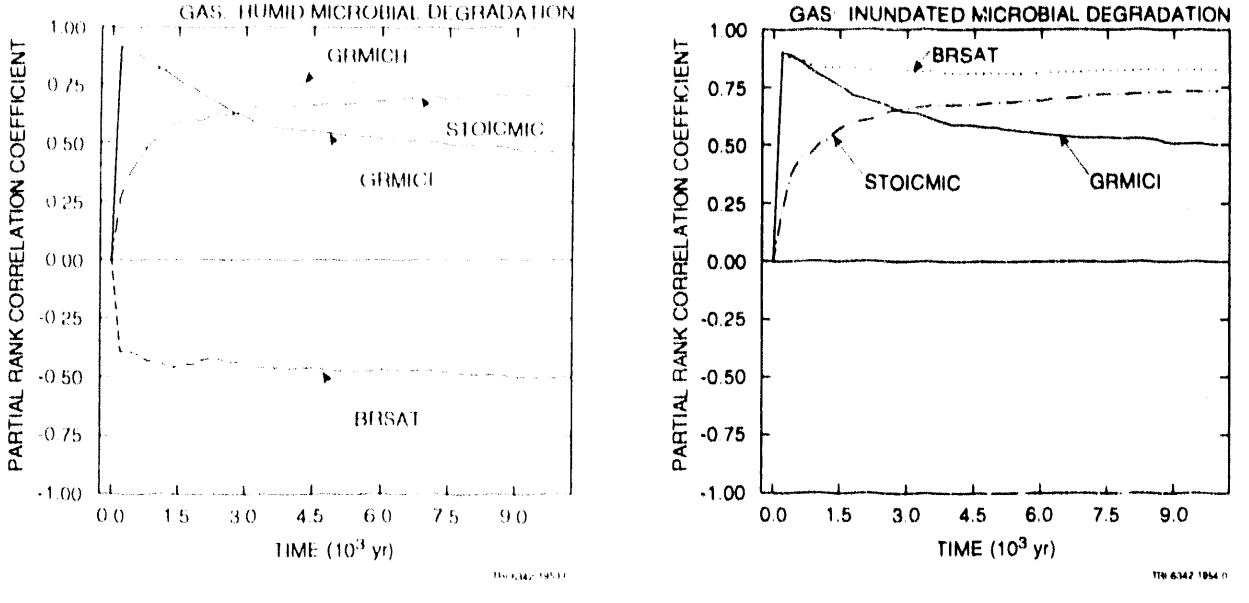

Figure 4-3. Uncertainty and sensitivity analysis results for gas generation due to corrosion of steel.

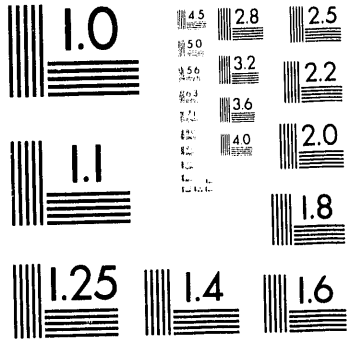
1.0
1.1
1.25
1.4
1.6
1.8
2.0
2.2
2.5
2.8
3.2
3.6
4.0
4.5
5.0
5.6
6.3
7.1

2 of 2

produced per unit of cellulose consumed while increasing GRMICH and GRMICI increases the rate GRMICH•GRMICI of microbial degradation. The importance of GRMICI decreases over time, probably due to its influence on gas generation under both humid and inundated conditions and to the fact that it influences the rate at which gas is produced but not the total amount of gas that can be produced. In addition, increasing BRSAT (initial brine saturation) tends to decrease gas production under humid conditions by increasing the amount of cellulose that is exposed to microbial degradation under inundated conditions. For cumulative gas production under inundated conditions, increasing each of BRSAT, STOICMIC and GRMICI increases gas production.

The regression analyses for cumulative gas production over 10,000 yr due to microbial degradation under humid and inundated conditions, respectively, are presented in Table 4-3. These analyses are for the gas production values appearing above 10,000 yr in the two upper frames of Figure 4-3. For gas production under humid conditions, the variables GRMICH (scale factor used in definition of gas-generation rate due to microbial degradation of cellulosics under humid conditions), STOICMIC (stoichiometric coefficient for microbial degradation of cellulosics), BRSAT (initial brine saturation), VWOOD (fraction of total waste volume that is occupied by IDB combustible waste category) and GRMICI (gas-generation rate due to microbial degradation of cellulosics under inundated conditions) can account for 72% of the observed variability in gas production, with gas production tending to increase with increasing values for GRMICH, STOICMIC, VWOOD and GRMICI and tending to decrease with increasing values for BRSAT. For gas production under inundated conditions, the variables BRSAT and STOICMIC can account for 57% of the observed variability in gas production, with gas production tending to increase as each of these variables increases. When the two additional variables GRMICI and GRMICH are added to the regression model, 67% of the variability in gas production can be accounted for, with gas production tending to increase as GRMICI increases and tending to decrease as GRMICH increases.

4.3.3 Total Gas Production

The upper two frames in Figure 4-4 show total gas production due to corrosion and microbial degradation and were obtained by combining the corresponding results in Figures 4-2 and 4-3 for gas production under humid and inundated conditions. Typically, low gas production under humid conditions is associated with higher gas production under inundated conditions and vice versa. As a result, the gas production curves in Figure 4-4 tend to lie farther above the abscissa than many of the

Table 4-3. Stepwise Regression Analyses with Rank-Transformed Data for Cumulative Gas Production over 10,000 yr Due to Microbial Degradation under Humid and Inundated Conditions.

Total Gas Production over 10,000 yr (Humid Degradation)				Total Gas Production over 10,000 yr (Inundated Degradation)			
Step[a]	Variable[b]	SRC[c]	R^{2d}	Step[a]	Variable[b]	SRC[c]	R^{2d}
1	GRMICH	0.57	0.32	1	BRSAT	0.62	0.37
2	STOICMIC	0.46	0.52	2	STOICMIC	0.45	0.57
3	BRSAT	-0.26	0.59	3	GRMICI	0.26	0.63
4	VWOOD	0.25	0.65	4	GRMICH	-0.20	0.67
5	GRMICI	0.25	0.72				

[a] Steps in stepwise regression analysis
[b] Variables listed in order of selection in regression analysis
[c] Standardized regression coefficients in final regression model
[d] Cumulative R^2 value with entry of each variable into regression model

individual curves in Figures 4-2 and 4-3. Overall, the gas production due to corrosion tends to be approximately two to three times the gas production due to microbial degradation. Gas production associated with microbial degradation of cellulosics has more curves close to zero than gas production due to corrosion due to the assignment of a range of possible values for STOICMIC (stoichiometric coefficient for microbial degradation of cellulosics) that extends to zero, which results in no gas generation due to microbial degradation.

The lower two frames in Figure 4-4 present sensitivity analysis results based on partial rank correlation coefficients. For cumulative gas production due to corrosion, increasing BRSAT (initial brine saturation), GRCORI (gas-generation rate for corrosion of steel under inundated conditions) and GRCORH (scale factor used in definition of gas-generation rate for corrosion of steel under humid conditions) tends to increase gas production. Increasing BRSAT, GRCORI and GRCORH tends to increase the rate of gas production and hence cumulative gas production. In contrast, a negative effect is indicated for STOICCOR (stoichometric factor for corrosion of steel), which results because increasing STOICCOR decreases the amount of gas produced per unit of steel consumed in the corrosion process. For cumulative gas production due to microbial degradation, GRMICI (gas-generation rate due to microbial degradation of cellulosics under inundated conditions) and BRSAT (initial brine saturation) have

Cumulative Gas Production

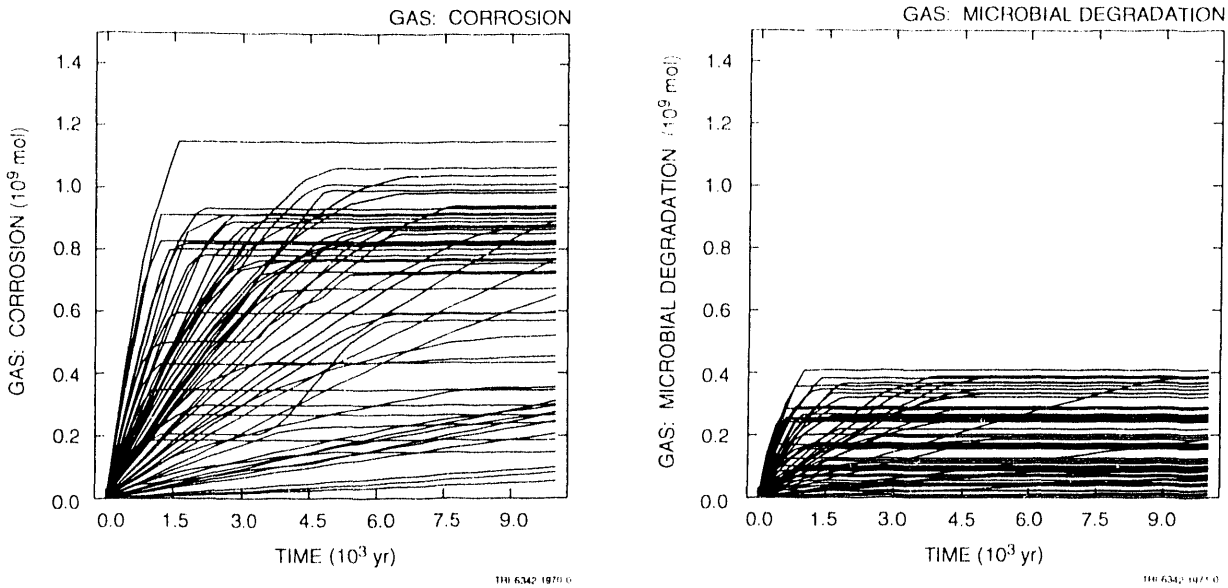

Partial Rank Correlation Coefficients for Cumulative Gas Production

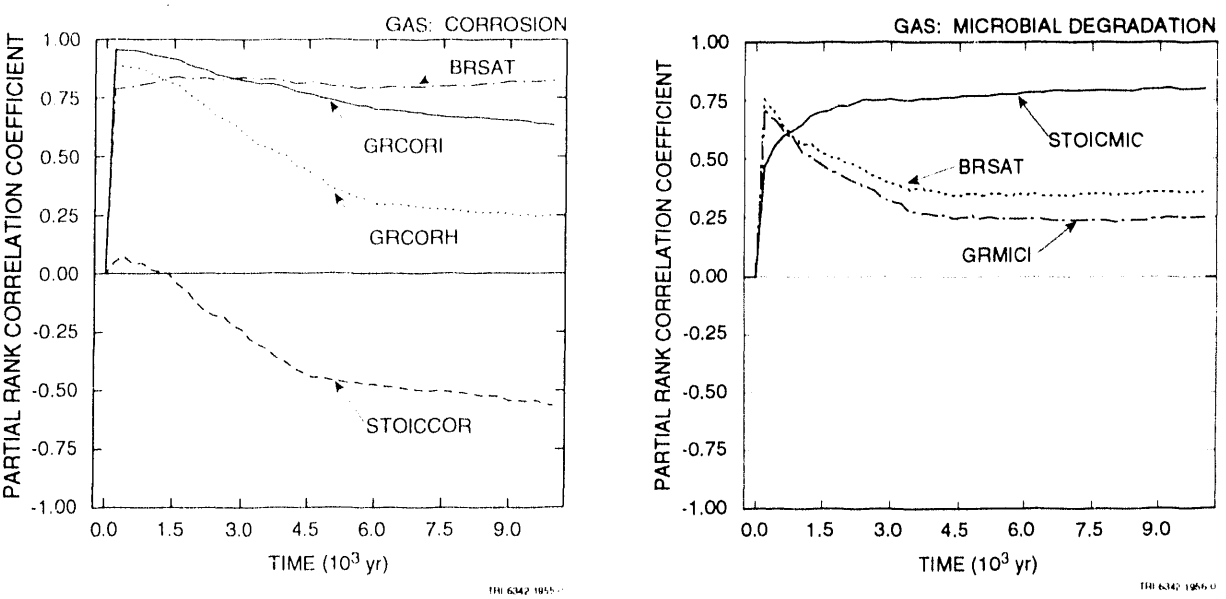

Figure 4-4. Uncertainty and sensitivity analysis results for gas generation due to corrosion of steel and microbial degradation of cellulosics.

positive effects at early times and then decrease in importance. In contrast, STOICMIC (stoichiometric coefficient for microbial degradation of cellulosics) has an increasingly important positive effect with time and ultimately dominates the variability in cumulative gas production.

The two regression analyses in Table 4-4 are for cumulative gas production over 10,000 yr due to corrosion and microbial degradation, respectively. Thus, these analyses are for the gas production values appearing above 10,000 yr in the two upper frames of Figure 4-4. The regression analysis for gas production due to corrosion selected the variables BRSAT (initial brine saturation), GRCORI (gas-generation rate for corrosion of steel under inundated conditions) STOICCOR (stoichiometric factor for corrosion of steel) and VMETAL (fraction of total waste volume that is occupied by IDB metals and glass waste category), with BRSAT, GRCORI and VMETAL having a positive effect on gas production and STOICCOR having a negative effect on gas production. Collectively, these four variables can account for 70% of the variability in gas production due to corrosion.

Table 4-4. Stepwise Regression Analysis with Rank-Transformed Data for Total Gas Production Due to Corrosion over 10,000 yr and Total Gas Generation Due to Microbial Degradation over 10,000 yr.

Total Gas Production over 10,000 yr (Corrosion)				Total Gas Production over 10,000 yr (Microbial Degradation)			
Step[a]	Variable[b]	SRC[c]	R^{2d}	Step[a]	Variable[b]	SRC[c]	R^{2d}
1	BRSAT	0.64	0.43	1	STOICMIC	0.68	0.44
2	GRCORI	0.35	0.56	2	GRMICI	0.36	0.56
3	STOICCOR	-0.31	0.66	3	VWOOD	0.24	0.62
4	VMETAL	0.21	0.70	4	BRSAT	0.20	0.66

[a] Steps in stepwise regression analysis
[b] Variables listed in order of selection in regression analysis
[c] Standardized regression coefficients in final regression model
[d] Cumulative R^2 value with entry of each variable into regression model

The regression analysis in Table 4-4 for gas production due to microbial degradation can account for 66% of the observed variability in gas production. In particular, STOICMIC (stoichiometric coefficient for microbial degradation of cellulosics) was found to account for 44% of the observed variability and small additional effects were indicated for GRMICI (gas-generation rate due to microbial degradation of cellulosics under

inundated conditions), VWOOD (fraction of total waste volume occupied by IDB combustible waste category) and BRSAT (initial brine saturation).

The gas production due to corrosion and to microbial degradation can be combined to produce the total gas production results shown in the upper frame of Figure 4-5. Most sample elements show a period of rapid gas production in the first few thousand years, with considerably reduced rates of gas production at later times. As examination of the two upper frames in Figure 4-6 shows, the inventory of steel and cellulosics is often exhausted or significantly depleted after the first few thousand years.

The lower frame in Figure 4-5 presents sensitivity analysis results based on partial rank correlation coefficients. At early times, total gas production is dominated by GRCORI (gas-generation rate for corrosion of steel under inundated conditions), GRCORH (scale factor used in definition of gas-generation rate for corrosion of steel under humid conditions), GRMICI (gas-generation rate for microbial degradation of cellulosics under inundated conditions), GRMICH (scale factor used in definition of gas-generation rate for microbial degradation of cellulosics under humid conditions) and BRSAT (initial brine saturation), with total gas generation tending to increase as each of these variables increases. As time increases, GRCORI, GRCORH, GRMICI and GRMICH become less important and have little effect on total gas generation over 10,000 yr. In contrast, STOICMIC (stoichiometric coefficient for microbial degradation of cellulosics) has little effect on total gas production at early times but increases in importance with increasing time due to the fact that total microbial gas production is determined primarily by STOICMIC.

A regression analysis for cumulative gas production over 10,000 yr due to both corrosion and microbial degradation is presented in Table 4-5. The first variable selected in the analysis is BRSAT (initial brine saturation), which has a positive regression coefficient and can account for 42% of the variability in total gas production. The indicated effect for BRSAT is consistent with its dominant influence on gas generation due to corrosion as indicated in Figure 4-4 and Table 4-4. The next variables selected in the regression analysis are STOICMIC (stoichiometric coefficient for microbial degradation of cellulosics) and STOICCOR (stoichiometric factor for corrosion of steel). The positive regression coefficient for STOICMIC and the negative regression coefficient for STOICCOR are consistent with the effects of these variables on gas generation due to microbial degradation and corrosion, respectively. Collectively, BRSAT, STOICMIC and STOICCOR can account for 60% of the variability in total gas production over 10,000 yr.

Cumulative Gas Production

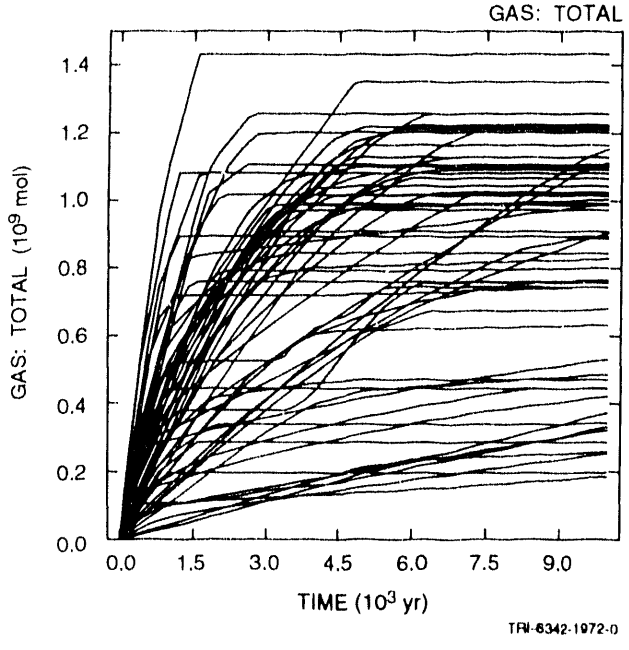

Partial Rank Correlation Coefficients for Cumulative Gas Production

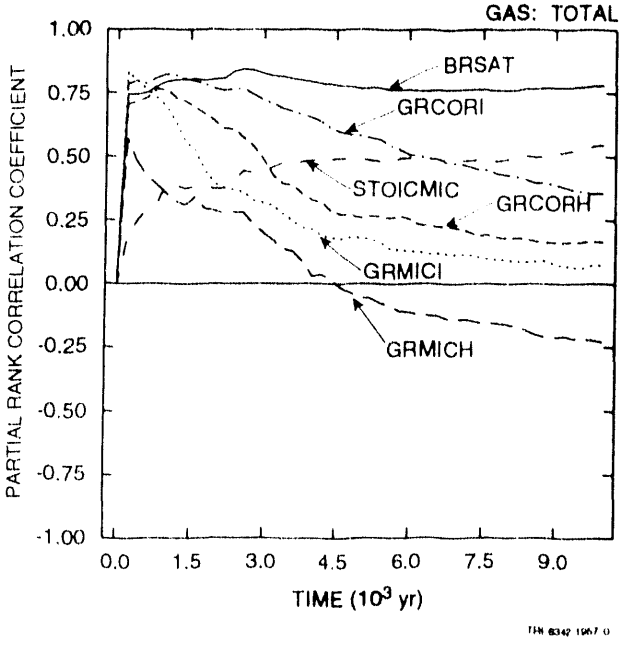

Figure 4-5. Uncertainty and sensitivity analysis results for total gas production due to both corrosion of steel and microbial degradation of cellulosics.

Steel and Cellulosic Inventories

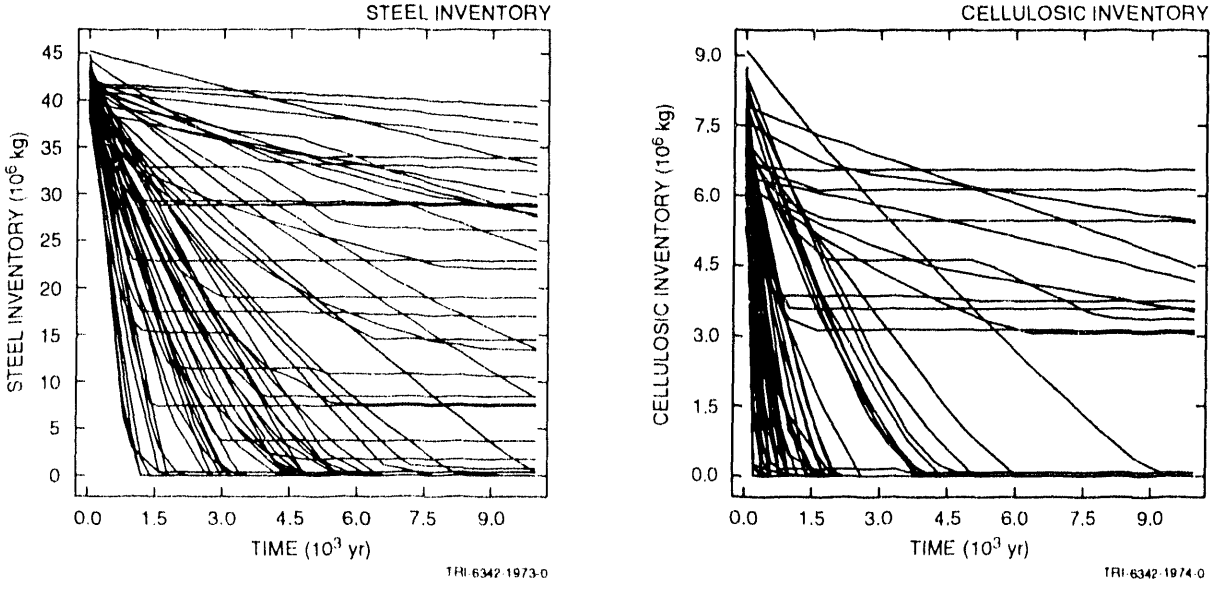

Partial Rank Correlation Coefficients for Steel and Cellulosic Iventories

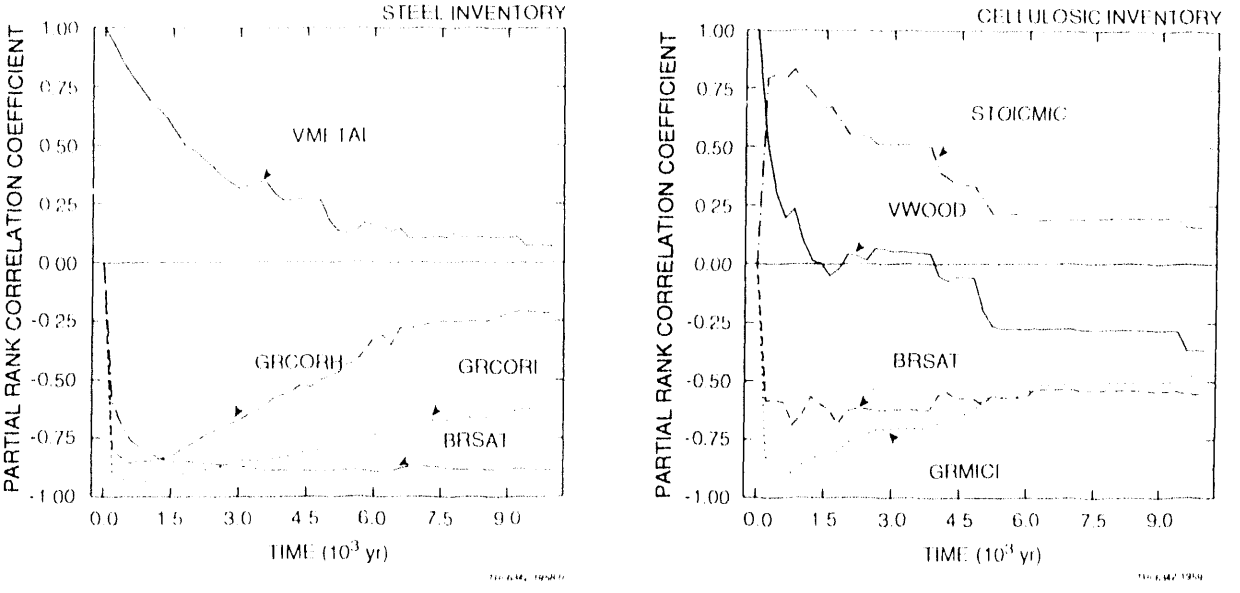

Figure 4-6. Uncertainty and sensitivity analysis results for steel and cellulosic inventories in repository.

Table 4-5. Stepwise Regression Analysis with Rank-Transformed Data for Total Gas Production Over 10,000 yr Due to Both Corrosion and Microbial Degradation.

Total Gas Production over 10,000 yr (Corrosion and Microbial)			
Step[a]	Variable[b]	SRC[c]	R^{2d}
1	BRSAT	0.64	0.42
2	STOICMIC	0.33	0.52
3	STOICCOR	-0.28	0.60

[a] Steps in stepwise regression analysis
[b] Variables listed in order of selection in regression analysis
[c] Standardized regression coefficients in final regression model
[d] Cumulative R^2 value with entry of each variable into regression model

As previously indicated, the upper two frames in Figure 4-6 show the time-dependent steel and cellulosic inventories associated with the individual sample elements. The lower two frames present sensitivity analyses based on partial rank correlation coefficients. The steel inventory is initially dominated by VMETAL (faction of total waste volume occupied by IDB metals and glass category), with the importance of this variable decreasing with time. The variables GRCORI (gas-generation rate for corrosion of steel under inundated conditions), GRCORH (scale factor used in definition of gas-generation rate for corrosion of steel under humid conditions) and BRSAT (initial brine saturation) have negative effects on the steel inventory. As with VMETAL, the importance of GRCORI and GRCORH tends to decrease with time; in contrast, the importance of BRSAT remains relatively fixed. The negative relationships involving GRCORI, GRCORH and BRSAT result from their effects in increasing the rate of corrosion. Further, the corrosion process stops when all the brine in a computational cell is consumed. Thus, increasing BRSAT increases the amount of steel that can be consumed by corrosion before the corrosion process is stopped due to brine depletion in the absence of brine inflow from the Salado Formation. The cellulosic inventory is initially dominated by VWOOD (fraction of total waste volume that is occupied by IDB combustible waste category), with the importance of this variable decreasing rapidly with time. The variable GRMICI (gas-generation rate due to microbial degradation of cellulosics under inundated conditions) shows a negative effect on cellulosic inventory due to its effect in increasing the rate at which cellulosics are consumed. Similarly, BRSAT shows a negative effect because cellulose is consumed more rapidly under inundated than under humid conditions. The positive effect indicated for STOICMIC

(stoichiometric coefficient for microbial degradation of cellulosics) probably results because increased values for STOICMIC lead to increased rates of gas generation, which in turn lead to humid conditions and thus lower rates of microbial degradation of cellulosics.

4.3.4 Gas Saturation and Pressure in Waste

Time-dependent values for average gas saturation in the waste (i.e., averaged over entire repository) and gas pressure in the waste are presented in the two upper frames of Figure 4-7. For most sample elements, gas saturation increases monotonically with time, although there may be a small drop in gas saturation in the first few hundred years. As the partial rank correlation coefficients for gas saturation in the lower left frame of Figure 4-7 show, increasing each of GRCORI (gas-generation rate for corrosion of steel under inundated conditions), GRCORH (scale factor used in definition of gas-generation rate for corrosion of steel under humid conditions), TZPOR (scale factor used in definition of transition zone and disturbed rock zone porosity) and STOICCOR (stoichiometric factor for corrosion of steel) tends to increase gas saturation, and increasing each of BRSAT (initial brine saturation) and SALPOR (porosity in Salado Formation halite and anhydrite under undisturbed conditions) tends to decrease gas saturation. The effects for GRCORI, GRCORH, BRSAT and SALPOR result because increasing each of GRCORI and GRCORH increases the amount of gas in the panel and increasing each of BRSAT and SALPOR increases the amount of brine in the panel. The dominant effect of SALPOR on net brine flow into the waste panel is indicated by the partial correlation coefficients shown in the lower right frame of Figure 4-8. A positive effect is indicated for TZPOR, which probably results from increased brine flow from the repository to the underlying disturbed rock zone and transition zone. The cause of the positive effect indicated for STOICCOR is not immediately apparent, as increasing STOICCOR tends to decrease gas production. However, as discussed in conjunction with Figures 2-13 and 3-10, increasing STOICCOR also tends to decrease the pore volume in the repository. In turn, decreasing pore volume tends to decrease the amount of brine initially in the repository, which is set as a fraction of the initial pore volume. Corrosion is assumed to proceed at a constant rate in each computational cell until the brine contained in the cell is consumed. As a result, large values of STOICCOR will lead to a larger percentage of the available brine being consumed; in turn, this frees up more space that can be occupied by gas and thus increases the gas saturation.

As shown in the upper right frame of Figure 4-7, time-dependent gas pressure in the repository tends to increase initially and then to decrease, with the rate of decrease being slower than the rate of increase.

Gas Saturation and Gas Pressure in Repository

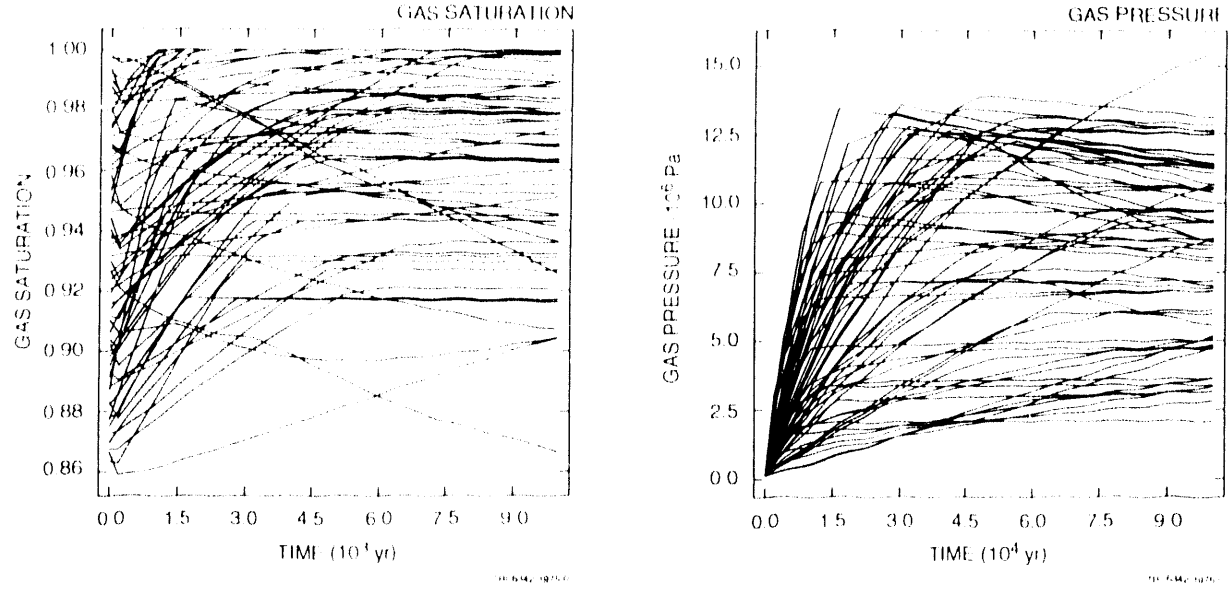

Partial Rank Correlation Coefficients for Gas Saturation and Gas Pressure in Repository

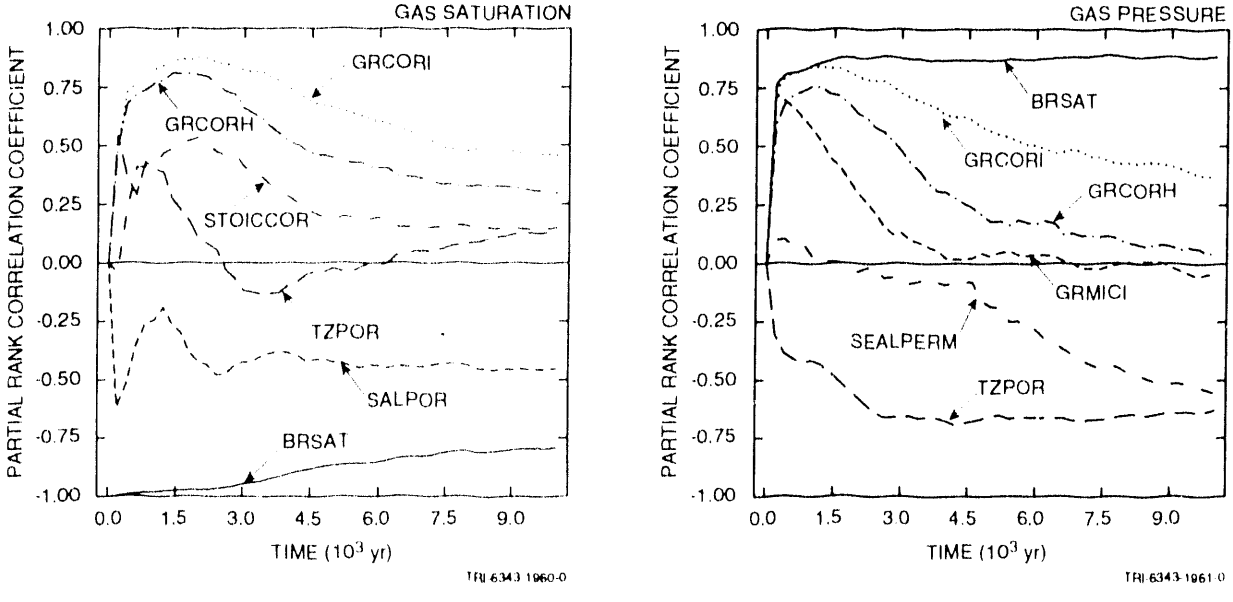

Figure 4-7. Uncertainty and sensitivity analysis results for average gas saturation and gas pressure in repository.

Total and Net Brine Inflow to Repository

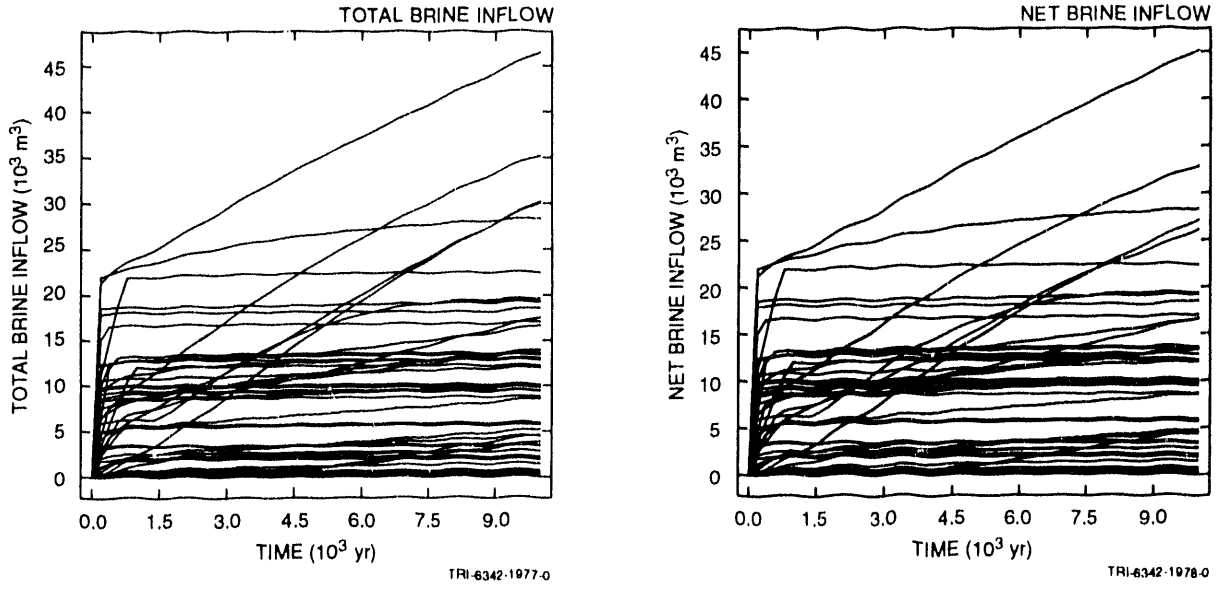

Partial Rank Correlation Coefficients for Total and Net Brine Inflow to Repository

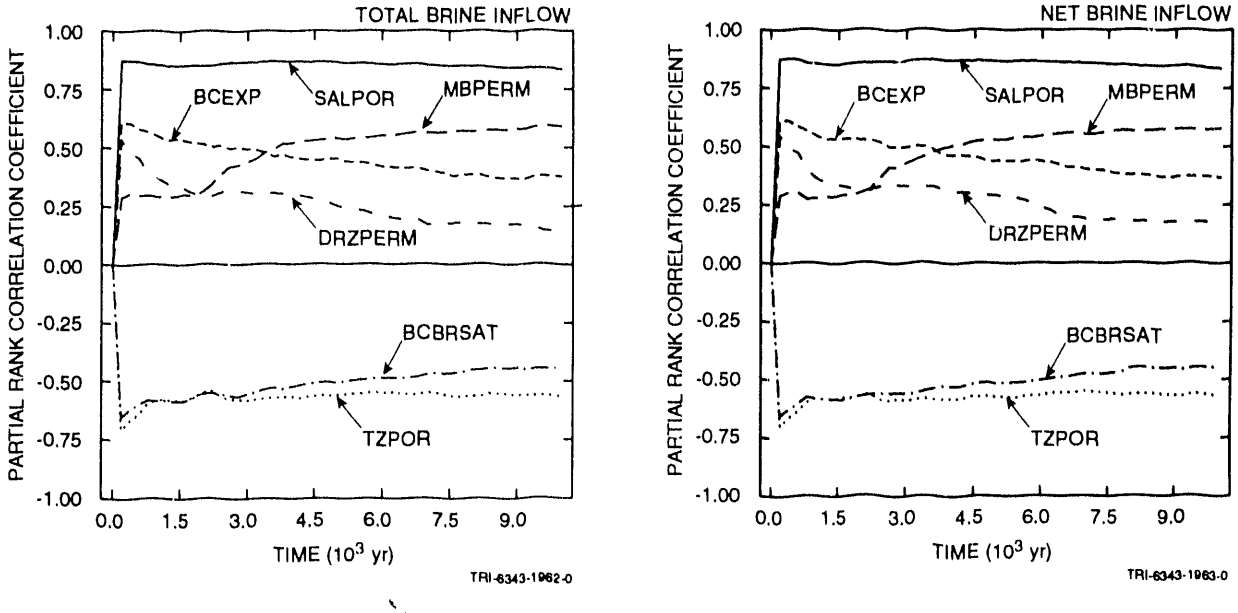

Figure 4-8. Uncertainty and sensitivity analysis results for total and net brine inflow to repository.

Only one sample element produces gas pressures that are close to the lithostatic pressure of 14.8 MPa. The partial rank correlation coefficients for gas pressure in the lower right frame of Figure 4-7 indicate that gas pressure is dominated by BRSAT (initial brine saturation) and TZPOR (scale factor used in definition of transition zone and disturbed rock zone porosity). Increasing BRSAT increases gas pressure by increasing gas production, and increasing TZPOR decreases gas pressure by increasing the pore volume available for gas storage. In addition, GRCORH (scale factor used in definition of gas-generation rate for corrosion of steel under humid conditions), GRCORI (gas-generation rate for corrosion of steel under inundated conditions) and GRMICI (gas-generation rate due to microbial degradation of cellulosics under inundated conditions) have positive effects on gas pressure at early times. At later times SEALPERM (shaft seal permeability) has a negative effect on gas pressure due to the reduced resistance to gas flow up the shaft that results as SEALPERM increases.

Regression analyses for gas saturation and gas pressure at 10,000 yr are presented in Table 4-6. These analyses are for the gas saturation and gas pressure values appearing above 10,000 yr in Figure 4-7. For gas saturation at 10,000 yr, the dominant variable is BRSAT (initial brine saturation), which can account for 44% of the observed uncertainty. Increasing BRSAT tends to reduce gas saturation by increasing the pore volume that is occupied by brine. After BRSAT, the regression analysis selects GRCORI (gas-generation rate for corrosion of steel under inundated conditions), SALPOR (porosity in Salado Formation halite and anhydrite under undisturbed conditions) and MBPERM (permeability in anhydrite marker beds in Salado Formation under undisturbed conditions), with each of these variables accounting for 6% to 7% of the uncertainty in gas saturation. Increasing GRCORI tends to increase gas saturation by increasing gas production. In contrast, increasing each of SALPOR and MBPERM tends to decrease gas saturation. As shown in Table 4-7, the negative effects on gas saturation indicated for SALPOR and MBPERM result from the positive effects on brine inflow to the repository (i.e., increasing each of SALPOR and MBPERM tends to increase the amount of brine flowing into the repository, which in turn reduces the amount of pore space that can be occupied by gas). Collectively, BRSAT, GRCORI, SALPOR and MBPERM can account for 64% of the uncertainty in gas saturation at 10,000 yr.

For gas pressure at 10,000 yr, BRSAT (initial brine saturation) is again the dominant variable and can account for 59% of the uncertainty. Increasing BRSAT tends to increase gas pressure by both increasing gas generation and reducing the pore volume available for gas storage. The next variable selected in the regression analysis is TZPOR (scale factor used in definition of transition zone and disturbed rock zone porosity),

Table 4-6. Stepwise Regression Analyses with Rank-Transformed Data for Gas Saturation and Gas Pressure in Repository at 10,000 yr.

Gas Saturation at 10,000 yr				Gas Pressure at 10,000 yr			
Step[a]	Variable[b]	SRC[c]	R^{2d}	Step[a]	Variable[b]	SRC[c]	R^{2d}
1	BRSAT	-0.67	0.44	1	BRSAT	0.74	0.59
2	GRCORI	0.28	0.51	2	TZPOR	-0.31	0.68
3	SALPOR	-0.27	0.58	3	SEALPERM	-0.27	0.74
4	MBPERM	-0.23	0.64	4	STOICCOR	-0.17	0.77
				5	GRCORI	0.15	0.79

[a] Steps in stepwise regression analysis
[b] Variables listed in order of selection in regression analysis
[c] Standardized regression coefficients in final regression model
[d] Cumulative R^2 value with entry of each variable into regression model

Table 4-7. Stepwise Regression Analyses with Rank-Transformed Data for Total and Net Brine Inflow to the Repository over 10,000 yr.

Total Brine Inflow over 10,000 yr				Net Brine Inflow over 10,000 yr			
Step[a]	Variable[b]	SRC[c]	R^{2d}	Step[a]	Variable[b]	SRC[c]	R^{2d}
1	SALPOR	0.65	0.39	1	SALPOR	0.66	0.40
2	MBPERM	0.32	0.51	2	MBPERM	0.31	0.51
3	TZPOR	-0.31	0.60	3	TZPOR	-0.31	0.61
4	BRSAT	-0.23	0.66	4	BRSAT	-0.23	0.66
5	BCBRSAT	-0.19	0.69	5	BCBRSAT	-0.19	0.69
6	SALPERM	0.19	0.72	6	SALPERM	0.18	0.72
7	BCEXP	0.19	0.76	7	BCEXP	0.18	0.76

[a] Steps in stepwise regression analysis
[b] Variables listed in order of selection in regression analysis
[c] Standardized regression coefficients in final regression model
[d] Cumulative R^2 value with entry of each variable into regression model

with gas pressure tending to decrease as TZPOR increases. This negative effect results because increasing TZPOR results in more pore volume for gas storage and hence in reduced gas pressures. The variable TZPOR accounts for 9% of the uncertainty of gas pressure. An additional 6% of the uncertainty is accounted for by SEALPERM (shaft seal permeability), with gas pressure tending to decrease as SEALPERM increases. This negative

effect results because increasing SEALPERM results in more gas flow out of the waste panel and hence in lower gas pressures. Small effects are also indicated for STOICCOR (stoichiometric factor for corrosion of steel) and GRCORI (gas-generation rate for corrosion of steel under inundated conditions), with gas pressure tending to decrease as STOICCOR increases and to increase as GRCORI increases. These effects result because increasing STOICCOR decreases gas generation due to corrosion and increasing GRCORI increases gas generation due to corrosion. Collectively, BRSAT, TZPOR, SEALPERM, STOICCOR and GRCORI can account for 79% of the uncertainty in gas pressure at 10,000 yr.

Total and net brine inflow are summarized in Figure 4-8. As comparison of the two sets of inflow results in Figure 4-8 shows, there is essentially no difference between total and net brine inflow. This is considerably different from the results shown in Figure 2-12 for Case 1, where there is a substantial difference between total and net inflow. As shown in Figure 4-8, brine inflow is controlled by SALPOR (porosity in Salado Formation halite and anhydrite under undisturbed conditions), MBPERM (permeability in anhydrite marker beds in Salado Formation under undisturbed conditions), BCEXP (Brooks and Corey exponent), DRZPERM (disturbed rock zone permeability), BCBRSAT (Brooks and Corey residual brine saturation) and TZPOR (scale factor used in definition of transition zone and disturbed rock zone porosity), with brine inflow tending to increase as SALPOR, MBPERM, BCEXP and DRZPERM increase and tending to decrease as BCBRSAT and TZPOR increase. Similar results are obtained in the regression analyses presented in Table 4-7 for total and net brine inflow to the repository over 10,000 yr (i.e., for the brine inflow values appearing above 10,000 yr in Figure 4-8). The positive effects for SALPOR and MBPERM result because increasing SALPOR increases the reservoir of brine in the Salado Formation potentially available for flow to the repository and increasing MBPERM reduces the resistance to brine flow in the anhydrite marker beds. The positive effect for DRZPERM results from reducing resistance to brine flow through the disturbed rock zone to the repository. The positive effect indicated for BCEXP and the negative effects indicated for BCBRSAT and TZPOR result from the role that these variables play in the definition of effective permeabilities for the transition and disturbed rock zones.

The 1991 WIPP performance assessment did not directly model closure of the waste panels. However, possible interaction of gas generation and panel closure was incorporated into the analysis by setting the initial pore volume in a waste panel to the volume necessary to contain all waste-generated gas at lithostatic pressure. As a result, initial pore volume is a function of STOICCOR (stoichiometric factor for corrosion of steel), STOICMIC (stoichiometric coefficient for microbial degradation of

cellulosics), VMETAL (fraction of total waste volume occupied by IDB metals and glass waste category) and VWOOD (fraction of total waste volume occupied by IDB combustible waste category). The behavior of pore volume for Case 3 is essentially the same as shown in Figures 2-13 and 3-10 for Cases 1 and 2.

4.3.5 Gas Movement in Anhydrite Marker Beds

As shown in Figure 4-1, there are three anhydrite marker beds in Case 3 into which gas can flow from the disturbed rock zone surrounding the repository: Marker Bed 139, Anhydrite Layers A and B, and Marker Bed 138. Gas flow occurs when the gas pressure in the disturbed rock zone exceeds the gas barrier pressure in the adjacent intact anhydrite layer. In BRAGFLO, the determination of whether or not gas flow occurs on the south end of the panel is made on the basis of the following pairs of adjacent computational cells: Cells (7,6) and (8,6) for Marker Bed 138, Cells (7,8) and (8,8) for Anhydrite Layers A and B, and Cells(7,15) and (8,15) for Marker Bed 139; a similar determination is made for the north end of the panel.

The gas barrier pressures in Cells (7,6), (7,8) and (7,15), the gas pressures in Cells (8,6), (8,8) and (8,15), and the differences between gas barrier pressure in the anhydrite and gas pressure in the disturbed rock zone for adjacent cells are shown in Figure 4-9. The gas barrier pressures initially drop as brine flows out of the anhydrite layers into the disturbed rock zone; then, as brine flows through the anhydrite layers to replenish the brine initially lost to the disturbed rock zone, the gas barrier pressures cease to decrease and begin to increase. The gas pressures in the disturbed rock zone increase initially and then often show a slow decrease. As shown by the differences between gas barrier pressures and gas pressures in the third column of plots in Figure 4-9, gas pressure rarely exceeds gas barrier pressure, with the result that there is little gas flow from the disturbed rock zone to the anhydrite layers. In particular, 6 sample elements result in gas flow from the disturbed rock zone to Marker Bed 138; 5 sample elements result in gas flow to Anhydrite Layers A and B, and 3 sample elements result in gas flow to Marker Bed 139.

As shown in Figure 4-10, sensitivity analysis results based on partial rank correlation coefficients can be used to determine the individual variables that are controlling the uncertainty in gas barrier pressures and gas pressures shown in Figure 4-9. Gas barrier pressure is initially controlled by MBPRES (pressure in anhydrite Marker Bed 139 under undisturbed conditions) and MBPERM (permeability in anhydrite marker beds in Salado Formation under undisturbed conditions), with the importance of

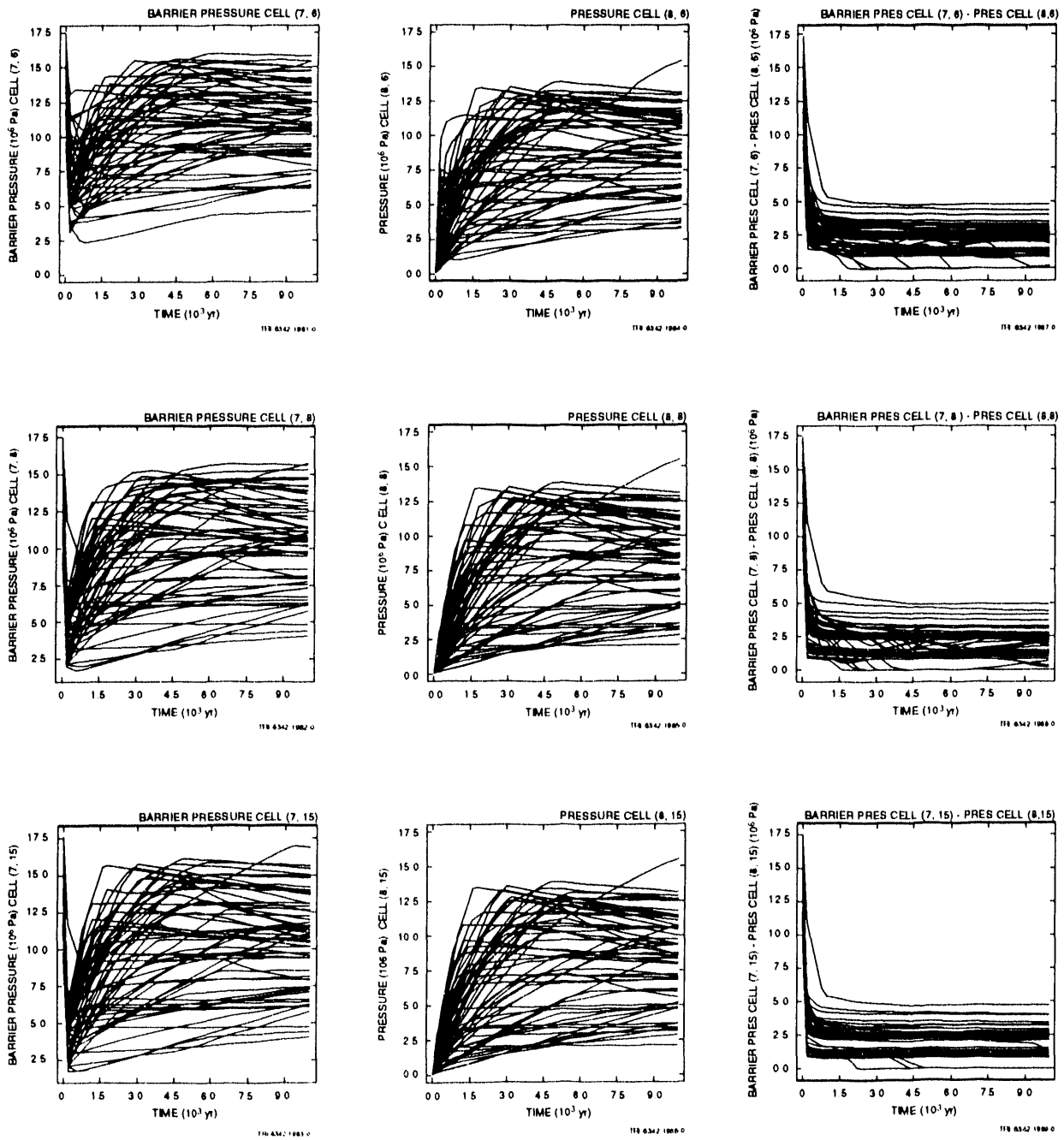

Figure 4-9. Gas barrier pressures in Computational Cells (7,6), (7,8) and (7,15), gas pressures in Computational Cells (8,6), (8,8) and (8,15), and differences between gas barrier pressure and gas pressure for adjacent computational cells. Location of individual computational cells is shown in Figure 4-1. Cells are identified by an ordered pair indicating cell and layer number in the computational grid.

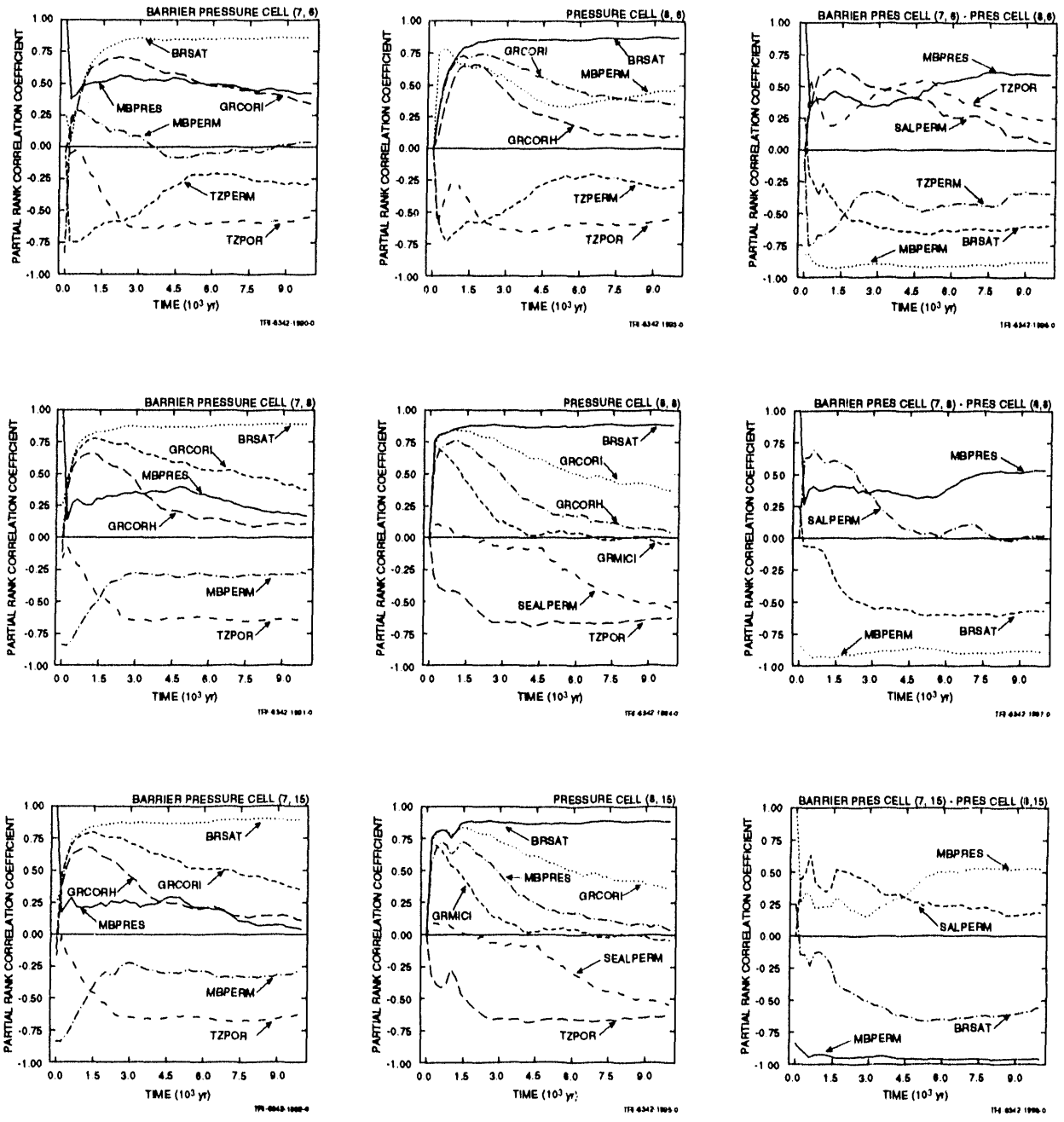

Figure 4-10. Partial rank correlation coefficients for gas barrier pressures in Computational Cells (7,6), (7,8) and (7,15), gas pressures in Computational Cells (8,6), (8,8) and (8,15), and differences between gas barrier pressure and gas pressure for adjacent computational cells. Location of individual computational cells is shown in Figure 4-1. Cells are identified by an ordered pair indicating cell and layer number in the computational mesh.

MBPRES and MBPERM decreasing with time. Increasing MBPRES tends to increase the gas barrier pressure while increasing MBPERM tends to decrease the gas barrier pressure. At later times, the uncertainty in gas barrier pressure is dominated by BRSAT (initial brine saturation) and TZPOR (scale factor used in definition of transition zone and disturbed rock zone porosity), with gas barrier pressure tending to increase as BRSAT increases and decrease as TZPOR increases.

The gas pressures in the disturbed rock zone are controlled by BRSAT (initial brine saturation) and TZPOR (scale factor used in definition of transition zone and disturbed rock zone porosity), with gas pressure tending to increase as BRSAT increases and decrease as TZPOR increases. The positive effect for BRSAT results because increasing BRSAT tends to increase gas generation and hence increase gas pressure. The negative effect for TZPOR results because increasing TZPOR tends to increase the pore volume available for gas storage and hence decrease gas pressure.

The differences between gas barrier pressure and gas pressure are initially dominated by MBPRES (pressure in anhydrite Marker Bed 139 under undisturbed conditions) and MBPERM (permeability in anhydrite marker beds in Salado Formation under undisturbed conditions), with the differences tending to increase as MBPRES increases and decrease as MBPERM increases. The early effects of MBPRES and MBPERM results from their corresponding effects on gas barrier pressure, which completely controls the differences between gas barrier pressure and gas pressure at early times due to the small values for gas pressure. With increasing time, MBPRES drops rapidly in importance. However, MBPERM remains the dominant variable at all times in determining the difference between gas barrier pressure and gas pressure, and hence in determining whether or not gas flow takes place from the disturbed rock zone to the anhydrite marker beds. Increasing BRSAT (initial brine saturation) tends to decrease the difference between gas barrier pressure and gas pressure. Interestingly, increasing BRSAT also tends to increase both gas barrier pressure and gas pressure; thus, BRSAT is having a larger absolute effect on gas pressure than on gas barrier pressure.

4.3.6 Gas and Brine Flow through Shaft Seal

A summary of the results for gas and brine flow through the shaft seal is given in Figure 4-11. Of the 60 sample elements, 45 result in nonzero gas flows to the Culebra, with these flows ranging up to approximately 10^7 m^3 over 10,000 yr. As the sensitivity analysis in the lower left frame of Figure 4-11 shows, gas flow through the seal is dominated by BRSAT (initial brine saturation), GRCORI (gas-generation rate for corrosion of steel under inundated conditions), SEALPERM (shaft seal permeability), GRCORH (scale

Cumulative Gas and Brine Flow through Shaft to Culebra

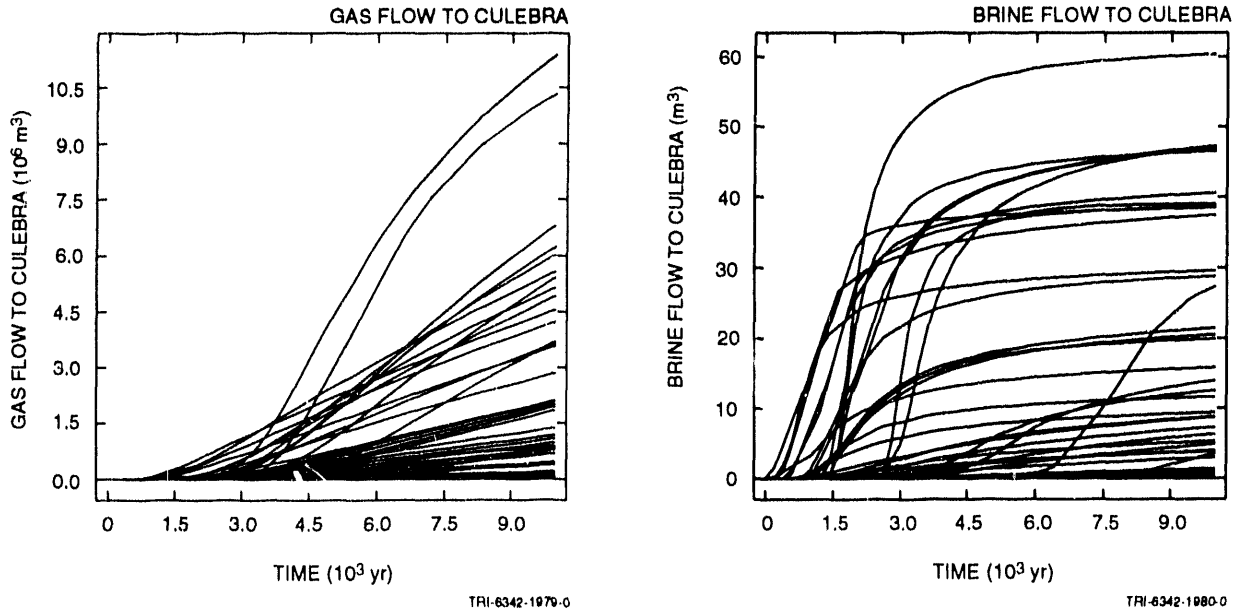

Partial Rank Correlation Coefficients for Cumulative Gas and Brine Flow through Shaft to Culebra

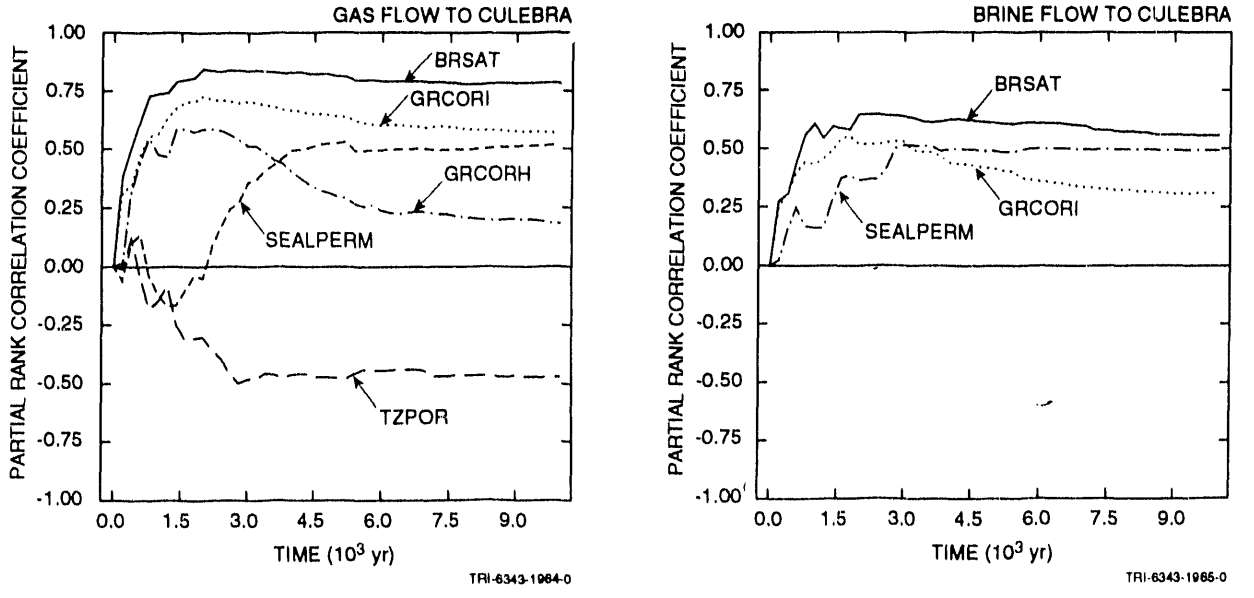

Figure 4-11. Uncertainty and sensitivity analysis results for cumulative gas and brine flow through shaft to Culebra.

factor used in definition of gas-generation rate for corrosion of steel under inundated conditions), and TZPOR (scale factor used in definition of transition zone and disturbed rock zone porosity). Increasing each of BRSAT, GRCORI and GRCORH increases gas generation, and thus increases both gas pressure in the waste panel and resultant gas flow through the shaft seal. The positive effect indicated for SEALPERM results from reduced resistance to gas flow up the shaft. The negative effect indicated for TZPOR results because increasing TZPOR increases the pore volume available for gas storage, with the result that both gas pressure and gas flow up the shaft is reduced.

A stepwise regression analysis for cumulative gas flow through the shaft over 10,000 yr is presented in Table 4-8. The cumulative gas flows used as values for the dependent variable in this regression analysis appear above 10,000 yr in the upper left frame of Figure 4-11. The variables BRSAT (initial brine saturation), GRCORI (gas-generation rate for corrosion of steel under inundated conditions) and SEALPERM (shaft seal permeability) appear in the regression analysis with positive regression coefficients; thus, increasing each of these variables tends to increase gas release. The positive effects for BRSAT and GRCORI result because increasing each of these variables tends to increase the total amount of gas generated in the panel, and the positive effect for SEALPERM results because increasing SEALPERM reduces to the resistance to gas flow through the shaft. The variable TZPOR (scale factor used in definition of transition zone and disturbed rock zone porosity) appears in the regression analysis with a negative regression coefficient; thus increasing TZPOR tends to reduce gas flow through the shaft. The negative effect for TZPOR results because increasing TZPOR tends to increase the pore space available for gas storage, thereby reducing gas pressure in the waste panel and thus gas flow up the shaft. Collectively, BRSAT, GRCORI, SEALPERM and TZPOR can account for 67% of the uncertainty in cumulative gas flow through the shaft over 10,000 yr.

Examination of the scatterplots in Figure 4-12 provides additional perspective on the effects of individual variables identified in the regression analysis in Table 4-8 for cumulative gas flow through the shaft. In particular, scatterplots are provided for BRSAT (initial brine saturation), SEALPERM (shaft seal permeability) and TZPOR (scale factor used in definition of transition zone and disturbed rock zone porosity), with plots using logarithmically-transformed variables appearing in the left column of Figure 4-12 and plots using rank-transformed variables appearing in the right column of Figure 4-12. An interesting pattern involving BRSAT and SEALPERM appears in Figure 4-12, with the 15 zero gas flows all associated with the smaller values of BRSAT but a well-defined relationship existing between SEALPERM and the nonzero gas flows. In

Table 4-8. Stepwise Regression Analyses with Rank-Transformed Data for Cumulative Gas and Brine Flow through Shaft Seal over 10,000 yr.

Cumulative Gas Flow (m^3) over 10,000 yr				Cumulative Brine Flow (m^3) over 10,000 yr			
Step[a]	Variable[b]	SRC[c]	R^2[d]	Step[a]	Variable[b]	SRC[c]	R^2[d]
1	BRSAT	0.62	0.37	1	BRSAT	0.43	0.16
2	GRCORI	0.35	0.49	2	SEALPERM	0.40	0.32
3	SEALPERM	0.31	0.60				
4	TZPOR	-0.26	0.67				

[a] Steps in stepwise regression analysis
[b] Variables listed in order of selection in regression analysis
[c] Standardized regression coefficients in final regression model
[d] Cumulative R^2 value with entry of each variable into regression model

particular, a stronger linear relationship (in rank or log space) exists between SEALPERM and the nonzero gas flows than exists between BRSAT and the nonzero gas flows. However, because the zero gas flows are associated with the smaller values of BRSAT but are spread randomly over the range of SEALPERM, the regression analysis in Table 4-8 identifies BRSAT as having a stronger relationship with gas flow than SEALPERM. As the rank scatterplot for TZPOR shows, gas flow through the shaft tends to decrease as TZPOR increases, although there is considerable variability around this trend.

Cumulative brine flow to the Culebra is shown in the upper right frame of Figure 4-11. Only 16 of the 60 sample elements result in brine flow through the shaft to the Culebra. Further, the flows that do occur tend to be small (i.e., $\leq$ 60 m^3 over 10,000 yr). A sensitivity analysis based on partial rank correlation coefficients for cumulative brine flow to the Culebra is presented in the lower right frame of Figure 4-11. Positive effects are indicated for BRSAT (initial brine saturation), GRCORI (gas-generation rate for corrosion of steel under inundated conditions) and SEALPERM (shaft seal permeability). The positive effects for BRSAT and SEALPERM result because increasing BRSAT reduces the amount of additional brine required to fill the repository and increasing SEALPERM reduces resistance to brine flow up the shaft. The reason for the selection of GRCORI is not apparent and could be spurious. As a reminder, only 16 of the 60 sample elements resulted in nonzero brine flows to the Culebra. This large number of zero values makes it difficult for partial correlation coefficients to identify the dominant variables and also increases the likelihood that spurious variables will be selected. The stepwise

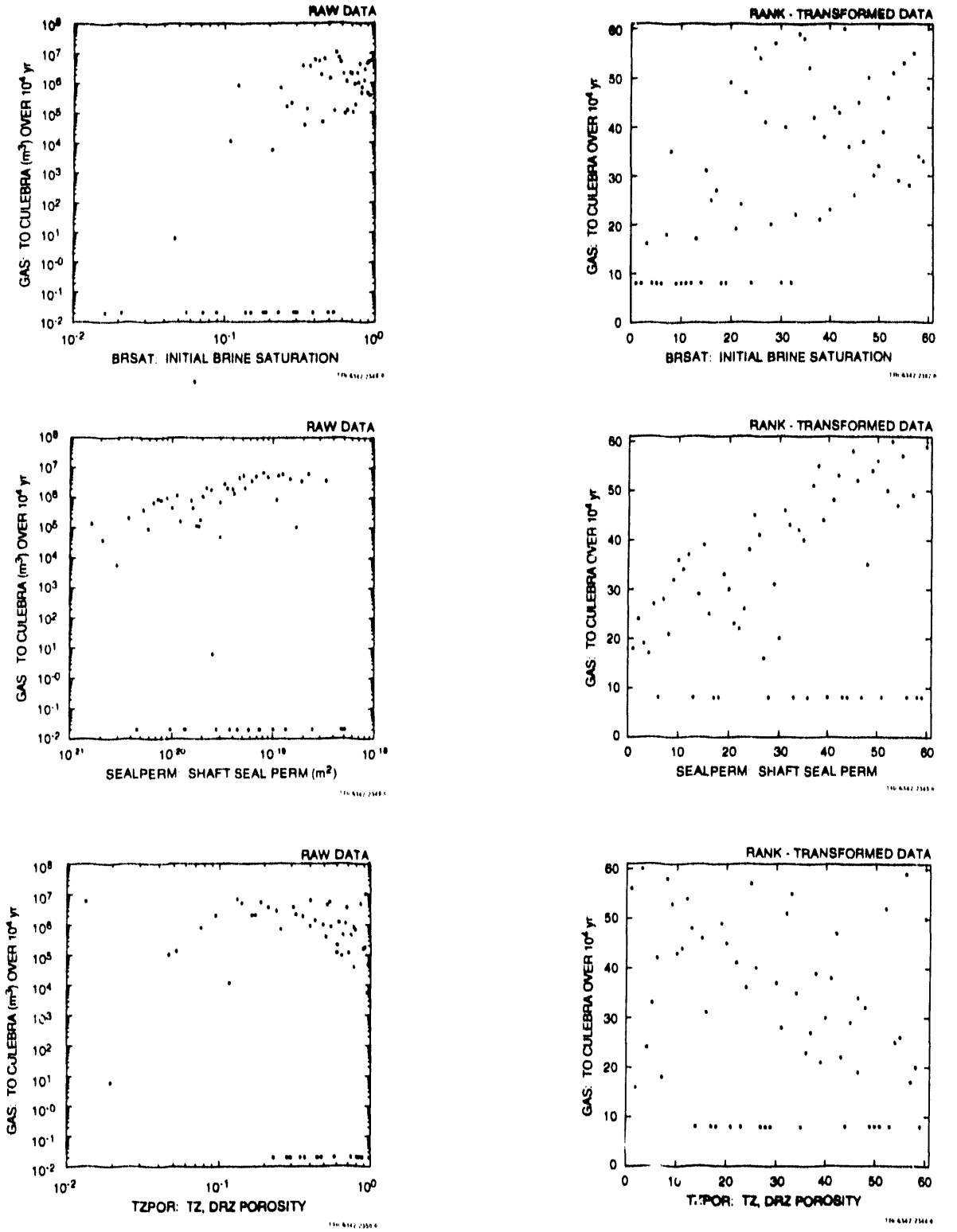

Figure 4-12. Scatterplots for cumulative gas flow through shaft seal over 10,000 yr with raw and rank-transformed data for the variables BRSAT (initial brine saturation), SEALPERM (shaft seal permeability) and TZPOR (scale factor used in definition of transition zone and disturbed rock zone porosity).

regression analysis in Table 4-8 for cumulative brine flow to the Culebra over 10^4 yr indicates positive effects for BRSAT and SEALPERM, but with an R^2 value of only 0.32.

The scatterplots in Figure 4-13 provide more insight on the variables controlling brine flow to the Culebra than the partial correlation analysis in Figure 4-11 or the stepwise regression analysis in Table 4-8. As shown in these scatterplots, there is a well-defined relationship between brine flow and SEALPERM (shaft seal permeability), with brine flow tending to increase as SEALPERM increases. However, as was the case for gas flow, this relationship is complicated by the apparent random appearance of zero brine flows scattered over the range of SEALPERM. As shown by the scatterplots for BRSAT (initial brine saturation), these zero flows tend to be associated with the smaller values of BRSAT. Also, the scatterplots for TZPOR (scale factor used in definition of transition zone and disturbed rock zone porosity) suggest that there may also be a tendency for zero brine flows to be associated with larger values for TZPOR. The association of zero brine flows with small values of BRSAT results because of both more volume for storage of brine flowing into the waste panel and increased consumption of this brine in corrosion of steel and microbial degradation of cellulosics. If the association of zero brine flows with the larger values of TZPOR is real, it probably results because increasing TZPOR increases the pore volume in the disturbed rock zone available for the storage of brine.

4.4 Discussion

The amount of brine reaching the repository is not adequate to assure the consumption of the steel and cellulosic inventories by corrosion and microbial degradation. The sensitivity analyses indicate that the dominate variable with respect to total steel and cellulosic consumption is initial brine saturation of the waste, with total consumption showing a tendency to increase as initial brine saturation increases. In consistency with the corrosion and microbial degradation processes being brine limited, variables affecting the rates of these processes are important for cumulative gas production at early times but are less important for total gas production over 10,000 yr. The cellulosic inventory is more likely to be completely consumed than the steel inventory.

For most sample elements, the gas saturation averaged over the entire repository exceeds 0.9 within a few hundred years of repository closure. Thus, brine saturation is below residual saturation in most of the repository. This low brine saturation precludes brine flow through the associated regions of the repository. As a result, radionuclides cannot be

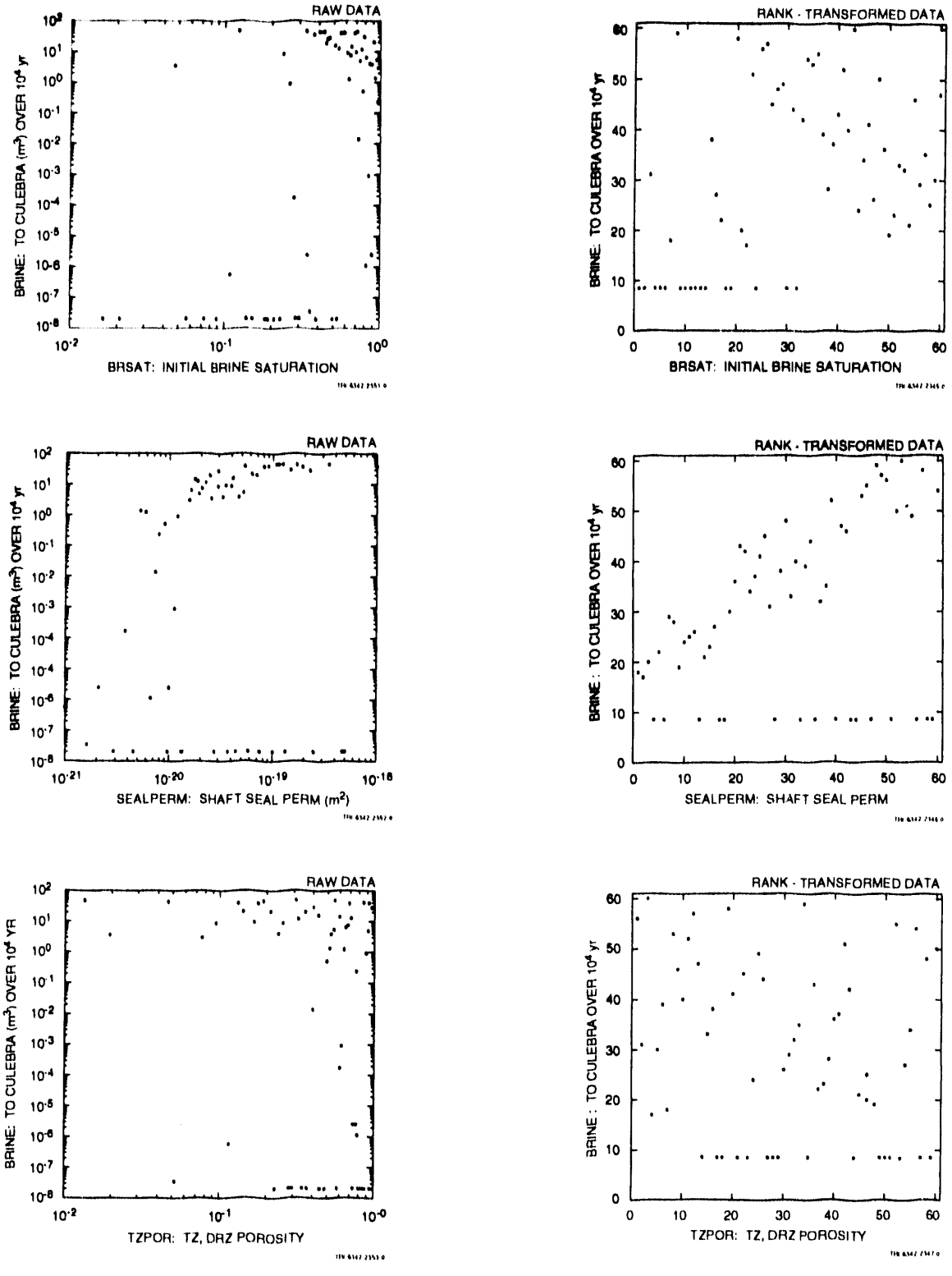

Figure 4-13. Scatterplots for cumulative brine flow through shaft seal over 10,000 yr with raw and rank-transformed data for the variables BRSAT (initial brine saturation), SEALPERM (shaft seal permeability) and TZPOR (scale factor used in definition of transition zone and disturbed rock zone porosity).

transported out of most of the repository by flowing brine under the conditions that existed in this analysis.

The short, low permeability seals considered in this analysis did not offer sufficient resistance to preclude gas and brine flow up the shaft to the Culebra. Of the 60 sample elements used in this analysis, 45 resulted in nonzero gas flows to the Culebra and 16 resulted in nonzero brine flows to the Culebra. The nonzero flows showed a strong tendency to be associated with the larger values for initial brine saturation in the waste. However, given that a nonzero flow to the Culebra occurred, its size tended to increase as shaft seal permeability increased.

To provide a correction for the competing effects of waste panel expansion due to gas pressure and waste panel compaction due to overburden pressure, the initial pore volume of the repository was set to the volume necessary to contain all potential waste-generated gas at lithostatic pressure (i.e., 14.8 MPa). As a result, gas pressure in the repository typically remained below lithostatic pressure. Thus, gas movement up the shaft is occurring in the presence of an effective bound of 14.8 MPa on gas pressure in the repository.

There was little gas movement away from the repository in the anhydrite marker beds. For most sample elements, gas pressure did not rise to levels necessary to exceed the gas barrier pressures associated with undisturbed anhydrite.

5. DISCUSSION

Five primary topics were investigated in this analysis: (1) gas production due to corrosion, (2) gas production due to microbial degradation, (3) gas migration into anhydrite marker beds in the Salado Formation, (4) gas migration through a system of shaft seals to the Culebra Dolomite, and (5) gas migration through a single shaft seal to the Culebra Dolomite. A summary of the most important variables for each of these topics is given in Table 5-1.

Table 5-1. Important Variables Identified in Uncertainty and Sensitivity Analyses for Gas and Brine Migration

Total Gas Production Due to Corrosion
• Initial brine saturation of waste • Stoichiometric factor for corrosion of steel • Gas generation rate for corrosion of steel under inundated conditions • Fraction of total waste volume occupied by IDB metals and glass waste category
Total Gas Production Due to Microbial Degradation
• Stoichiometric coefficient for microbial degradation of cellulosics • Gas generation rate due to microbial degradation of cellulosics under inundated conditions • Fraction of total waste volume occupied by IDB combustible waste category
Gas Migration into Anhydrite Marker Beds
• Gas barrier pressure, which is defined as a function of anhydrite permeability
Gas Migration through Shaft to Culebra Dolomite for a System of Shaft Seals with Panel Seals and Disturbed Rock Zone Permeability Sufficiently Low to Prevent Significant Amounts of Gas from Bypassing Panel Seals (i.e., Case 2)
• Initial brine saturation of waste • Permeability of seals between waste panels • Permeability of shaft seals
Gas Migration through Shaft to Culebra Dolomite for a Single Shaft Seal without Panel Seals (i.e., Case 3)
• Initial brine saturation • Gas generation rate for corrosion of steel under inundated conditions • Permeability of shaft seals • Porosity of distributed rock zone

Initial brine saturation in the waste was the most important variable with respect to total gas production due to corrosion. For many observations in the analysis, the consumption of steel by corrosion was limited by the amount of brine in the repository. As a result, initial brine saturation often controlled the amount of steel that was consumed by corrosion and hence the amount of gas produced by corrosion. The stoichiometric factor for corrosion defined the proportion of two different corrosion reactions, with each reaction producing a different amount of gas per mole of steel consumed by corrosion. Factors affecting the rate of gas generation due to corrosion were important early (i.e., before 3000 yr) but had less effect on total gas generation over 10,000 yr. For most observations, gas generation due to corrosion stopped before 10,000 yr due to either brine depletion or steel depletion, with the result that the rate of corrosion was not the dominant factor in determining the amount of gas produced over 10,000 yr. The initial inventory of steel has a positive effect on the amount of gas produced by corrosion, although this effect is less than the effects for initial brine saturation, the stoichiometric factor for corrosion and the gas generation rate due to the relatively small range of uncertainty assigned to the initial steel inventory. When the corrosion processes run to completion, the total amount of gas generated is determined by the stoichiometric factor for corrosion and the initial steel inventory.

The stoichiometric coefficient was the most important variable with respect to total gas production due to microbial degradation of cellulosics. As for gas production due to corrosion, factors affecting the rate of microbial degradation were important at early times but had less effect on the total gas production over 10,000 yr. A small positive effect was also indicated for the initial inventory of cellulosics, with this effect tending to be obscured by the large uncertainty assigned to the stoichiometric coefficient. When the microbial degradation processes run to completion, the total amount of gas generated is determined by the stoichiometric coefficient and the initial inventory of cellulosics. Overall, the cellulosics showed a greater tendency to be completely consumed over 10,000 yr than was shown by steel. The amount of gas produced by corrosion tended to be several times the amount of gas produced by microbial degradation. This difference between total gas production results in large part from the stoichiometric coefficient for microbial degradation, which was assigned an uncertainty range that extends to zero.

Gas migration into the anhydrite marker beds was dominated by the gas barrier pressure that had to be overcome for gas to move from the disturbed

rock zone to the undisturbed anhydrite. For most sample elements, gas pressures in the disturbed rock zone never reached levels that were sufficient to overcome the gas barrier pressure associated with the first computational cell in the undisturbed anhydrite. For all three cases considered in this study, the gas barrier pressure was defined as a function of the permeability of undisturbed anhydrite.

Three analysis cases were considered in this study: (1) Fully consolidated shaft, (2) System of shaft seals with panel seals, and (3) Single shaft seal without panel seals. Case 1 does not result in any meaningful gas or brine movement from the repository to the Culebra Dolomite and was included in this analysis to facilitate observing the factors affecting gas and brine migration into the anhydrite marker beds of the Salado Formation in the presence of an effective shaft seal system. Case 2 provides a more realistic representation of the repository in that the analysis includes the waste panels, the seals between the waste panels, and a system of three shaft seals. Case 3 was included in the analysis to investigate the effect that a single, short, low permeability shaft seal might have on gas and brine migration to the Culebra Dolomite. To provide a bounding perspective on the effect of the permeability of this single shaft seal on gas and brine migration to the Culebra Dolomite, no seals were assumed to exist between the panels in the repository.

For Case 2, gas migration through the shaft was dominated by initial brine saturation of the waste, permeability of seals between waste panels, and permeability of shaft seals. No single variable played a dominant role, although the strongest effect was due to initial brine saturation. Of the 22 sample elements used in this analysis, 18 resulted in gas migration to the Culebra Dolomite. In contrast, only 4 sample elements resulted in the movement of brine away from the waste panels.

For Case 3, gas migration through the shaft was dominated by initial brine saturation of the waste and shaft seal permeability. Initial brine saturation tends to act as a switch, with no gas release to the Culebra Dolomite often resulting when initial brine saturation is small (i.e., < 0.15). However, given that a gas release to the Culebra Dolomite occurs, the size of this release shows a strong tendency to increase as the shaft seal permeability increases. A similar pattern involving initial brine saturation and shaft seal permeability also occurs for the movement of brine through the shaft to the Culebra Dolomite. Of the 60 sample elements used in this analysis, 45 resulted in nonzero gas flows to the Culebra and 16 resulted in nonzero brine flows to the Culebra. Thus, the short, low permeability shaft seal considered in this analysis did not offer sufficient resistance to preclude gas and brine flow from the repository to the Culebra.

REFERENCES

Allen, D.M. 1971. *The Prediction Sum of Squares as a Criterion for Selecting Predictor Variables*. Report No. 23. Lexington, KY: Department of Statistics, University of Kentucky. (Copy on file at the Waste Management and Transportation Library, Sandia National Laboratories, Albuquerque, NM.)

Bertram-Howery, S.G., and R.L. Hunter, eds. 1989. *Preliminary Plan for Disposal-System Characterization and Long-Term Performance Evaluation of the Waste Isolation Pilot Plant*. SAND89-0178. Albuquerque, NM: Sandia National Laboratories.

Bertram-Howery, S.G., M.G. Marietta, R.P. Rechard, P.N. Swift, D.R. Anderson, B.L. Baker, J.E. Bean, Jr., W. Beyeler, K.F. Brinster, R.V. Guzowski, J.C. Helton, R.D. McCurley, D.K. Rudeen, J.D. Schreiber, and P. Vaughn. 1990. *Preliminary Comparison with 40 CFR Part 191, Subpart B for the Waste Isolation Pilot Plant, December 1990*. SAND90-2347. Albuquerque, NM: Sandia National Laboratories.

Beyer, W.H., ed. 1968. *CRC Handbook of Tables for Probability and Statistics*. 2nd ed. Cleveland, OH: Chemical Rubber Co.

David, F.N. 1938. *Tables of the Ordinates and Probability Integral of the Distribution of the Correlation Coefficient in Small Samples*. London, England: Biometrika Office, University College; Cambridge, England: The University Press.

Davies, P.B. 1991. *Evaluation of the Role of Threshold Pressure in Controlling Flow of Waste-Generated Gas into Bedded Salt at the Waste Isolation Pilot Plant*. SAND90-3246. Albuquerque, NM: Sandia National Laboratories.

Draper, N.R., and H. Smith. 1981. *Applied Regression Analysis*. 2nd ed. New York, NY: Wiley.

Helton, J. C. 1983. "Health Effects Associated with Unit Radionuclide Releases to the Environment," *Technical Assistance for Regulatory Development: Review and Evaluation of the Draft EPA Standard 40 CFR 191 for Disposal of High-Level Waste*. NUREG/CR-3235, SAND87-1557. Albuquerque, NM: Sandia National Laboratories. Vol. 5.

Helton, J.C. [1992.] "Uncertainty and Sensitivity Analysis Techniques for Use in Performance Assessment for Radioactive Waste Disposal," *Reliability Engineering and System Safety*. (Copy on file at the Waste Management and Transportation Library, Sandia National Laboratories, Albuquerque, NM.)

Helton, J.C., J.W. Garner, R.D. McCurley, and D.K. Rudeen. 1991. *Sensitivity Analysis Techniques and Results for Performance Assessment at the Waste Isolation Pilot Plant*. SAND90-7103. Albuquerque, NM: Sandia National Laboratories.

Helton, J.C., J.W. Garner, R.P. Rechard, D.K. Rudeen and P.N. Swift. 1992. *Preliminary Comparison with 40 CFR Part 191, Subpart B for the Waste Isolation Pilot Plant, December 1991, Volume 4: Uncertainty and Sensitivity Analysis Results*. SAND91-0893/4. Albuquerque, NM: Sandia National Laboratories.

Iman, R.L., and W.J. Conover. 1979. "The Use of the Rank Transform in Regression," *Technometrics*. Vol. 21, no. 4, 499-509.

Iman, R.L., and W.J. Conover. 1982. "A Distribution-Free Approach to Inducing Rank Correlation Among Input Variables," *Communications in Statistics: Simulation and Computation*. Vol 11, no. 3, 311-334.

Iman, R.L., and J.M. Davenport. 1982. "Rank Correlation Plots for Use with Correlated Input Variables," *Communications in Statistics: Simulation and Computation*. Vol. 11, no. 3, 335-360.

Iman, R.L., and M.J. Shortencarier. 1984. *A FORTRAN 77 Program and User's Guide for the Generation of Latin Hypercube and Random Samples for Use with Computer Models*. NUREG/CR-3624, SAND83-2365. Albuquerque, NM: Sandia National Laboratories.

Iman, R.L., J.M. Davenport, E.L. Frost, and M.J. Shortencarier. 1980. *Stepwise Regression with PRESS and Rank Regression (Program User's Guide)*. SAND79-1472. Albuquerque, NM: Sandia National Laboratories.

Iman, R.L., M.J. Shortencarier, and J.D. Johnson. 1985. *A FORTRAN 77 Program and User's Guide for the Calculation of Partial Correlation and Standardized Regression Coefficients*. NUREG/CR-4122, SAND85-0044. Albuquerque, NM: Sandia National Laboratories.

Lappin, A.R., R.L. Hunter, D.P. Garber, P.B. Davies, R.L. Beauheim, D.J. Borns, L.H. Brush, B.M. Butcher, T. Cauffman, M.S.Y. Chu, L.S. Gomez, R.V. Guzowski, H.J. Iuzzolino, V. Kelley, S.J. Lambert, M.G. Marietta, J.W. Mercer, E.J. Nowak, J. Pickens, R.P. Rechard, M. Reeves, K.L. Robinson, and M.D. Siegel. 1989. *Systems Analysis, Long-Term Radionuclide Transport, and Dose Assessments, Waste Isolation Pilot Plant (WIPP), Southeastern New Mexico; March 1989*. SAND89-0462. Albuquerque, NM: Sandia National Laboratories.

Marietta, M.G., S.G. Bertram-Howery, D.R. Anderson, K.F. Brinster, R.V. Guzowski, H. Iuzzolino, and R.P. Rechard. 1989. *Performance Assessment Methodology Demonstration: Methodology Development for Evaluating Compliance with EPA 40 CFR 191, Subpart B, for the Waste Isolation Pilot Plant*. SAND89-2027. Albuquerque, NM: Sandia National Laboratories.

McKay, M.D., R.J. Beckman, and W.J. Conover. 1979. "A Comparison of Three Methods for Selecting Values of Input Variables in the Analysis of Output from a Computer Code," *Technometrics*. Vol. 21, no. 2, 239-245.

Nowak, E.J., J.R. Tillerson, and T.M. Torres. 1990. *Initial Reference Seal System Design: Waste Isolation Pilot Plant*. SAND90-0355. Albuquerque, NM: Sandia National Laboratories.

Powers, D.W., S.J. Lambert, S-E. Shaffer, L.R. Hill, and W.D. Weart, eds. 1978. *Geological Characterization Report, Waste Isolation Pilot Plant (WIPP) Site, Southeastern New Mexico*. SAND78-1596. Albuquerque, NM: Sandia National Laboratories. Vols. 1-II.

Rechard, R.P., W. Beyeler, R.D. McCurley, D.K. Rudeen, J.E. Bean, and J.D. Schreiber. 1990. *Parameter Sensitivity Studies of Selected Components of the Waste Isolation Pilot Plant Repository/Shaft Systems*. SAND89-2030. Albuquerque, NM: Sandia National Laboratories.

U.S. DOE (Department of Energy). 1980. *Final Environmental Impact Statement: Waste Isolation Pilot Plant*. DOE/EIS-0026. Washington, DC: U.S. Department of Energy. Vols. 1-2.

U.S. DOE (Department of Energy). 1990. *Final Supplement Environmental Impact Statement, Waste Isolation Pilot Plant*. DOE/EIS-0026-FS. Washington, DC: U.S. Department of Energy, Office of Environmental Restoration and Waste Management. Vols. 1-13.

U.S. DOE (Department of Energy). 1991. *Strategy for the Waste Isolation Pilot Plant Test Phase, Revised Draft #3*. DOE/EM/48063-2. Washington, DC: U.S. Department of Energy, Office of Waste Operations. (Copy on file at the Waste Management and Transportation Library, Sandia National Laboratories, Albuquerque, NM.)

U.S. EPA (Environmental Protection Agency). 1985. "Environmental Standards for the Management and Disposal of Spent Nuclear Fuel, High-Level and Transuranic Radioactive Wastes; Final Rule, 40 CFR Part 191," *Federal Register*. Vol. 50, no. 182, 38066-38089.

U.S. EPA (Environmental Protection Agency). 1986. "Land Disposal Restrictions," *Code of Federal Regulations 40, Part 268*. Washington, DC: Office of the Federal Register, National Archives and Records Administration.

Voss, C.I. 1974. *SUTRA (Saturated-Unsaturated Transport): A Finite-Element Simulation Model for Saturated-Unsaturated, Fluid-Density-Dependent Ground-Water Flow with Energy Transport or Chemically-Reactive Single-Species Solute Transport*. Water-Resources Investigations Report 84-4369. Reston, VA: U.S. Geological Survey National Center.

WIPP PA (Performance Assessment) Division. 1991a. *Preliminary Comparison with 40 CFR Part 191, Subpart B for the Waste Isolation Pilot Plant, December 1991, Volume 1: Methodology and Results*. SAND91-0893/1. Albuquerque, NM: Sandia National Laboratories.

WIPP PA (Performance Assessment) Division. 1991b. *Preliminary Comparison with 40 CFR Part 191, Subpart B for the Waste Isolation Pilot Plant, December 1991, Volume 2: Probability and Consequence Modeling.* SAND91-0893/2. Albuquerque, NM: Sandia National Laboratories.

WIPP PA (Performance Assessment) Division. 1991c. *Preliminary Comparison with 40 CFR Part 191, Subpart B for the Waste Isolation Pilot Plant, December 1991, Volume 3: Reference Data.* SAND91-0893/3. Albuquerque, NM: Sandia National Laboratories.

WIPP PA (Performance Assessment) Department. 1992. *Long-Term Gas and Brine Migration at the Waste Isolation Pilot Plant: Preliminary Sensitivity Analyses for Post-Closure 40 CFR 268 (RCRA), May 1992.* SAND92-1933. Albuquerque, NM: Sandia National Laboratories.

DISTRIBUTION

(Send Distribution list changes to M.M. Gruebel, Dept. 6342, Sandia National Laboratories, PO Box 5800, Albuquerque, NM 87185-5800)

Federal Agencies

US Department of Energy (6)
Office of Civilian Radioactive Waste Management
Attn: Deputy Director, RW-2
Associate Director, RW-10/50
Office of Program and Resources Management
Office of Contract Business Management
Director, Analysis and Verification Division, RW-22
Associate Director, RW-30
Office of Systems and Compliance
Associate Director, RW-40
Office of Storage and Transportation
Director, RW-4/5
Office of Strategic Planning and International Programs
Office of External Relations
Forrestal Building
Washington, DC 20585

US Department of Energy
Albuquerque Operations Office
Attn: National Atomic Museum Library
PO Box 5400
Albuquerque, NM 87185

US Department of Energy (2)
Office of Environmental Restoration and Waste Management
Attn: EM-1
C. Frank, EM-50
Washington, DC 20585

US Department of Energy (3)
Office of Environmental Restoration and Waste Management
Attn: M. Frei, EM-34, Trevion II
Director, Waste Management Projects
Washington, DC 20585-0002

US Department of Energy
Office of Environmental Restoration and Waste Management
Attn: J. Lytle, EM-30, Trevion II
Washington, DC 20585-0002

US Department of Energy
Office of Environmental Restoration and Waste Management
Attn: S. Schneider, EM-342, Trevion II
Washington, DC 20585-0002

US Department of Energy (3)
WIPP Task Force
Attn: G.H. Daly
S. Fucigna
B. Bower
12800 Middlebrook Rd., Suite 400
Germantown, MD 20874

US Department of Energy (4)
Office of Environment, Safety and Health
Attn: R.P. Berube, EH-20
C. Borgstrum, EH-25
R. Pelletier, EH-231
K. Taimi, EH-232
Washington, DC 20585

US Department of Energy (6)
WIPP Project Integration Office
Attn: S. Alcorn
W.J. Arthur III
J. Coffey
L.W. Gage
P.J. Higgins
D.A. Olona
PO Box 5400
Albuquerque, NM 87115-5400

US Department of Energy (2)
WIPP Project Integration Satellite Office
Attn: R. Batra
R. Becker
PO Box 3090, Mail Stop 525
Carlsbad, NM 88221-3090

US Department of Energy (10)
WIPP Project Site Office (Carlsbad)
Attn: A. Hunt (4)
V. Daub (4)
J. Lippis
K. Hunter
PO Box 3090
Carlsbad, NM 88221-3090

US Department of Energy
Research & Waste Management Division
Attn: Director
PO Box E
Oak Ridge, TN 37831

US Department of Energy (2)
Idaho Operations Office
Fuel Processing and Waste
Management Division
785 DOE Place
Idaho Falls, ID 83402

US Department of Energy
Savannah River Operations Office
Defense Waste Processing
Facility Project Office
Attn: W.D. Pearson
PO Box A
Aiken, SC 29802

US Department of Energy (2)
Richland Operations Office
Nuclear Fuel Cycle & Production
Division
Attn: R.E. Gerton
825 Jadwin Ave.
PO Box 500
Richland, WA 99352

US Department of Energy
Office of Geologic Disposal
Yucca Mountain Project Office
Attn: Associate Director, RW-20
PO Box 98608
Las Vegas, NV 89193-8608

US Department of Energy (3)
Nevada Operations Office
Attn: J.R. Boland
D. Livingston
P.K. Fitzsimmons
2753 S. Highland Drive
Las Vegas, NV 89183-8518

US Department of Energy (2)
Technical Information Center
PO Box 62
Oak Ridge, TN 37831

US Department of Energy
Los Alamos Area Office
528 35th Street
Los Alamos, NM 87544

US Department of Energy (2)
Chicago Operations Office
Attn: J.C. Haugen
9800 South Cass Avenue
Argonne, IL 60439

US Department of Energy (3)
Rocky Flats Area Office
Attn: W.C. Rask
G. Huffman
T. Lukow
PO Box 928
Golden, CO 80402-0928

US Department of Energy
Dayton Area Office
Attn: R. Grandfield
PO Box 66
Miamisburg, OH 45343-0066

US Department of Energy
Attn: E. Young
Room E-178
GAO/RCED/GTN
Washington, DC 20545

US Bureau of Land Management
Carlsbad Office
101 E. Mermod
Carlsbad, NM 88220

US Bureau of Land Management
New Mexico State Office
PO Box 1449
Santa Fe, NM 87507

US Environmental Protection
Agency (2)
Radiation Protection Programs
Attn: M. Oge
ANR-460
Washington, DC 20460

US Environmental Protection
Agency, Region 6
Attn: C. Byrum, 6T-ET
1445 Ross Ave.
Dallas, TX 75202

US Geological Survey (2)
Water Resources Division
Attn: C. Peters
4501 Indian School NE
Suite 200
Albuquerque, NM 87110

US Nuclear Regulatory Commission
Division of Waste Management
Attn: H. Marson
Mail Stop 4-H-3
Washington, DC 20555

US Nuclear Regulatory Commission (4)
Advisory Committee on Nuclear Waste
Attn: D. Moeller
M.J. Steindler
P.W. Pomeroy
W.J. Hinze
7920 Norfolk Ave.
Bethesda, MD 20814

Defense Nuclear Facilities Safety Board
Attn: D. Winters
625 Indiana Ave. NW
Suite 700
Washington, DC 20004

Nuclear Waste Technical Review Board
Attn: Library (2)
1100 Wilson Blvd.
Suite 910
Arlington, VA 22209-2297

Energy and Science Division
Office of Management and Budget
Attn: K. Yuracko
725 17th Street NW
Washington, DC 20503

State Agencies

New Mexico Bureau of Mines
and Mineral Resources
Socorro, NM 87801

New Mexico Energy, Minerals and
Natural Resources Department
Attn: Librarian
2040 South Pacheco
Santa Fe, NM 87505

New Mexico Energy, Minerals and
Natural Resources Department
New Mexico Radioactive Task Force (2)
(Governor's WIPP Task Force)
Attn: A. Lockwood, Chairman
C. Wentz, Policy Analyst
2040 South Pacheco
Santa Fe, NM 87505

Bob Forrest
Mayor, City of Carlsbad
PO Box 1569
Carlsbad, NM 88221

Carlsbad Department of Development
Executive Director
Attn: C. Bernard
PO Box 1090
Carlsbad, NM 88221

New Mexico Environment Department
Secretary of the Environment (3)
Attn: J. Espinosa
PO Box 968
1190 St. Francis Drive
Santa Fe, NM 87503-0968

New Mexico Environment Department
Attn: P. McCasland
WIPP Project Site Office
PO Box 3090
Carlsbad, NM 88221-3090

New Mexico State Engineer's Office
Attn: M. Chudnoff
PO Box 25102
Santa Fe, NM 87504-5102

Environmental Evaluation Group (5)
Attn: R. Neill
7007 Wyoming Blvd. NE, Suite F-2
Albuquerque, NM 87109

Advisory Committee on Nuclear Facility Safety

John F. Ahearne
Executive Director, Sigma Xi
99 Alexander Drive
Research Triangle Park, NC 27709

James E. Martin
109 Observatory Road
Ann Arbor, MI 48109

WIPP Panel of National Research Council's Board on Radioactive Waste Management

Charles Fairhurst, Chairman
Department of Civil and
Mineral Engineering
University of Minnesota
500 Pillsbury Dr. SE
Minneapolis, MN 55455-0220

John O. Blomeke
3833 Sandy Shore Drive
Lenoir City, TN 37771-9803

John D. Bredehoeft
Western Region Hydrologist
Water Resources Division
US Geological Survey (M/S 439)
345 Middlefield Road
Menlo Park, CA 94025

Rodney C. Ewing
Department of Geology
University of New Mexico
Albuquerque, NM 87131

B. John Garrick
PLG, Inc.
4590 MacArthur Blvd.
Suite 400
Newport Beach, CA 92660-2027

Leonard F. Konikow
US Geological Survey
431 National Center
Reston, VA 22092

Jeremiah O'Driscoll
505 Valley Hill Drive
Atlanta, GA 30350

Chris G. Whipple
ICF Kaiser Engineers
1800 Harrison St.
Oakland, CA 94612-3430

National Research Council (3)
Board on Radioactive
Waste Management
RM HA456
Attn: P.B. Myers (2)
G.J. Grube
2101 Constitution Ave.
Washington, DC 20418

Performance Assessment Peer Review Panel

G. Ross Heath
College of Ocean and Fishery
Sciences, HN-15
583 Henderson Hall
University of Washington
Seattle, WA 98195

Thomas H. Pigford
Department of Nuclear Engineering
4159 Etcheverry Hall
University of California
Berkeley, CA 94720

Thomas A. Cotton
JK Research Associates, Inc.
4429 Butterworth Place NW
Washington, DC 20016

Robert J. Budnitz
President, Future Resources
Associates, Inc.
2000 Center Street, Suite 418
Berkeley, CA 94704

C. John Mann
Department of Geology
245 Natural History Bldg.
1301 West Green Street
University of Illinois
Urbana, IL 61801

Frank W. Schwartz
Department of Geology and Mineralogy
The Ohio State University
Scott Hall
1090 Carmack Rd.
Columbus, OH 43210

National Laboratories

Argonne National Laboratory (2)
Attn: A. Smith
D. Tomasko
9700 South Cass, Bldg. 201
Argonne, IL 60439

Battelle Pacific Northwest
Laboratory (2)
Attn: S. Bates
R.E. Westerman
MSIN P8-44
Battelle Boulevard
Richland, WA 99352

Idaho National Engineering
Laboratory (2)
Attn: H. Loo
R. Klinger
Mail Stop 5108
Idaho Falls, ID 83403-4000

Los Alamos National Laboratory (5)
Attn: B. Erdal, CNC-11
M. Ennis, HS-12
Mail Stop J900
S. Kosiewicz, EM-7
Mail Stop J595
L. Soholt, EM-13
Mail Stop M992
J. Wenzel, HS-12
Mail Stop K482
PO Box 1663
Los Alamos, NM 87545

Oak Ridge National Laboratory
Transuranic Waste Manager
Attn: D.W. Turner
Bldg. 3047
PO Box 2008
Oak Ridge, TN 37831-6060

Pacific Northwest Laboratory
Attn: B. Kennedy
PO Box 999
Richland, WA 99352

Westinghouse-Savannah River
Technology Center (4)
Attn: N. Bibler
J.R. Harbour
M.J. Plodinec
G.G. Wicks
Aiken, SC 29802

Corporations/Members of the Public

Battelle Memorial Institute
Attn: R. Root
J. Kircher
505 Marquette NW
Suite 1
Albuquerque, NM 87102

Benchmark Environmental Corp.
Attn: C. Frederickson
4501 Indian School NE
Suite 105
Albuquerque, NM 87110

Beta Corporation Int.
Attn: E. Bonano
6613 Esther NE
Albuquerque, NM 87109

City of Albuquerque
Public Works Department
Utility Planning Division
Attn: W.K. Summers
PO Box 1293
Albuquerque, NM 87103

Deuel and Associates, Inc.
Attn: R.W. Prindle
7208 Jefferson NE
Albuquerque, NM 87109

Disposal Safety, Inc.
Attn: B. Ross
1660 L Street NW, Suite 314
Washington, DC 20036

Ecodynamics (2)
Attn: P. Roache
R. Blaine
PO Box 9229
Albuquerque, NM 87119-9229

EG & G Idaho (3)
1955 Fremont Street
Attn: C. Atwood
C. Hertzler
T.I. Clements
Idaho Falls, ID 83415

Geomatrix
Attn: K. Coppersmith
100 Pine St., Suite 1000
San Francisco, CA 94111

Golder Associates, Inc.
Attn: R. Kossik
4104 148th Avenue NE
Redmond, WA 98052

INTERA, Inc.
Attn: A.M. LaVenue
1650 University Blvd. NE, Suite 300
Albuquerque, NM 87102

INTERA, Inc.
Attn: J.F. Pickens
6850 Austin Center Blvd., Suite 300
Austin, TX 78731

INTERA, Inc.
Attn: W. Stensrud
PO Box 2123
Carlsbad, NM 88221

INTERA, Inc.
Attn: W. Nelson
101 Convention Center Drive
Suite 540
Las Vegas, NV 89109

IT Corporation (2)
Attn: R.F. McKinney
J. Myers
Regional Office
Suite 700
5301 Central Avenue NE
Albuquerque, NM 87108

John Hart and Associates, P.A.
Attn: J.S. Hart
2815 Candelaria Road NW
Albuquerque, NM 87107

John Hart and Associates, P.A.
Attn: K. Lickliter
1009 North Washington
Tacoma, WA 98406

MAC Technical Services Co.
Attn: D.K. Duncan
8418 Zuni Road SE
Suite 200
Albuquerque, NM 87108

Newman and Holtzinger
Attn: C. Mallon
1615 L Street NW
Suite 1000
Washington, DC 20036

RE/SPEC, Inc. (2)
Attn: W. Coons
4775 Indian School NE
Suite 300
Albuquerque, NM 87110

RE/SPEC, Inc.
Attn: J.L. Ratigan
PO Box 725
Rapid City, SD 57709

Reynolds Electric and Engineering
Company, Inc.
Attn: E.W. Kendall
Building 790
Warehouse Row
PO Box 98521
Las Vegas, NV 89193-8521

Science Applications International
Corporation (SAIC)
Attn: H.R. Pratt
10260 Campus Point Drive
San Diego, CA 92121

Science Applications International
Corporation (2)
Attn: D.C.Royer
C.G. Pflum
101 Convention Center Dr.
Las Vegas, NV 89109

Science Applications International
Corporation (3)
Attn: M. Davis
R. Guzowski
J. Tollison
2109 Air Park Road SE
Albuquerque, NM 87106

Science Applications International
Corporation (2)
Attn: J. Young
D. Lester
18706 North Creek Parkway, Suite 110
Bothell, WA 98011

Southwest Research Institute
Center for Nuclear Waste Regulatory
Analysis (2)
Attn: P.K. Nair
6220 Culebra Road
San Antonio, TX 78228-0510

Systems, Science, and Software (2)
Attn: E. Peterson
P. Lagus
Box 1620
La Jolla, CA 92038

TASC
Attn: S.G. Oston
55 Walkers Brook Drive
Reading, MA 01867

Tech Reps, Inc. (7)
Attn: J. Chapman
C. Crawford
D. Marchand
T. Peterson
J. Stikar
D. Scott
M. Minahan
5000 Marble NE, Suite 222
Albuquerque, NM 87110

Tolan, Beeson & Associates
Attn: T.L. Tolan
2320 W. 15th Avenue
Kennewick, WA 99337

TRW Environmental Safety Systems (2)
Attn: I. Sacks, Suite 800
L. Wildman, Suite 1300
2650 Park Tower Drive
Vienna, VA 22180-7306

Sanford Cohen and Associates
Attn: J. Channell
7101 Carriage Rd NE
Albuquerque, NM 87109

Westinghouse Electric Corporation (5)
Attn: Library
C. Cox
L. Fitch
B.A. Howard
R.F. Kehrman
PO Box 2078
Carlsbad, NM 88221

Westinghouse Hanford Company
Attn: D.E. Wood, MSIN H0-32
PO Box 1970
Richland, WA 99352

Western Water Consultants
Attn: P.A. Rechard
PO Box 4128
Laramie, WY 82071

Western Water Consultants
Attn: D. Fritz
1949 Sugarland Drive #134
Sheridan, WY 82801-5720

P. Drez
8816 Cherry Hills Road NE
Albuquerque, NM 87111

David Lechel
9600 Allende Rd. NE
Albuquerque, NM 87109

C.A. Marchese
PO Box 21790
Albuquerque, NM 87154

Arend Meijer
3821 Anderson SE
Albuquerque, NM 87108

D.W. Powers
Star Route Box 87
Anthony, TX 79821

Shirley Thieda
PO Box 2109, RR1
Bernalillo, NM 87004

Jack Urich
c/o CARD
144 Harvard SE
Albuquerque, NM 87106

Universities

University of California
Mechanical, Aerospace, and
Nuclear Engineering Department (2)
Attn: W. Kastenberg
D. Browne
5532 Boelter Hall
Los Angeles, CA 90024

University of California
Engineering and Applied Science Attn:
D. Okrent
48-121A Engineering IV
Los Angeles, CA 90024-1597

University of California
Mine Engineering Department
Rock Mechanics Engineering
Attn: N. Cook
Berkeley, CA 94720

University of Hawaii at Hilo
Business Administration
Attn: S. Hora
Hilo, HI 96720-4091

University of New Mexico
Geology Department
Attn: Library
Albuquerque, NM 87131

University of New Mexico
Research Administration
Attn: H. Schreyer
102 Scholes Hall
Albuquerque, NM 87131

University of Wyoming
Department of Civil Engineering
Attn: V.R. Hasfurther
Laramie, WY 82071

University of Wyoming
Department of Geology
Attn: J.I. Drever
Laramie, WY 82071

University of Wyoming
Department of Mathematics
Attn: R.E. Ewing
Laramie, WY 82071

Libraries

Thomas Brannigan Library
Attn: D. Dresp
106 W. Hadley St.
Las Cruces, NM 88001

New Mexico State Library
Attn: N. McCallan
325 Don Gaspar
Santa Fe, NM 87503

New Mexico Tech
Martin Speere Memorial Library
Campus Street
Socorro, NM 87810

New Mexico Junior College
Pannell Library
Attn: R. Hill
Lovington Highway
Hobbs, NM 88240

Carlsbad Municipal Library
WIPP Public Reading Room
Attn: L. Hubbard
101 S. Halagueno St.
Carlsbad, NM 88220

University of New Mexico
Zimmerman Library
Government Publications Department
Albuquerque, NM 87131

NEA/Performance Assessment Advisory Group (PAAG)

P. Duerden
ANSTO
Lucas Heights Research Laboratories
Private Mail Bag No. 1
Menai, NSW 2234
AUSTRALIA

Gordon S. Linsley
Division of Nuclear Fuel Cycle and
Waste Management
International Atomic Energy Agency
PO Box 100
A-1400 Vienna, AUSTRIA

Nicolo Cadelli
Commission of the European
Communities
200, Rue de la Loi
B-1049 Brussels, BELGIUM

R. Heremans
Organisme Nationale des Déchets
Radioactifs et des Matiéres Fissiles
(ONDRAF)
Place Madou 1, Boitec 24/25
B-1030 Brussels, BELGIUM

J. Marivoet
Centre d'Etudes de l'Energie
Nucléaire (CEN/SCK)
Boeretang 200
B-2400 Mol, BELGIUM

P. Conlon
Waste Management Division
Atomic Energy Control Board (AECB)
PO Box 1046
Ottawa, Ontario KIP 559, CANADA

A.G. Wikjord
Manager, Environmental and Safety
Assessment Branch
Atomic Energy of Canada Limited
Whiteshell Research Establishment
Pinewa, Manitoba ROE 1LO
CANADA

Teollisuuden Voima Oy (TVO) (2)
Attn: Timo Äikäs
Jukka-Pekka Salo
Annankatu 42 C
SF-00100 Helsinki Suomi
FINLAND

Timo Vieno
Technical Research Centre of Finlar
(VTT)
Nuclear Energy Laboratory
PO Box 208
SF-02151 Espoo, FINLAND

Division de la Sécurité et de la
Protection de l'Environment (DSPE)
Commissariat á l'Energie Atomique
Agence Nationale pour la Gestion des
Déchets Radioactifs (ANDRA) (2)
Attn: Gérald Ouzounian
M. Claude Ringeard
Route du Panorama Robert Schuman
B. P. No. 38
F-92266 Fontenay-aux-Roses Cedex
FRANCE

Claudio Pescatore
Division of Radiation Protection and
Waste Management
OECD Nuclear Energy Agency
38, Boulevard Suchet
F-75016 Paris, FRANCE

M. Dominique Greneche
Commissariat á l'Energie Atomique
IPSN/DAS/SASICC/SAED
B.P. No. 6
F-92265 Fontenay-aux-Roses Cedex
FRANCE

Robert Fabriol
Bureau de Recherches Géologiques et
Miniéres (BRGM)
B.P. 6009
45060 Orléans Cedex 2, FRANCE

P. Bogorinski
Gesellschaft für Reaktorsicherheit
(GRS) MBH
Schwertnergasse 1
D-5000 Köln 1, GERMANY

R. Storck
GSF - Institut für Tieflagerung
Theodor-Heuss-Strabe 4
D-3300 Braunschweig, GERMANY

Ferrucio Gera
ISMES S.p.A
Via del Crociferi 44
I-00187 Rome, ITALY

Hiroyuki Umeki
Isolation System Research Program
Radioactive Waste Management Project
Power Reactor and Nuclear Fuel
Development Corporation (PNC)
1-9-13, Akasaka, Minato-ku
Tokyo 107, JAPAN

P. Carboneras Martinez
ENRESA
Calle Emilio Vargas, 7
R-28043 Madrid
SPAIN

Tönis Papp
Swedish Nuclear Fuel and Waste
Management Co.
Box 5864
S 102 48 Stockholm
SWEDEN

Conny Hägg
Swedish Radiation Protection
Institute (SSI)
Box 60204
S-104 01 Stockholm
SWEDEN

J. Hadermann
Paul Scherrer Institute
Waste Management Programme
CH-5232 Villigen PSI
SWITZERLAND

J. Vigfusson
HSK-Swiss Nuclear Safety Inspectorate
Federal Office of Energy
CH-5232 Villigen-HSK
SWITZERLAND

D.E. Billington
Departmental Manager—Assessment
Studies
Radwaste Disposal R&D Division
AEA Decommissioning & Radwaste
Harwell Laboratory, B60
Didcot Oxfordshire OX11 ORA
UNITED KINGDOM

P. Grimwood
Waste Management Unit
BNFL
Sellafield
Seascale, Cumbria CA20 1PG
UNITED KINGDOM

Alan J. Hooper
UK Nirex Ltd
Curie Avenue
Harwell, Didcot
Oxfordshire, OX11 ORH
UNITED KINGDOM

Jerry M. Boak
Yucca Mountain Project Office
US Department of Energy
PO Box 98608
Las Vegas, NV 89193

Seth M. Coplan (Chairman)
US Nuclear Regulatory Commission
Division of High-Level Waste Management
Mail Stop 4-H-3
Washington, DC 20555

A.E. Van Luik
INTERA/M&O
The Valley Bank Center
101 Convention Center Dr.
Las Vegas, NV 89109

NEA/Probabilistic System Assessment Group (PSAG)

Shaheed Hossain
Division of Nuclear Fuel Cycle and Waste Management
International Atomic Energy Agency
Wagramerstrasse 5
PO Box 100
A-1400 Vienna, AUSTRIA

Alexander Nies (PSAC Chairman)
Gesellschaft für Strahlen- und Institut für Tieflagerung
Abteilung für Endlagersicherheit
Theodor-Heuss-Strasse 4
D-3300 Braunschweig, GERMANY

Eduard Hofer
Gesellschaft für Reaktorsicherheit (GRS) MBH
Forschungsgelände
D-8046 Garching, GERMANY

Andrea Saltelli
Commission of the European Communities
Joint Resarch Centre of Ispra
I-21020 Ispra (Varese)
ITALY

Alejandro Alonso
Cátedra de Tecnología Nuclear
E.T.S. de Ingenieros Industriales
José Gutiérrez Abascal, 2
E-28006 Madrid, SPAIN

ENRESA (2)
Attn: M. A. Cuñado
F. J. Elorza
Calle Emilio Vargas, 7
E-28043 Madrid, SPAIN

Pedro Prado
CIEMAT
Instituto de Tecnología Nuclear
Avenida Complutense, 22
E-28040 Madrid, SPAIN

Nils A. Kjellbert
Swedish Nuclear Fuel and Waste Management Company (SKB)
Box 5864
S-102 48 Stockholm, SWEDEN

Björn Cronhjort
Royal Institute of Technology
Automatic Control
S-100 44 Stockholm, SWEDEN

Richard A. Klos
Paul-Scherrer Institute (PSI)
CH-5232 Villingen PSI, SWITZERLAND

Nationale Genossenschaft für die Lagerung Radioaktiver Abfälle (2)
Attn: C. McCombie
F. Van Dorp
Hardstrasse 73
CH-5430 Wettingen, SWITZERLAND

N. A. Chapman
Intera Information Technologies
Park View House
14B Burton Street
Melton Mowbray
Leicestershire LE13 1AE
UNITED KINGDOM

Daniel A. Galson
Galson Sciences Ltd.
35, Market Place
Oakham
Leicestershire LE15 6DT
UNITED KINGDOM

David P. Hodgkinson
Intera Information Technologies
45 Station Road, Chiltern House
Henley-on-Thames
Oxfordshire RG9 1AT
UNITED KINGDOM

Brian G.J. Thompson
Department of the Environment: Her Majesty's Inspectorate of Pollution
Room A5.33, Romney House
43 Marsham Street
London SW1P 2PY
UNITED KINGDOM

Intera Information Technologies
Attn: M.J.Apted
3609 South Wadsworth Blvd.
Denver, CO 80235

US Nuclear Regulatory Commission (2)
Attn: R. Codell
N. Eisenberg
Mail Stop 4-H-3
Washington, DC 20555

Battelle Pacific Northwest Laboratories
Attn: P.W. Eslinger
MS K2-32
PO Box 999
Richland, WA 99352

Center for Nuclear Waste Regulatory Analysis (CNWRA)
Southwest Research Institute
Attn: B. Sagar
PO Drawer 28510
6220 Culebra Road
San Antonio, TX 78284

Geostatistics Expert Working Group (GXG)

Rafael L. Bras
R.L. Bras Consulting Engineers
44 Percy Road
Lexington, MA 02173

Jesus Carrera
Universidad Politécnica de Cataluña
E.T.S.I. Caminos
Jordi, Girona 31
E-08034 Barcelona
SPAIN

Gedeon Dagan
Department of Fluid Mechanics and Heat Transfer
Tel Aviv University
PO Box 39040
Ramat Aviv, Tel Aviv 69978
ISRAEL

Ghislain de Marsily (GXG Chairman)
University Pierre et Marie Curie
Laboratorie de Geologie Applique
4, Place Jussieu
T.26 - 5e etage
75252 Paris Cedex 05, FRANCE

Alain Galli
Centre de Geostatistique
Ecole des Mines de Paris
35 Rue St. Honore
77035 Fontainebleau, FRANCE

Christian Ravenne
Geology and Geochemistry Division
Institut Francais du Pétrole
1 & 4, Av. de Bois-Préau B.P. 311
92506 Rueil Malmaison Cedex
FRANCE

Peter Grindrod
INTERA Information Technologies Ltd.
Chiltern House
45 Station Road
Henley-on-Thames
Oxfordshire, RG9 1AT, UNITED KINGDOM

Alan Gutjahr
Department of Mathematics
New Mexico Institute of Mining and Technology
Socorro, NM 87801

C. Peter Jackson
Harwell Laboratory
Theoretical Studies Department
Radwaste Disposal Division
Bldg. 424.4
Oxfordshire Didcot Oxon OX11 ORA
UNITED KINDGOM

Rae Mackay
Department of Civil Engineering
University of Newcastle Upon Tyne
Newcastle Upon Tyne NE1 7RU
UNITED KINGDOM

Steve Gorelick
Department of Applied Earth Sciences
Stanford University
Stanford, CA 94305-2225

Peter Kitanidis
60 Peter Coutts Circle
Stanford, CA 94305

Dennis McLaughlin
Parsons Laboratory
Room 48-209
Department of Civil Engineering
Massachusetts Institute of Technology
Cambridge, MA 02139

Shlomo P. Neuman
College of Engineering and Mines
Department of Hydrology and Water Resources
University of Arizona
Tucson, AZ 85721

Yoram Rubin
Department of Civil Engineering
University of California
Berkeley, CA 94720

Foreign Addresses

Studiecentrum Voor Kernenergie
Centre D'Energie Nucleaire
Attn: A. Bonne
SCK/CEN
Boeretang 200
B-2400 Mol
BELGIUM

Atomic Energy of Canada, Ltd. (3)
Whiteshell Research Establishment
Attn: M.E. Stevens
B.W. Goodwin
D. Wushke
Pinewa, Manitoba ROE 1LO, CANADA

Juhani Vira
Teollisuuden Voima Oy (TVO)
Annankatu 42 C
SF-00100 Helsinki Suomi
FINLAND

Jean-Pierre Olivier
OECD Nuclear Energy Agency (2)
38, Boulevard Suchet
F-75016 Paris
FRANCE

D. Alexandre, Deputy Director
ANDRA
31 Rue de la Federation
75015 Paris
FRANCE

Claude Sombret
Centre D'Etudes Nucleaires
De La Vallee Rhone
CEN/VALRHO
S.D.H.A. B.P. 171
30205 Bagnols-Sur-Ceze, FRANCE

Bundesministerium fur Forschung und Technologie
Postfach 200 706
5300 Bonn 2, GERMANY

Bundesanstalt fur Geowissenschaften und Rohstoffe
Attn: M. Langer
Postfach 510 153
3000 Hanover 51, GERMANY

Gesellschaft fur Reaktorsicherheit (GRS) (2)
Attn: B. Baltes
W. Muller
Schwertnergasse 1
D-5000 Cologne, GERMANY

Institut fur Tieflagerung (2)
Attn: K. Kuhn
Theodor-Heuss-Strasse 4
D-3300 Braunschweig, GERMANY

Physikalisch-Technische Bundesanstalt
Attn: P. Brenneke
Postfach 33 45
D-3300 Braunschweig, GERMANY

Shingo Tashiro
Japan Atomic Energy Research Institute
Tokai-Mura, Ibaraki-Ken
319-11, JAPAN

Netherlands Energy Research Foundation (ECN)
Attn: L.H. Vons
3 Westerduinweg
PO Box 1
1755 ZG Petten, THE NETHERLANDS

Johan Andersson
Swedish Nuclear Power Inspectorate
Statens Kärnkraftinspektion (SKI)
Box 27106
S-102 52 Stockholm, SWEDEN

Fred Karlsson
Svensk Karnbransleforsorjning
AB SKB
Box 5864
S-102 48 Stockholm, SWEDEN

Nationale Genossenschaft für die
Lagerung Radioaktiver Abfälle (2)
Attn: S. Vomvoris
P. Zuidema
Hardstrasse 73
CH-5430 Wettingen, SWITZERLAND

AEA Technology
Attn: J.H. Rees
D5W/29 Culham Laboratory
Abington
Oxfordshire OX14 3DB, UNITED KINGDOM

AEA Technology
Attn: W.R. Rodwell
044/A31 Winfrith Technical Centre
Dorchester
Dorset DT2 8DH, UNITED KINGDOM

AEA Technology
Attn: J.E. Tinson
B4244 Harwell Laboratory
Didcot, Oxfordshire OX11 ORA
UNITED KINGDOM

D.R. Knowles
British Nuclear Fuels, plc
Risley, Warrington
Cheshire WA3 6AS, 1002607
UNITED KINGDOM

Internal

1 A. Narath
20 O.E. Jones
1502 J.C. Cummings
1511 D.K. Gartling
6000 D.L. Hartley
6115 P.B. Davies
6115 R.L. Beauheim
6119 E.D. Gorham
6119 Staff (14)
6121 J.R. Tillerson
6121 Staff (7)
6233 J.C. Eichelberger
6300 D.E. Ellis
6302 L.E. Shephard
6303 S.Y. Pickering
6303 W.D. Weart
6305 S.A. Goldstein
6305 A.R. Lappin
6306 A.L. Stevens
6312 F.W. Bingham
6313 L.S. Costin
6331 P.A. Davis
6341 Sandia WIPP Central Files (100)
6342 D.R. Anderson
6342 J.C. Helton (20)
6342 Staff (30)
6343 V. Harper-Slaboszewicz
6343 Staff (3)
6345 R.C. Lincoln
6345 Staff (9)
6347 D.R. Schafer
6348 J.T. Holmes
6348 Staff (4)
6351 R.E. Thompson
6352 D.P. Garber
6352 S.E. Sharpton
6400 N.R. Ortiz
6613 R.M. Cranwell
6613 R.L. Iman
6613 C. Leigh
6622 M.S.Y. Chu
6641 R.E. Luna, Acting
7141 Technical Library (5)
7151 Technical Publications
7613-2 Document Processing for
DOE/OSTI (10)
8523-2 Central Technical Files

☆ U.S. GOVERNMENT PRINTING OFFICE 1993—774-122/80238

DATE

FILMED

11/24/93

END